U.PORTO

Universidade do Porto
FEUP Faculdade de Engenharia

Film thickness and friction in grease lubricated rough contacts

António Couto Vieira

Dissertation submitted to
Faculdade de Engenharia da Universidade do Porto
for the degree of:

Mestre em Engenharia Mecânica

Supervisor:
David Emanuel Gonçalves, PhD
INEGI - CETRIB

Co-Supervisor:
Jorge Seabra, Professor
DEMec - FEUP

INEGI - CETRIB
and
Faculdade de Engenharia da Universidade do Porto
Departamento de Engenharia Mecânica

Porto, 2017

The work presented in this dissertation was performed at
INEGI - CETRIB
and Department of Mechanical Engineering of the
Faculty of Engineering of
University of Porto
Porto, Portugal.

António Couto Vieira
E-mail: up201502882@fe.up.pt

Faculdade de Engenharia da Universidade do Porto - DEMec
INEGI - CETRIB
Rua Dr. Roberto Frias s/n, Sala M111
4200-465 Porto
Portugal

Abstract

Greases are vastly used in mechanical components, specially in rolling bearings. It is important to understand grease lubrication mechanisms in order to optimize these machine elements performance, however grease lubrication is not as well understood as oil lubrication, so it is still very hard to predict grease performance.

The purpose of this work is to study the mechanisms of grease lubrication on rough contacts and the influence of the surfaces' roughness and grease formulation on the grease's friction behaviour and film thickness build-up. In order to understand the influence of the grease components on the grease lubrication, base oils and thickeners were physically and chemically characterized. Furthermore, the influence of the operating conditions on the film thickness and friction behaviour of lubricating grease is analysed through experimental tests performed on single rolling contacts.

The behaviour of dry greases, greases who lost a great amount of bled oil, was also investigated. This study allows the understanding of the thickener concentration influence on the grease tribological behaviour.

Keywords: Lubrication, Grease, Rough Contacts, Greases' friction behaviour, Greases' film thickness

To my family and friends...

Acknowledgements

I would like to express my gratitude to every person that contributed to execution of this work, directly or indirectly, specially to CETRIB and in particularly to my supervisors, David Gonçalves and Jorge Seabra, for the precious assistance and knowledge they passed me during the execution of this work.

I would like to thank three professors which marked my academical path, and inspired me to follow this master's degree specialization and taught me that work is not work when you enjoy what you do. To Prof. Armando Vilaça Campos, Paulo Tavares de Castro and Jorge Seabra, I express my profound gratitude.

I want to thank my friends for all the good and relaxing moments we have shared, and my family for being always present, specially to my brother, grandmother and mother without whom I could not get this degree. Finally, I would like to express my gratitude and love to my girlfriend, for being my company of all hours.

Contents

Abstract **i**

Acknowledgements **v**

1 Introduction **1**
1.1 Introduction . . . 1
1.2 Motivation . . . 1
1.3 Objectives . . . 2
1.4 Layout . . . 2

2 Background Theory **3**
2.1 History of tribology and lubrication . . . 3
2.2 Grease composition and properties . . . 4
2.3 Grease Base Oil . . . 5
2.3.1 Oil Properties . . . 5
2.3.2 Base oil types . . . 9
2.4 Grease Thickeners . . . 10

3 Experimental Characterization **13**
3.1 Introduction . . . 13
3.2 Tested Greases . . . 13
3.3 Base Oil Properties . . . 14
3.3.1 Dynamic Viscosity . . . 14
3.3.2 Density . . . 16
3.3.3 Influence of temperature on viscosity . . . 17
3.3.4 Pressure-viscosity . . . 18
3.4 Oil/Thickener Separation . . . 19
3.5 Fourier Transform Infrared spectroscopy - FTIR . . . 20
3.6 Oil bleeding . . . 25
3.7 Surface Roughness Measurements . . . 25
3.8 Closure . . . 27

4 Film Thickness of fully flooded grease lubricated contacts **29**
4.1 Introduction . . . 29
4.2 Experimental procedure . . . 30
4.3 Base oil film thickness . . . 31
4.3.1 Introduction . . . 31
4.3.2 Specific film thickness . . . 32
4.3.3 Results . . . 33
4.4 Grease film thickness . . . 36

4.4.1 Introduction 36
4.4.2 Results 36
4.5 Closure 40

5 Friction behaviour of fully flooded grease lubricated contacts 41
5.1 Introduction 41
5.2 Introductory notes on Stribeck Curves 41
5.3 Measurement Procedure 42
5.4 Oil Lubricated Contacts - Results 43
5.5 Grease Lubricated Contacts - Results 53
5.6 Grease friction vs Base oil friction 65
5.7 Grease friction vs Dry Grease friction 70
5.8 Closure 77

6 Conclusion 79
6.1 Conclusions 79
6.2 Future Work 80

References 81

A Graphic Results 87

List of Figures

2.1 Viscosity explanation [30] . . . 6
2.2 Flow characteristics of Newtonian and non-Newtonian lubricants: A. viscosity as a function of shear stress; B. shear rate as a function of shear stress. [30] . . . 6
2.3 VI explanation [30] . . . 7
2.4 Development of viscosity against pressure: 1. aromatic oil; 2. naphthenic oil; 3. paraffinic oil; 4. biodegradable polyolester [30] . . . 8

3.1 SV10 device . . . 14
3.2 Base oils dynamic viscosities (η) . . . 15
3.3 Base oils kinematic viscosities (ν) . . . 16
3.4 Base oils thermal-viscosities (β) . . . 18
3.5 Base oils pressure-viscosities (α) . . . 19
3.6 LiM FTIR Spectra . . . 21
3.7 CaLiM FTIR Spectra . . . 22
3.8 ClayM FTIR Spectra . . . 23
3.9 PPAO FTIR Spectra . . . 24
3.10 Bleeding apparatus . . . 25

4.1 EHD2 device . . . 30
4.2 Stribeck curve. . . . 32
4.3 Base oils film thickness measurements . . . 34
4.4 Base oils film thickness measurements . . . 35
4.5 Greases film thickness measurements . . . 38

5.1 Base oils' Specific Film Thickness for the smooth disk (σ = 44 nm) . . . 45
5.2 Base oils' Specific Film Thickness for the intermediate disk (σ = 212 nm) . . . 46
5.3 Base oils' Specific Film Thickness for the rough disk (σ = 574 nm) . . . 47
5.4 Base oils friction measurements . . . 51
5.5 Greases Specific Film Thickness - Smooth disk (Ra = 0.02 μm) . . . 55
5.6 Greases Specific Film Thickness - Intermediate disk (Ra = 0.1 μm) . . . 56
5.7 Greases Specific Film Thickness - Rough disk (Ra = 0.5 μm) . . . 57
5.8 Grease friction measurements . . . 59
5.9 Stribeck curves . . . 61
5.10 Grease Stribeck curve and film thickness . . . 63
5.11 LiM - Base oil vs Grease . . . 66
5.12 CaLiM - Base oil vs Grease . . . 67
5.13 ClayM - Base oil vs Grease . . . 68
5.14 PPAO - Base oil vs Grease . . . 69
5.15 LiM - Dry vs Standard Grease . . . 71

5.16 CaLiM - Dry vs Standard Grease 72
5.17 ClayM - Dry vs Standard Grease 73
5.18 PPAO - Dry vs Standard Grease 74
5.19 Dry Greases traction curves for the intermediate disk (Ra=0.1 μm) 75
5.20 Dry Greases traction curves for the rough disk (Ra=0.5 μm) 76

A.1 LiM Base Oil Film Thickness 87
A.2 CaLiM Base Oil Film Thickness 88
A.3 ClayM Base Oil Film Thickness 88
A.4 PPAO Base Oil Film Thickness 89
A.5 LiM Base Oil Stribeck Curve T=40°C 89
A.6 LiM Base Oil Stribeck Curve T=80°C 90
A.7 LiM Base Oil Stribeck Curve T=110°C 90
A.8 CaLiM Base Oil Stribeck Curve T=40°C 91
A.9 CaLiM Base Oil Stribeck Curve T=80°C 91
A.10 CaLiM Base Oil Stribeck Curve T=110°C 92
A.11 ClayM Base Oil Stribeck Curve T=40°C 92
A.12 ClayM Base Oil Stribeck Curve T=80°C 93
A.13 ClayM Base Oil Stribeck Curve T=110°C 93
A.14 PPAO Base Oil Stribeck Curve T=40°C 94
A.15 PPAO Base Oil Stribeck Curve T=80°C 94
A.16 PPAO Base Oil Stribeck Curve T=110°C 95
A.17 LiM Grease Film Thickness 95
A.18 CaLiM Grease Film Thickness 96
A.19 ClayM Grease Film Thickness 96
A.20 PPAO Grease Film Thickness 97
A.21 LiM Grease Stribeck Curve T=40°C 98
A.22 LiM Grease Stribeck Curve T=80°C 98
A.23 LiM Grease Stribeck Curve T=110°C 99
A.24 CaLiM Grease Stribeck Curve T=40°C 99
A.25 CaLiM Grease Stribeck Curve T=80°C 100
A.26 CaLiM Grease Stribeck Curve T=110°C 100
A.27 ClayM Grease Stribeck Curve T=40°C 101
A.28 ClayM Grease Stribeck Curve T=80°C 101
A.29 ClayM Grease Stribeck Curve T=110°C 102
A.30 PPAO Grease Stribeck Curve T=40°C 102
A.31 PPAO Grease Stribeck Curve T=80°C 103
A.32 PPAO Grease Stribeck Curve T=110°C 103
A.33 LiM Dry Grease Stribeck Curve Ra=100 nm 104
A.34 LiM Dry Grease Stribeck Curve Ra=500 nm 104
A.35 CaLiM Dry Grease Stribeck Curve Ra=100 nm 105
A.36 CaLiM Dry Grease Stribeck Curve Ra=500 nm 105
A.37 ClayM Dry Grease Stribeck Curve Ra=100 nm 106
A.38 ClayM Dry Grease Stribeck Curve Ra=500 nm 106
A.39 PPAO Dry Grease Stribeck Curve Ra=100 nm 107
A.40 PPAO Dry Grease Stribeck Curve Ra=500 nm 107

List of Tables

3.1 Greases formulation 13
3.2 Base oils dynamic viscosity /mPa.s· 15
3.3 Base oils VI 16
3.4 Density Measurements (T_0 - room temperature $\simeq$ 22^oC) 16
3.5 Vogel's equation parameters 17
3.6 Thermal-viscosity at test temperature /^{o}C^{-1} 17
3.7 Values of s and t used on Gold's equation. 18
3.8 Pressure-viscosity at test temperatures /Pa^{-1} $\times 10^{-9}$ 19
3.9 Roughness parameters of each disk and sphere /μm 26

4.1 Ball-on-disk test conditions for film thickness measurements 31
4.2 Characteristic Λ values for each lubrication regime 32
4.3 Optimized Pressure-viscosities /Pa^{-1} $\times 10^{-9}$ 35
4.4 Plateau thickness and transition speed for each grease 37
4.5 Ratio between grease and base oil film thicknesses $\left(\frac{h_G}{h_{BO}}\right)$ 39

5.1 Test specimens details 43
5.2 Test conditions 43
5.3 $\frac{\alpha}{VI}$ ratio /Pa^{-1} $\times 10^{-12}$ 48

List of Symbols

Symbol	Description	Units
a	Hertzian half-width	m
E	Young modulus	Pa
E^*	Effective Young modulus$\left(\frac{1}{E^*} = \frac{(1-\nu_1^2)}{E_1} + \frac{(1-\nu_2^2)}{E_2}\right)$	Pa
F_n	Normal Load	N
G	Transverse shear modulus	Pa
h_G	Grease central film thickness	m
h_{BO}	Base oil central film thickness	m
h_R	Residual central film thickness	m
k	Thermal conductivity	$W \cdot m^{-1} \cdot K^{-1}$
L	Lubricant Thermal Parameter	-
R_a	Mean Roughness	m
R_q	Root Mean Square Roughness	m
R_x	Equivalent radius of contact in the x direction $\left(\frac{1}{R_x} = \frac{1}{2} \cdot \left(\frac{1}{R_{x1}} + \frac{1}{R_{x2}}\right)\right)$	m
S	Hersey parameter	m^{-1}
S_P	Modified Hersey parameter [Brandão *et al.*]	-
S_{PR}	Modified Hersey parameter	-
SRR	Slide-to-Roll Ratio	-
T	Temperature	^oC
U_0	Entrainment Speed	$m \cdot s^{-1}$
U_i	Tangential Speed of the contacting surface i	$m \cdot s^{-1}$
α	Pressure-viscosity	Pa^{-1}
β	Temperature-viscosity coefficient	$^oC^{-1}$
ϕ_T	Thermal correction factor for the Hamrock & Dowson equation	-
γ	Shear Strain	-
$\dot{\gamma}$	Shear Rate	s^{-1}
η	Dynamic Viscosity	Pa·s
Λ	Specific Film Thickness	-
μ	Friction coefficient	-
ν	Kinematic Viscosity	$m^2 \cdot s^{-1}$
ν	Poisson coefficient	-
ρ	Density	$kg \cdot m^{-3}$
σ_i	Root Mean Square Roughness of Surface i	m
σ	Composite Roughness	m
τ	Shear Stress	Pa
τ_y	Yield Shear Stress	Pa

Acronym	**Description**
COF	Coefficient of Friction
$CaLi$	Lithium-Calcium soap thickener
$Clay$	Clay thickener
EHL	Elastohydrodynamic Lubrication
$FTIR$	Fourier Transform Infrared Spectroscopy
Li	Lithium soap thickener
M	Mineral Base oil
PAO	Poly-Alpha-Olefin Base oil
P	Polypropylene thickener

Chapter 1

Introduction

1.1 Introduction

Depending on the application, roller bearings can be lubricated with oil, grease, pastes, or lubricating varnishes, however, most of the roller bearings are grease lubrication. Greases, which can include solid or liquid lubricant additives, enable customization for almost every application and aspects like temperature, speed range or maximum bearable pressure can be modified with the use of additives or even thickeners. Greases are generally used in areas where a continuous supply of oil cannot be secured, such as open bearings or gears, or on high loads and/or low speeds demands.

During the last decades, several researches have been developed in order to better comprehend the mechanisms which rule greases lubrication [1–5], including the prediction of grease film thickness [6; 7] and traction behaviour [8; 9], however these predictions only take into account the base oil properties and neglect the thickener and additives contribution, as well as the interaction between all the grease components. It is known that thickener crosses the contact contributing to film thickness generation [10; 11], base oil properties and thickener concentration also contribute to the lubricant film formation [9] and that greases form a thicker film than its respective base oil [10; 12].

1.2 Motivation

Due to their proliferation as a lubricant, it is important to understand greases' lubrication mechanisms, their friction behaviour and how these two factors are related, in order to improve grease manufacturing and formulation and consequently optimize machine elements performance.

It is still difficult to predict the lubrication regime in grease lubricated contacts, not only because the active lubricant inside the contact is unknown (depending on the operating conditions the thickener and/or the base oil could define the film behaviour), but also because the relationship between the film thickness and friction with the roughness of the surfaces is hard to understand.

This work aims to study the influence of the operating conditions on the grease film thickness build-up, and on the friction behaviour, as well as the influence of the base oil and thickener on the performance of different grease formulations. These studies are based on results from experimental tests, where the lubricant's film thickness and coefficient of friction were measured.

1.3 Objectives

Fully formulated lubricating greases and their base oils will be tested in a dedicated ball-on-disc device. The base oils and thickeners of the tested greases cover a wide range of commercial products. Film thickness and friction measurements will be performed, using surfaces of different roughness, in order to characterize the greases' tribological behaviour. Dry greases, greases with high thickener content, will also be tested.

1.4 Layout

This manuscript consists on six chapters.

Chapter 1 - Introduction

This chapter approaches the importance of grease lubrication on machine elements, and clarifies this thesis' objectives.

Chapter 2 - Background Theory

In this chapter, the history of lubrication is briefly summarized. General remarks about grease lubrication are referred, such as its components and main properties.

Chapter 3 - Experimental Characterization

The experimental techniques and materials used to characterize greases, base oils and thickeners are described. The results of these characterization procedures are also presented.

Chapter 4 - Film Thickness of fully flooded grease lubricated contacts

This chapter presents the results of film thickness measurements of greases and their respective base oils, which were carried out on a ball-on-disk apparatus. Film thickness predictions of Newtonian fluids are discussed and compared to the experimental results. The experimental procedures, and post-test analyses are also shown here.

Chapter 5 - Friction behaviour of fully flooded grease lubricated contacts

Greases and base oils friction behaviour are described and discussed, for a wide range of operating conditions. The influence of roughness on the lubricant's friction behaviour is analysed. The experimental procedures and the post-test analyses are also presented in this chapter.

Chapter 6 - Conclusion

The main conclusions of this work are discussed and suggestions for future work are presented.

Chapter 2

Background Theory

2.1 History of tribology and lubrication

Since the beginning of mankind, the concept of friction was understood by our ancestors. A very important milestone in the history of tribology was the invention of the wheel. Records show the use of wheels from 3500 b.C., illustrating our ancestors' concern with friction reduction in translationary motion. The transportation of large stone building blocks and monuments required the know-how of frictional devices and lubricants, such as water lubricated sleds. Certain specimens of egyptian chariots, from around 1400 b.C. showed that Egyptians used animal fats, such as tallow, to lubricate chariot axels [13; 14].

Since the Renaissance that Tribology had a large development. Leonardo Da Vinci, invented what was the first prototype of a roller bearing. His work on friction originated in studies of the rotational resistance of axles and the mechanics of screw threads. He focused on all kinds of friction and drew a distinction between sliding and rolling friction. At the end of that period (1493-1500) he was confident about the laws of friction [15].

In his Principia from 1687 [16], Sir Isaac Newton laid down the foundations of viscosity and was able to bring out the concept of Newtonian and Non-Newtonian Fluids, which had a great impact on the study of lubricants as we know it nowadays. French physicist Guillaume Amontons rediscovered the rules of friction after he studied dry sliding between two flat surfaces (1699). He postulated two laws which are only applicable to dry friction. Amontons stated that the force of friction is directly proportional to the applied load (Amontons' 1st Law), he also stated that the force of friction is independent of the apparent area of contact (Amontons' 2nd Law).

In the following century, Charles-Augustin Coulomb (1736-1806) added a third law that the friction force is independent of velocity, once motion starts, making a clear distinction between static friction and kinetic friction.

Further developments were associated with the growth of industrialization in the latter part of the eighteenth century. Early developments in the petroleum industry started in Scotland, Canada, and the United States in the 1850s.

Despite the essential laws of viscous flow were postulated by Sir Isaac Newton in 1668, scientific understanding of lubricated bearing operations did not occur until the end of the nineteenth century. Indeed, the beginning of our understanding of the principle of hydrodynamic lubrication was made possible by the experimental studies of Beauchamp Tower (1884) [17] and the theoretical interpretations of Osborne Reynolds (1886) [18].

The formulation of the elastohydrodynamic problem lubrication goes back to 1886, when Reynolds published his famous article where he derived the differential equation describing the pressure distribution and load-carrying capacity of lubricating films for journal bearings. In 1916, Martin and Gumbel applied Reynolds' equation to the lubrication of gears and found film thicknesses that were too small to explain the full-film lubrication that was observed here. In 1941 Meldahl [19] included elastic deformations caused by the contact pressures, but still the film thickness predictions were too small. In 1945 Ertel [20] (published under the name of Grubin in 1949 [21]), included a pressure–viscosity effect on the film thickness and finally a full-film could be predicted. Since then, this type of lubrication has been called elastohydrodynamic lubrication (EHL). Formulae for line contacts, based on numerical calculations, were developed by Petrusevich [22] and Dowson and Higginson [23]. In 1972 Kauzlarich and Greenwood [24] solved the line contact problem for grease lubrication. Later, in 1976, Hamrock and Dowson [25–28] solved the circular problem for oil lubrication. Their curve fit to numerical solutions is still the most widely used film thickness formula in EHL.

As the science and knowledge about lubrication evolved, the manufacture of more complex lubricants was possible. During the period around 1930 and 1940, a great amount of work was made around synthetic lubricants and the use of additives, it was also around this period that calcium, and lithium thickened greases were developed. We had to wait until the 1990s, to see the development of polypropylene greases.

2.2 Grease composition and properties

The *American Society for Testing and Materials* (ASTM) defines lubricating grease as: "A solid to semifluid product of dispersion of a thickening agent in liquid lubricant." which means that a grease is nothing more rather than an oil blended with a thickener. ASTM also states: "Other ingredients imparting special properties may be included", referring to grease additives (ASTM D 288, Standard Definitions of Terms Relating to Petroleum). Another definition, in a more rheological point of view, is: "a lubricant which under certain loads and within its range of temperature application, exhibits the properties of a solid body, undergoes plastic strain and starts to flow like a liquid should the load reach the critical point, and regains solid body like properties after the removal of stress".

This definition, proposed by Sinitsyn [29], incloses another very important detail: greases are both solid and liquid depending on external factors like the level of stress it is subdued, temperature, etc., yet it exhibits an extra property comparing to a liquid lubricant, a yield stress, τ_y.

Thus there are three components which integrate a lubricating grease: base oil (65 to 95 wt %), thickener (5 to 35 wt %) and additives (0 to 10 wt%). The base oil and additives are the major components in grease formulations, and thereafter, exert considerable influence on the behaviour of the grease. The thickener is usually a soap, which may diversify in size from 1 to 100 μm, or dispersions of small particles. Ergo, greases have a matrix structure; the scale of which can vary from simple particle interaction to the formation of extended fibre networks. Such structure or composition endows this type of

lubricant with a variety of viscoelastic and semi-plastic properties which cannot be found in fluid lubrication. Though each component has its role in the lubrication process, grease lubrication also depends on their interaction and on the manufacturing process, which makes the comprehension and characterization of each of the components' influence on the process rather difficult.

Greases can be used in a wide variety of environments. Operating temperatures for grease lubricated applications range from subzero, -70°C to temperatures exceeding 300°C for high temperature applications. Greases are also used in vacuum atmospheres, common on space applications, yet, commonly, the operating environment involves wet and humid atmospheres, exposure to salt water and many other types of corrosive agents that affect the performance of machine elements.

2.3 Grease Base Oil

As the most abundant component on greases, base-oils play a key role on the greases lubrication. As a matter of fact, the base-oil will provide most of the properties to the grease, which can be slightly altered by the thickener and the additives, such as: solubility, oxidation stability, evaporation loss, low temperature properties and viscosity.

2.3.1 Oil Properties

Viscosity

Perhaps the most important property of a base fluid, viscosity plays a key role in a grease formulation. Base fluid viscosity defines many of the grease's characteristics, such as heat transfer, oil bleed rate, load capacity, etc.

Viscosity is a measure of a fluid's resistance to flow. It describes the internal friction of a moving fluid. A fluid with large viscosity resists motion because its molecular structure grants a lot of internal friction. A fluid with low viscosity flows easily because its molecular makeup results in very little friction when it is in motion.

Viscosity and its dimensions are best explained with a model of parallel layers of fluid which could be viewed molecularly (Figure 2.1). If this packet of fluid layers is sheared (τ), the individual fluid layers are displaced in the direction of the shearing force. The upper layers move faster than the lower layers because molecular forces act to resist movement between the layers. These forces create resistance to shearing and this resistance is given the term dynamic viscosity. The difference in velocity between two given fluid layers, related to their linear displacement, is referred to as shear rate ($\dot{\gamma}$) . This velocity gradient is proportional to the shear stress (τ). The proportionality constant η is called dynamic viscosity and has the units Pa·s, equation (2.1) and (2.2).

$$\dot{\gamma} = \frac{dv}{dy} \quad \left[\mathrm{s}^{-1}\right] \tag{2.1}$$

$$\eta = \frac{\tau}{\dot{\gamma}} \quad [\mathrm{Pa.s}] \tag{2.2}$$

The experimental determination of viscosity in run-out or capillary tubes is influenced by the weight of the fluid. The relationship between dynamic viscosity and specific gravity

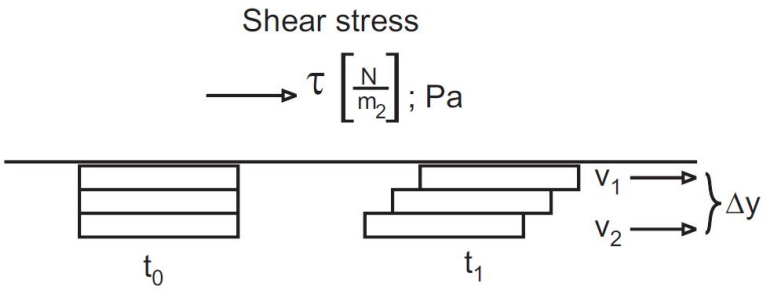


Figure 2.1: Viscosity explanation [30]

is referred to as kinematic viscosity ν.

$$\nu = \frac{\eta}{\rho} \qquad \left[\mathrm{m}^2 \cdot \mathrm{s}^{-1}\right] \tag{2.3}$$

Fluids which present proportionality between shear stress and shear rate are classified as Newtonian fluids, that is, the viscosity of Newtonian fluids is independent of shear rate. Deviations from this Newtonian behavior are sometimes referred to as structural viscosity. Those viscosities are named as apparent viscosities.

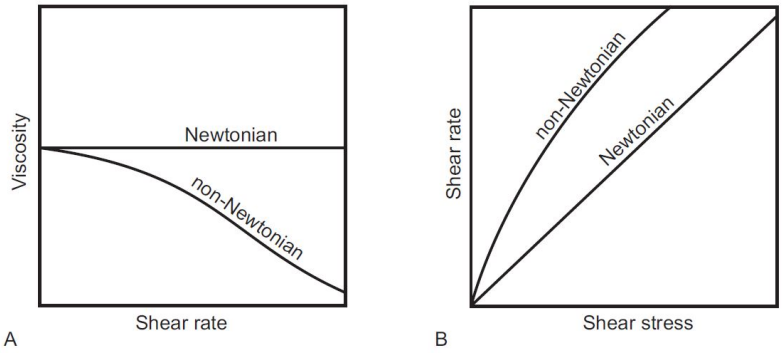


Figure 2.2: Flow characteristics of Newtonian and non-Newtonian lubricants: A. viscosity as a function of shear stress; B. shear rate as a function of shear stress. [30]

Influence of Temperature on Viscosity

The viscosity of all oils used for lubrication purposes drops significantly as their temperature increases. In linear systems, this η–T behavior is hyperbolic and the interpolation between two measured viscosities is problematic. For these reasons, η–T behavior has been studied and researched along the years and many models have been developed. One of these models is the Cameron's law [31]:

$$\eta = \eta_0 \cdot e^{-\beta \cdot \Delta T} \tag{2.4}$$

where η_0 is the dynamic viscosity at a reference temperature, β is the thermal-viscosity coefficient and ΔT is the temperature variation(T - T_0).

The most accurate expression and the most accepted amongst the engineer community is described in ASTM D341 standard[32]:

$$\log\log(\nu + a) = n + m\log(T) \tag{2.5}$$

where ν is the kinematic viscosity, T is the temperature in Kelvin and m, n and a are experimentally determined lubricant dependent constants.

Yet, lubricant manufacturers tend to use another parameter that gives expeditious and concise information about the influence of temperature on viscosity, VI - Viscosity Index - which can be calculated by the following equation:

$$VI = \frac{L - U}{L - H} \times 100 \tag{2.6}$$

where L and H correspond to the viscosity of the reference oil at 100°C and 40°C, respectively, and U is the viscosity at 40°C of the oil in analysis.

As shown in the figure, oils, whose VI is high show lower temperature dependency on viscosity and vice versa.

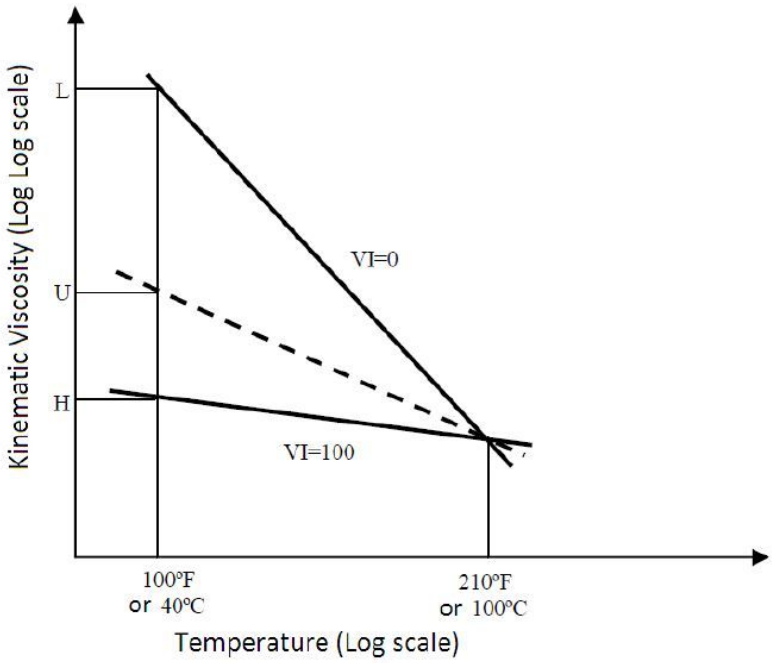


Figure 2.3: VI explanation [30]

Influence of Pressure on Viscosity

The importance of viscosity-pressure dependency was, and still is, underestimated for several lubrication applications. Piezo-viscous properties have an important role on the calculus of elastohydrodynamic lubricant films. Viscosity increases exponentially as pressure raises, metal-forming lubricants can be subject to such pressures that the viscosity of such oils can increase by a number powers of 10. Viscosity-pressure behavior can be described by the formula [33]:

$$\eta_p = \eta_0 \cdot e^{\alpha(p-p_0)} \tag{2.7}$$

where η_p is the dynamic viscosity at a pressure p, η_0 is the dynamic viscosity at 1 bar and α is the viscosity–pressure coefficient.

α can increase significantly with decreasing temperature which has an exponential effect on viscosity. Thus, practical lubrication technology needs consideration of pressure and temperature to make a reasonable evaluation of viscosity. Figure 2.4 shows the development of viscosity against pressure for a number of oils with different chemical structures.

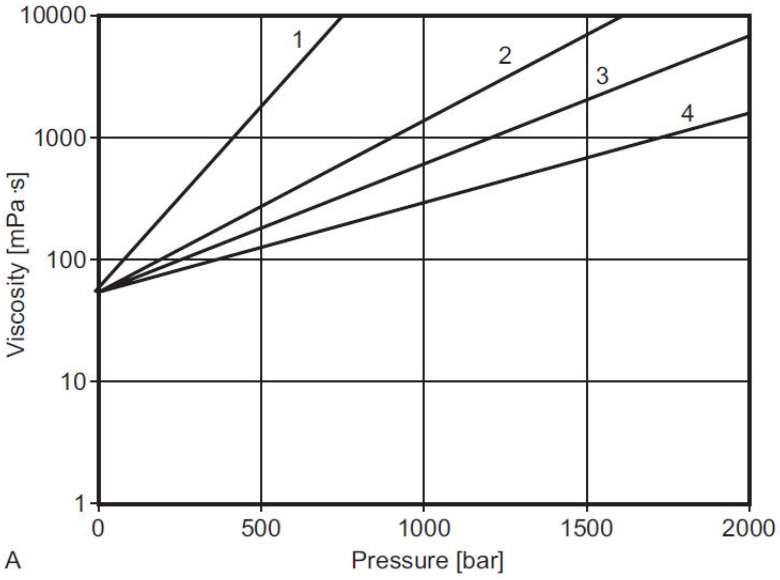


Figure 2.4: Development of viscosity against pressure: 1. aromatic oil; 2. naphthenic oil; 3. paraffinic oil; 4. biodegradable polyolester [30]

The Effect of Shear Rate on Viscosity

The definition of viscosity for Newtonian fluids is a proportionality between the shear stress τ and the shear rate $\dot{\gamma}$. This means that viscosity is not altered (with the exception of temperature and pressure dependence) even when subjected to greater shear forces, in a friction contact zone, or in other words, in isothermal and isobaric conditions.

Lubricants whose viscosity displays dependence on shear rate are known as non-Newtonian or fluids with structural viscosity.

Greases or oils that contain polymers with specific additives and mineral oils at low temperatures (long-chain paraffin effects) show a structure-viscous behavior. Most major

lubricant base oils such as hydrocarbon oils (mineral oil raffinates or synthetic hydrocarbons), synthetic esters and natural fatty oils can withstand very high shearing forces as found in highly loaded machine elements (e.g. gearboxes) and are independent of shear rate.

Bulk Density

Bulk density relates the mass of a lubricant with its volume. Temperature and pressure also affect its value. Temperature influence on bulk density is described in the following equation:

$$\rho(T) = \rho(T_0) \times [1 - \alpha_T(T - T_0)] \tag{2.8}$$

where T is an arbitrary temperature, α_T is the temperature-density coefficient and $\rho(T_0)$ is the density measured at reference temperature T_0.

Density variation with pressure can be estimated using the empirical equation proposed by Hamrock[34]:

$$\rho(p) = \rho(p_0) \times \left(1 + \frac{0.6p}{1 + 1.7p}\right) \tag{2.9}$$

where p is pressure and $\rho(p_0)$ is the bulk density measured at the atmospheric pressure p_0.

Thermal conductivity

Thermal conductivity is a material-specific property used for characterizing steady heat transport, thus it describes the transport of energy – in the form of heat – through a body of mass as the result of a temperature gradient [35]. Higher thermal conductivity favours heat evacuation, this property has linear variations with temperature.

2.3.2 Base oil types

The more commonly used base-oils can be divided into two main groups, mineral oils and synthetic fluids, nevertheless, in the past few years triglyceride oils have been more and more used as base-oil for grease manufacturing. Only the first two will have a more detailed approach in this thesis.

Mineral Base Oils

The largest portion of base fuilds used in greases dwell on a variety derivatives from the refining of crude oil and downstream petroleum raw materials. Mineral oils can comprehend a very wide range of chemical components, depending not only on the origin and composition of the crude oil, but as well on the refining processes to which they have been submitted to. [36]

Mineral oils can be divided in three groups: aromatic, naphthenic and paraffinic; historically speaking, due to their solubility characteristics, aromatic and naphthenic mineral oils have been used in large scale. However due to health concerns, oils of the aromatic

group were neglected, leading the paraffinic oils to the manufacturers' preferences.

Generally compared to other oil types, mineral oils present a higher viscosity at low temperatures, and a low Viscosity Index. Three of the greases selected were formulated with a mineral base-oil.

Synthetic Base Oils

Synthetic oils can be produced with a range of properties and characteristics that are uncommon amongst the conventional mineral oils, some good examples are a wider range of operating temperatures, a better chemical resistance, compatibility with polymeric components and seals. Moreover, their biodegradability has been an influencing factor to the selection of synthetics oils, because of environmental concerns [36].

Synthetic oils are often used as a base fluid for grease, amongst the types of synthetic oils that find application in grease lubrication are: esters, polyglycols, perfluoropolyethers, synthetic hydrocarbons like alkylated aromatics and polyalphaolefins, etc. This last type of synthetic oil can be found, as a base fluid, in one of studied greases, more specifically a polyalphaolefin.

2.4 Grease Thickeners

A significant part of the evolution in grease technology is due to the constant development of new thickeners. Their contribution has been such a key factor that grease manufacturers often classify or name their products according to the type of thickener used.

There are two main groups of thickeners [36]: metal soaps and inorganic compounds. The first being the most used type of thickener. Only the types of thickeners used in the tested greases will be presented here, strictly speaking, Lithium and Lithium-Calcium thickeners (metal soaps) and Polypropylene and Clay-based thickeners (inorganic compounds).

Lithium Soaps

In the first decades of the previous century, there was a lack of variety in grease thickeners, the traditional calcium, aluminium and sodium greases had to fulfill all the demands of grease lubrication.

Triggered by the aircraft industry development, lithium greases took grease lubrication to the next level, and for the first time, mechanical engineers had access to a grease which could be classified as truly multipurpose. Early lithium soaps were made from simple stearic acid, derived principally from beef tallow. Today, almost all lithium greases are based on the castor oil derivative, 12-hydroxy stearic acid.

Lithium greases show an excellent mechanical stability, a acceptable high-temperature performance, up to 120°C, and a good water resistance. This kind of advantages were not verified in any other existing grease at that time, that being said lithium greases experienced a considerable proliferation due to their unique characteristics. The major drawback using the lithium-12-hydroxy stearate grease is its pumpability at low temperatures.

Lithium-Calcium Soaps of stearate derivatives

The earliest greases were made by reacting lime with vegetable oils, or animal fats, before water, to produce a calcium soap. The resulting thickened oil was adequate for simple lubrication like cart wheels or water wheel shafts and bearings.

This type of calcium greases are still used nowadays for less demanding applications and their manufacturing process is very similar to the one used over 100 years ago. When the operating temperature is constantly above 50°C, water evaporation may result in the complete breakdown of consistency in the grease and it will revert to a fluid state.

Calcium grease present a relatively low cost and are used in cool, wet environments in situations such as marine applications, propeller housings and water pumps.

Recently, calcium thickeners are combined with soaps that are not water stabilised, this allows an increase in the operating temperature range, up to 110°C, while not losing the benefits of a traditional calcium grease like excellent adhesion, water resistance and the lower operating temperatures. Anhydrous calcium thickeners are normally based on 12-hydroxy stearic acid, just like their lithium counterparts and the resulting grease offers excellent mechanical stability.

Clay Thickeners

Since the beginning of the 20th century, fine clays were used in grease formulations as a thickener agent, mainly as an attempt to improve high-temperature performance. Nonetheless, the lack of a fibrous matrix structure limits the stability of clay-based greases and the nocuous effects of oxidation can still occur in the base oil at elevated temperatures, oxidation and separation leads to a abrasive clay residue being deposited on the machine surfaces, yet separation rate is very low. Despite these drawbacks, clay is still used in certain applications as a thickener of highly viscous base oils to produce compounds for use in open gear systems.

Polypropylene

Recently proliferated, this polymer thickener is composed by different polypropylene chains and rubber resulting in a polymer compound with an optimized crystalline- amorphous balance. This type of grease offers many advantages over standard multipurpose greases: controlled oil bleed, extended service life, resistance to water and aggressive chemicals, enhanced additive response and a high film thickness in the track (efficient surface separator).

Chapter 3

Experimental Characterization

3.1 Introduction

Lubrication is influenced by the contacting surfaces and the lubricant [37]. The contact between the two surfaces will generate high pressures, therefore elastic deformation of the surfaces will occur. If the surfaces roll, slide or spin relative to each other, the lubricant will be dragged into the converging gap of the contact due to the shear stresses applied on the lubricant by the surfaces. Thus, the generation of lubricant film is dependent of the applied load, surface speed and geometry, elasticity of the surfaces' materials and the viscosity and pressure– viscosity coefficient of the lubricant [25–28; 38; 39].

Other mechanical properties, such as the lubricant yield stress and transverse shear modulus (τ_y , G) are also important to understand lubrication mechanisms, although these last two were not addressed here.

In this chapter, base oils physical properties were measured and evaluated in order to perceive how their properties influence grease lubrication performance, that is film thickness and friction behaviour. Moreover, greases, base oils and thickeners chemical compositions were evaluated through FTIR spectroscopy, in order to understand how thickener and base oil natures affect greases' lubrication.

Roughness measurements of the test specimens were also conducted, in order to comprehend the influence of roughness on the lubricant friction behaviour.

3.2 Tested Greases

Four different lubricating greases were tested. These greases were named according to their chemical compositions (Thickener+Base Oil).

Three of these greases were formulated with different mineral based oil: LiM, CaLiM,ClayM; PPAO was formulated with a synthetic base oil, more specifically a polyalphaolefin (PAO).

All the details concerning the tested greases, their respective base oils and thickeners are shown in the following tables:

	LiM	CaLiM	ClayM	PPAO
Thickener	Lithium	Lithium-Calcium	Organophilic Clay	Polypropylene
Base oil type	Mineral	Mineral	Mineral	Synthetic

Table 3.1: Greases formulation

3.3 Base Oil Properties

Base oil properties were required in this work for the study of film thickness, mainly, but also for the study of the friction behaviour of base oils and greases. Base oil properties were primarily necessary to elaborate film thickness predictions.

Viscosity and bulk density were directly or experimentally measured, yet other properties like the influence of temperature on viscosity or the pressure-viscosity dependence were obtained indirectly by calculus based on experimental values and equations present on the bibliography.

3.3.1 Dynamic Viscosity

Dynamic viscosity was measured by using a *A&D SV10* device. This apparatus is a vibro-viscometer, so it measures viscosity by controlling the amplitude of sensor plates immersed in an oil sample and measuring the electric current to drive the sensor plates.

When the spring plates vibrate with a uniform frequency, the amplitude varies in response to the quantity of the frictional force produced by the viscosity between the sensor plates and the sample. The vibro-viscometer controls the driving electric current to vibrate the spring plates in order to develop uniform amplitude [40].

This viscometer has a temperature sensor and its software has the possibility to plot η *vs.* T curves.

Samples were heated in an oven to the temperature of 105°C (maximum temperature sustained by the sample cups), the samples were removed from the oven and placed in the SV10 device, which measured their viscosity as temperature decreases, from 100°C to room temperature.

Figure 3.2 show the η *vs.* T curves for the four base oils.

Since density was also determined (see following subsection), it is possible to evaluate the value of kinematic viscosity for each temperature using equation (2.3).

Figure 3.3 show the ν *vs.* T curves for the four base oils.

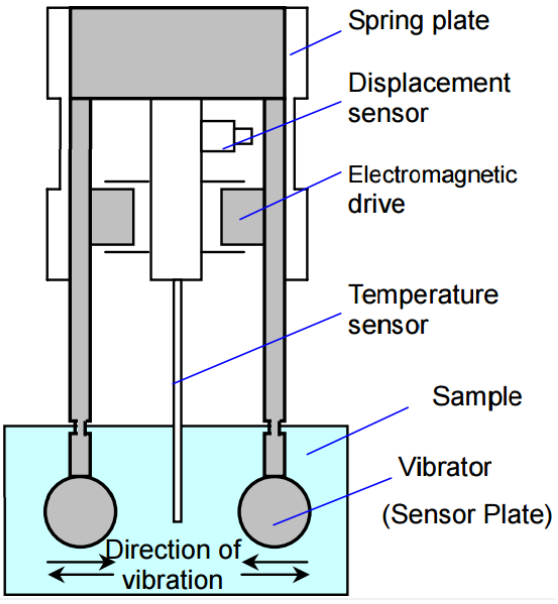
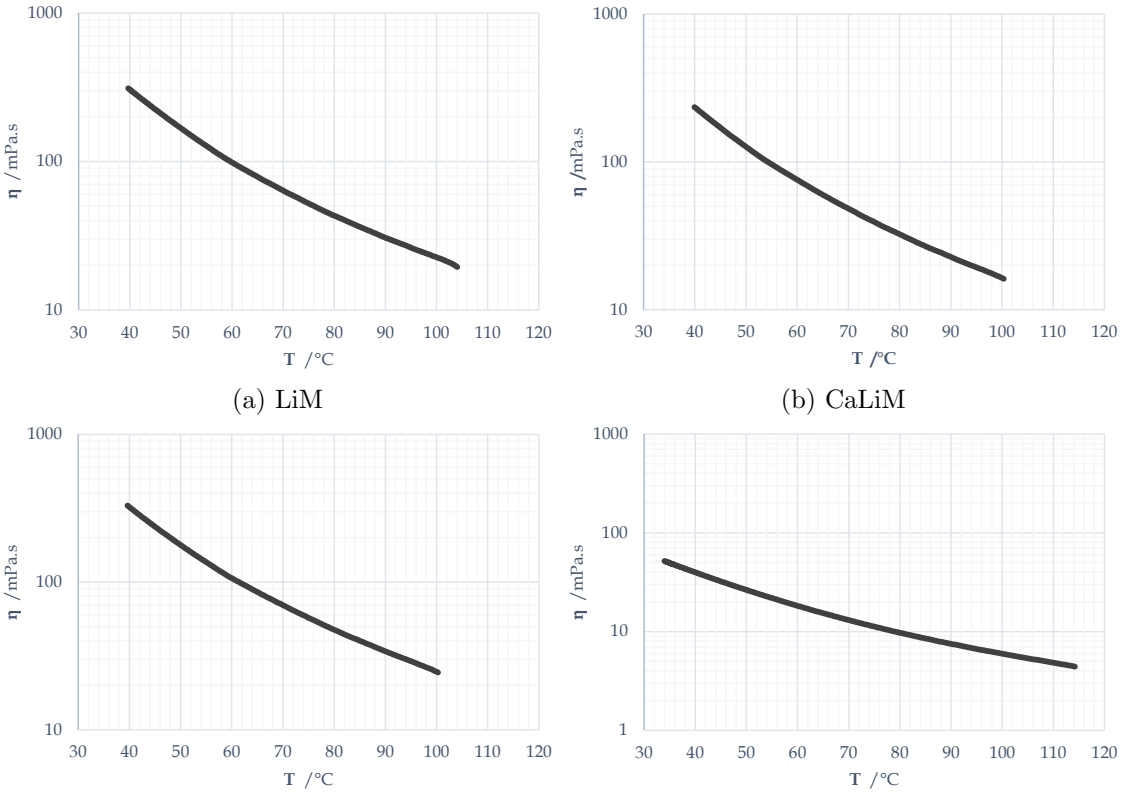


Figure 3.1: SV10 device

As it is visible on Table 3.2, the base oil with higher dynamic viscosity is ClayM, followed by LiM, CaLiM and finally PPAO. Also CaLiM show the lowest *VI* which indicates that its viscosity is strongly temperature dependent, this has an important influence on the grease behaviour at higher temperatures. ClayM and PPAO show the highest *VI* values so their viscosity are less dependent on temperature.



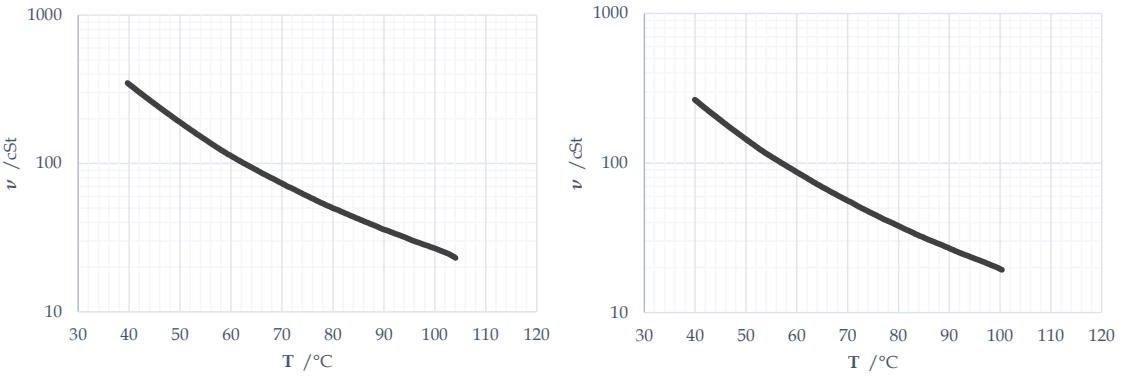
(a) LiM (b) CaLiM

(c) ClayM (d) PPAO

Figure 3.2: Base oils dynamic viscosities (η)

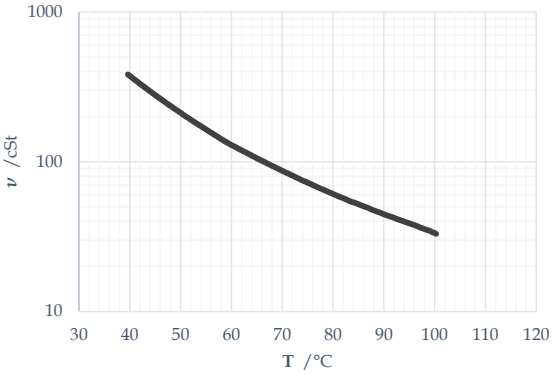
	LiM	CaLiM	ClayM	PPAO
η_{40}	281.19	234.44	323.30	39.77
η_{70}	63.90	48.32	70.07	13.04
η_{100}	11.63	16.34	24.70	5.99

Table 3.2: Base oils dynamic viscosity /mPa.s·

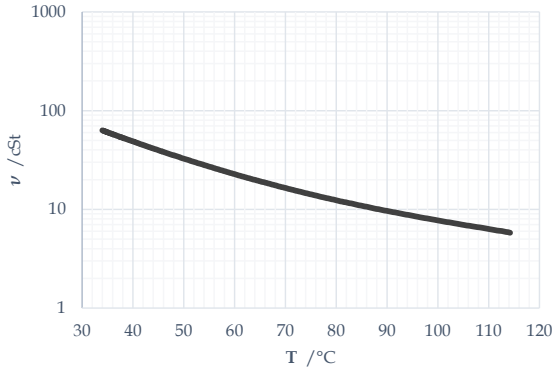


(a) LiM

(b) CaLiM



(c) ClayM



(d) PPAO

Figure 3.3: Base oils kinematic viscosities (ν)

	LiM	CaLiM	ClayM	PPAO
VI	104	83	128	126

Table 3.3: Base oils *VI*

3.3.2 Density

This property was measured using an Anton Paar DMA 35N densimeter, which support a temperature range from 15 up to 40ºC. It is known that temperature influences density, thus it is important to calculate the thermal expansion parameter, shown in equation (2.8).

Two measurements at different temperatures were made to evaluate the thermal expansion coefficient. Table 3.4 shows the calculated thermal expansion coefficients, as well as the density at room temperature, more or less, 22ºC.

	LiM	CaLiM	ClayM	PPAO	Units
$\rho(T_0)$	905.6	901.6	897	828.4	kg/m^3
$\rho(T_1)$	897	890.1	881	818.7	kg/m^3
α_T	-8.3$\times$ 10^{-4}	-9.1$\times$ 10^{-4}	-2.2$\times$ 10^{-3}	-8.7$\times$ 10^{-4}	ºC^{-1}
T_1	33.9	36.4	30.1	35.8	ºC

Table 3.4: Density Measurements (T_0 - room temperature $\simeq$ 22ºC)

3.3.3 Influence of temperature on viscosity

The influence of temperature on the base oils viscosity was also evaluated in this work. Using Vogel's equation [41] it is possible to plot a ν *vs.* T curve with just two viscosity values and their respective temperature. Vogel's equation in shown in equation (3.1). Since temperature-viscosity dependency coefficient β is defined as the derivative of viscosity in relation to temperature, using Vogel's equation this coefficient can be easily calculated through equation (3.2).

$$\nu = K \cdot \exp\left[\frac{b}{(\theta + c)}\right] \tag{3.1}$$

$$\beta = \frac{b}{(\theta + c)^2} \tag{3.2}$$

Hence, the Vogel curve that better fits the experimental measurements were calculated, by adjusting the b, c and K parameters, from which the β value was extracted for each of the testing temperatures. Those values are shown on Table 3.5, for each base oil.

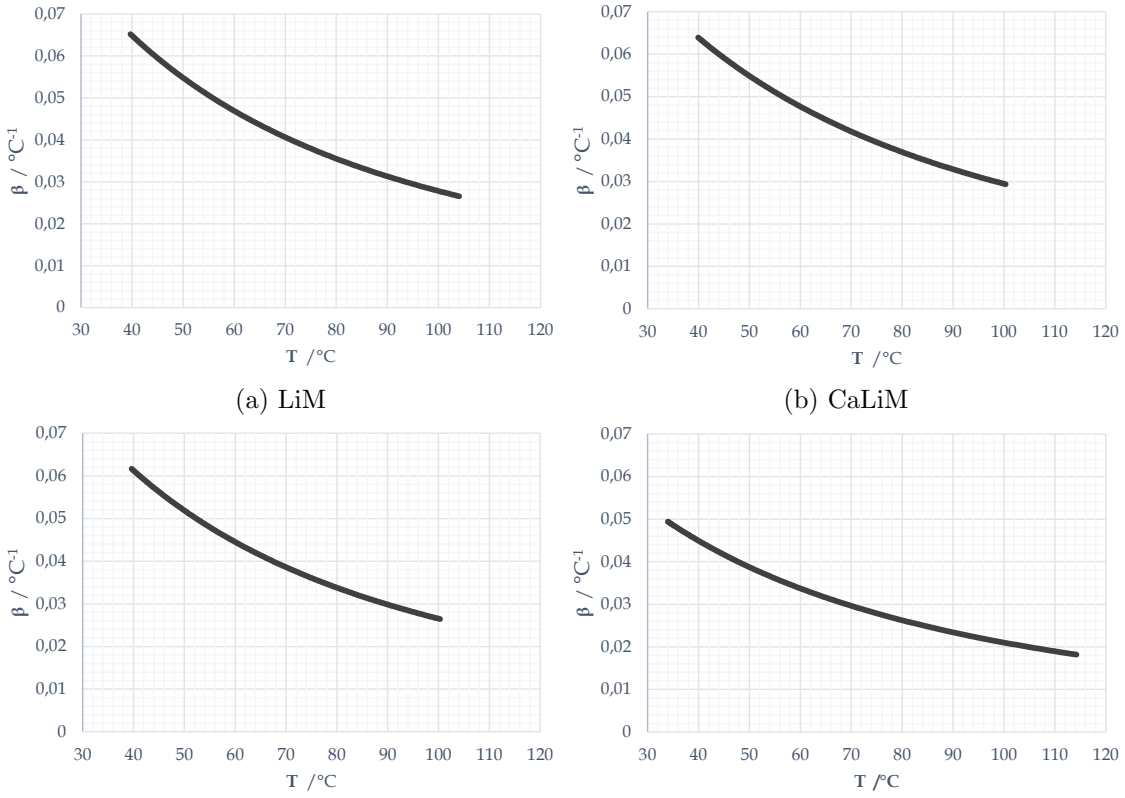
	LiM	CaLiM	ClayM	PPAO
b	840.49	1030.50	815.41	754.8
c	73.86	87.04	73.40	89.61
K	0.213	0.079	0.319	0.144

Table 3.5: Vogel's equation parameters

Figure 3.4 shows the β *vs.* T curves for each one of the base oils. The β values for each one of the testing temperatures are presented on Table 3.6.

	LiM	CaLiM	ClayM	PPAO
β_{40}	6.48×10^{-2}	6.39×10^{-2}	6.13×10^{-2}	4.42×10^{-2}
β_{70}	4.06×10^{-2}	4.18×10^{-2}	3.86×10^{-2}	2.96×10^{-2}
β_{100}	2.78×10^{-2}	2.94×10^{-2}	2.65×10^{-2}	2.10×10^{-2}

Table 3.6: Thermal-viscosity at test temperature $/^{o}C^{-1}$



(a) LiM

(b) CaLiM

(c) ClayM

(d) PPAO

Figure 3.4: Base oils thermal-viscosities (β)

3.3.4 Pressure-viscosity

Pressure-viscosity has a key role on the formation of a lubricant film. This property is very difficult to evaluate since it requires specific and expensive equipment to measure viscosity of fluids at high pressure and, therefore, the pressure-viscosity was estimated using Gold's equation [42]:

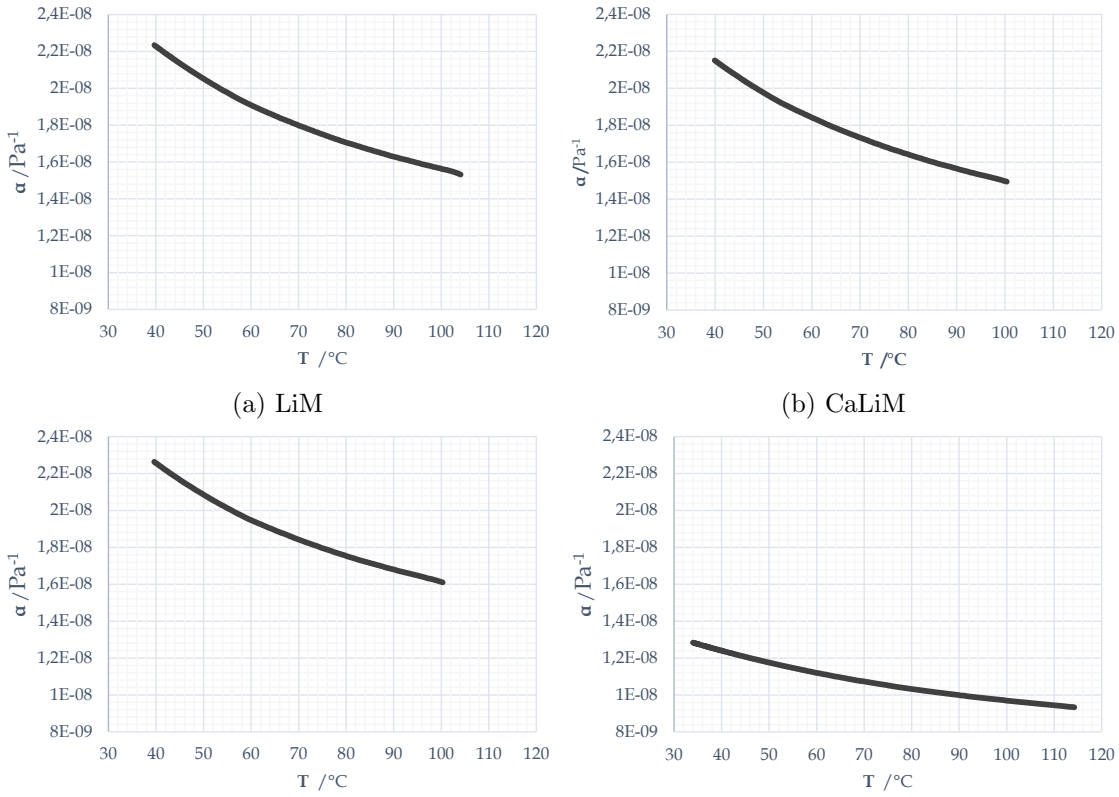
$$\alpha = s \cdot \nu^t \times 10^{-9} \tag{3.3}$$

where s and t are values specific of each oil nature, as shown on Table 3.7.

The pressure-viscosity values calculated for the three testing temperatures are shown on Table 3.8. Moreover, the α *vs.* T curves for each base oil are presented on Figure 3.5.

	Mineral	Esther	PAO
s	9.904	7.382	6.605
t	0.1390	0.1335	0.1360

Table 3.7: Values of s and t used on Gold's equation.



(a) LiM

(b) CaLiM

(c) ClayM

(d) PPAO

Figure 3.5: Base oils pressure-viscosities (α)

	LiM	CaLiM	ClayM	PPAO
α_{40}	22.8	21.5	22.6	12.4
α_{70}	18.0	17.3	18.4	10.7
α_{100}	15.6	15.0	16.1	9.70

Table 3.8: Pressure-viscosity at test temperatures /Pa^{-1} $\times 10^{-9}$

3.4 Oil/Thickener Separation

In order to analyse the chemical properties of the thickener, a method to separate the thickener from oil was applied, a sample of each grease was dissolved in petroleum ether by means of an ultrasonic device, this solution was then filtered through an 8 μm mesh paper filter pumped by a vacuum pump and then kept in the oven at 100°C for 1h, so that any residual ether or fluid evaporates from the filter. By the end of this procedure a sample of thickener was available to be analysed by FTIR spectroscopy.

3.5 Fourier Transform Infrared spectroscopy - FTIR

Fourier Transform Infrared spectroscopy uses infra-red radiation to collect data about the absorptivity or emissivity of a body. FTIR devices emit IR radiation, some of which is absorbed by the sample, and other is transmitted/redirected back to the receptor. This transmitted/redirected spectrum represents the molecular absorption and transmission, creating a molecular fingerprint of the sample. Thus FTIR produces direct information on molecular species of interest, including additives, fluid breakdown products, and external contamination, whereas two distinct molecular structures do not produce the same infrared spectrum. Ergo, all these characteristics make FTIR a very powerful tool, particularly for lubricant analysis.

In this thesis, FTIR technology was used to identify the different thickeners and base oils. The spectra of each grease, base oil and thickener was measured, identifying the peaks which are characteristic for each thickener and base oil natures.

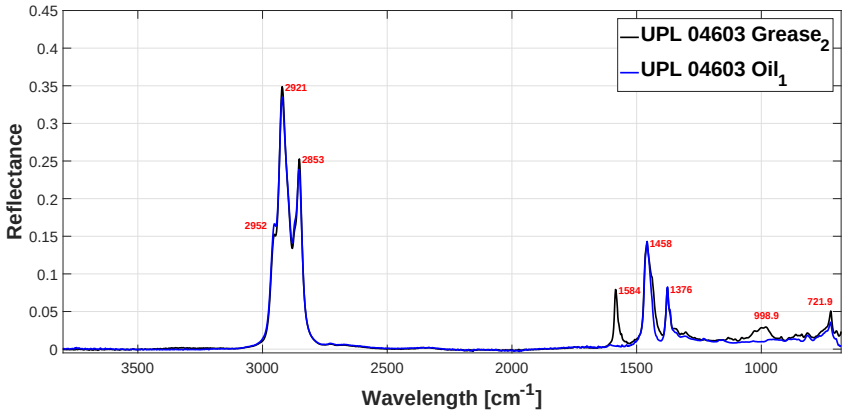
The spectra were obtained using an Agilent® Cary 630 FTIR device, with an Attenuated Total Reectance (ATR) accessory.

Before each measurement, the crystal was cleaned with petroleum ether and 16 scans were performed to assure the crystal was perfectly clean. After that, a background spectrum is obtained and the sample can be applied over the crystal. A total of 64 background scans and 128 sample scans were performed at a resolution of 4 cm^{-1}. All spectra were normalized to the CH_2 peak at approximately 1460 cm^{-1} to prevent disparities between spectra due to different sample thicknesses. To ensure that the results found with FTIR spectroscopy were representative of the sample, each spectrum was measured at least twice. This procedure was carried out for all the tested greases and their corresponding thickeners and base oils. Slight baseline corrections were made, when needed. The spectra were directly taken from the device's software without any kind of curve smoothing and a very good reproducibility was found.

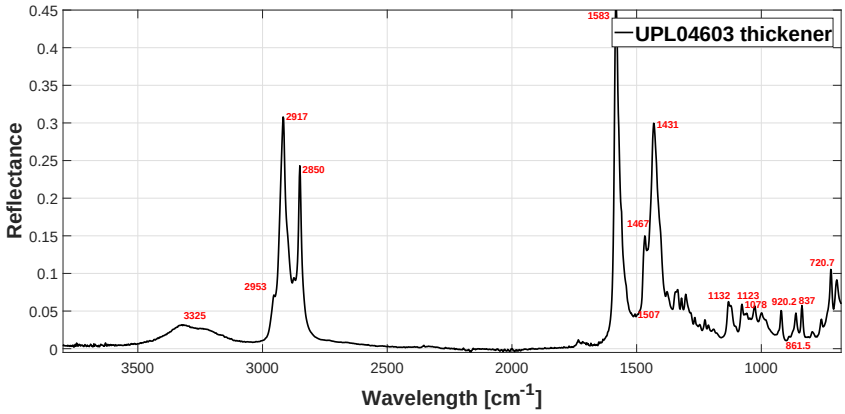
The Figure 3.6 shows the spectrum of LiM, its thickener and base oil. The thickener was obtained using the procedure described in the previous section.

Concerning this grease, base oil and thickener, the prime observations are listed bellow.

- The wide peak around 3300 cm^{-1} is characteristic of the thickener, it also present in the grease though it is not so visible as in the thickener spectrum. This peak is generally present in greases formulated with soap thickeners [43];
- The band which shows a strong reflectance around 3000-2800 cm^{-1} is inherent to all three - grease, base oil and thickener. This peak indicates the existence of an asymmetric C-H stretch of CH_2 and CH_3 molecules, a hydrocarbon structure present in both oil and thickener [44];
- The small peak present in the grease spectrum around 1584 cm^{-1} is typical of the thickener, since it can be found in the thickener spectra with an higher reflectance. This molecular structure, COO, is found in soap thickeners [1];
- The CH_2 deformation solely attributed to the thickener occurs at 1458 cm^{-1}[45];
- The CH_2 and CH_3 groups present in the base oil and the hydrocarbon soap thickener are responsible for the peaks at the following wavelengths [cm^{-1}]: 2952, 2921, 2853,1458,1376,721[44; 45].



(a) Grease and Base oil

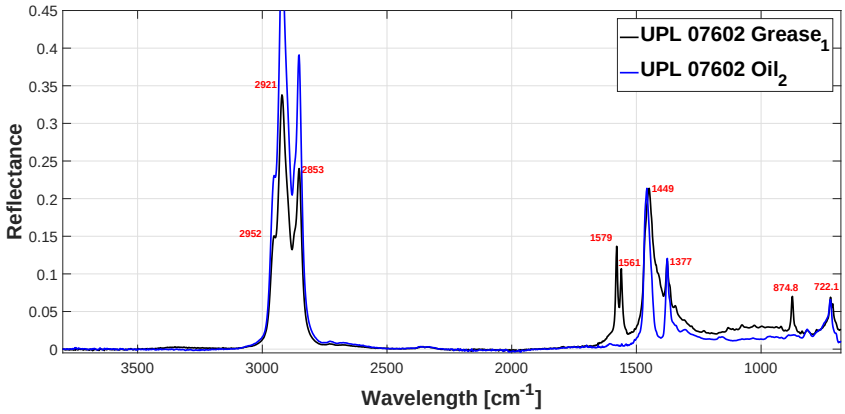


(b) Thickener

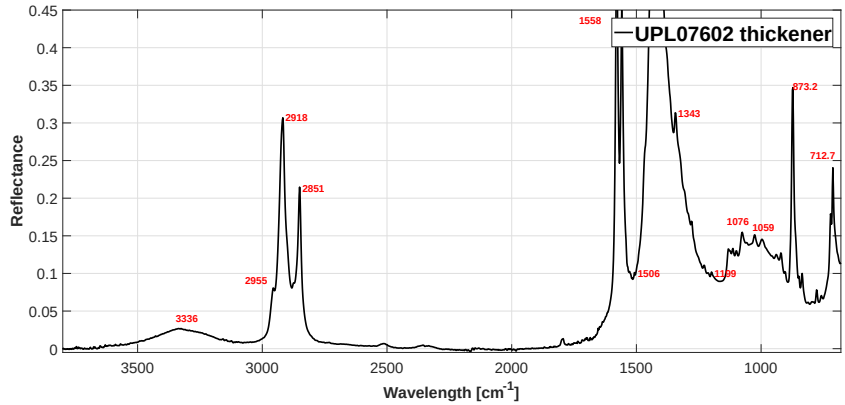
Figure 3.6: LiM FTIR Spectra

Figure 3.7 shows the spectra for the grease CaLiM, its base oil and thickener. This grease is also formulated with a mineral base oil but it is thickened with lithium and calcium, thus its spectrum and LiM spectrum are similar, with a few differences worth reference. The main characteristics of these spectra are:

- The wide band centered around 1430 cm^{-1} is characteristic of calcium and also its sharp bands at 874 and 712 cm^{-1} [46];
- The lithium-typical bands are still present around 1580 and 1560 cm^{-1}, this molecular structure, COO, is found in soap thickeners[1];
- Just like in LiM, the CH_2 and CH_3 groups present in the base oil and the hydrocarbon soap thickener are responsible for the peaks at the following wavelengths [cm^{-1}]: 2952, 2921, 2853,1449,1377,721 [44; 45];
- The broad peak around 3300 cm^{-1} is typical of the thickener, it also present in the grease though it is not so visible as in the thickener spectrum. This broad band is usually present in greases formulated with soap thickeners [43];
- The band which shows a strong reflectance around 3000-2800 cm^{-1} is characteristic of the three spectra. This peak indicates the presence of an asymmetric C-H stretch of CH_2 and CH_3 molecules, a hydrocarbon structure present in both oil and thickener [44].



(a) Grease and Base oil



(b) Thickener

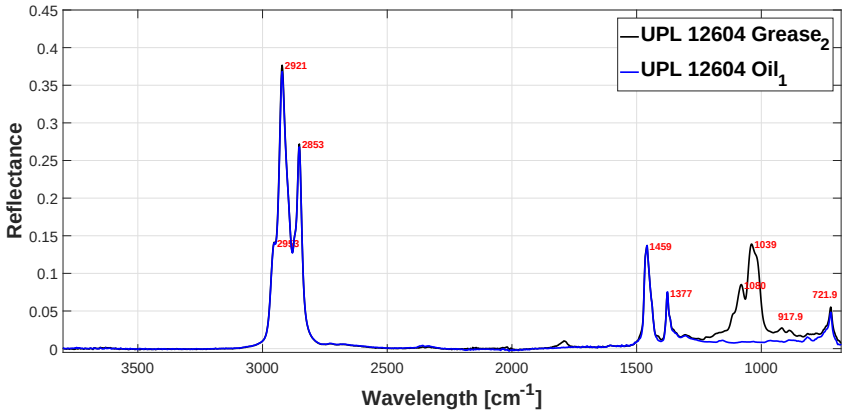
Figure 3.7: CaLiM FTIR Spectra

Just like the two already referred greases, ClayM is also formulated with a mineral base oil and a organophilic clay thickener. The typical peaks of a mineral oil will be visible in the grease and the base oil spectra, peaks concerning the clay thickener will be visible on the thickener and grease spectra. Hence, the major observations regarding this grease, its thickener and base oil are:

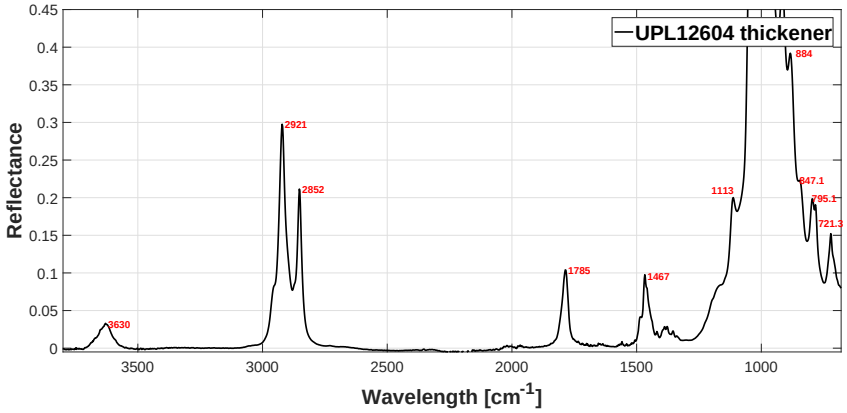
- The wide band around 3630 cm^{-1}, present on the thickener spectrum, indicates a free O-H stretching [47; 48];
- The broad band present in the other thickeners around 3300 cm^{-1} is not seen on the ClayM thickener, since the organophilic clay is not a soap thickener;
- The organic C-H bonds, verified in the CH_2 and CH_3 groups, present in the base oil, thickener and grease are responsible for the peaks at the following wavelengths [cm^{-1}]: 2952, 2921, 2853,1459,721. [44; 45];
- The band which shows a strong reflectance around 3000-2800 cm^{-1} is characteristic of the three spectra. This peak hints the presence of an asymmetric C-H stretch of CH_2 and CH_3 molecules, a hydrocarbon structure present in both oil and thickener [44];
- The broad band with strong reflectance around 1000 cm^{-1}, on the thickener spectra, is a Si–O stretching, typical of a clay [47; 48];

- There is a reflecting peak at 1720 cm⁻1 corresponding to a C=O stretching, which is characteristic of the clay thickener [47].

Figure 3.8 shows the spectra of the ClayM grease, base oil and thickener.



(a) Grease and Base oil

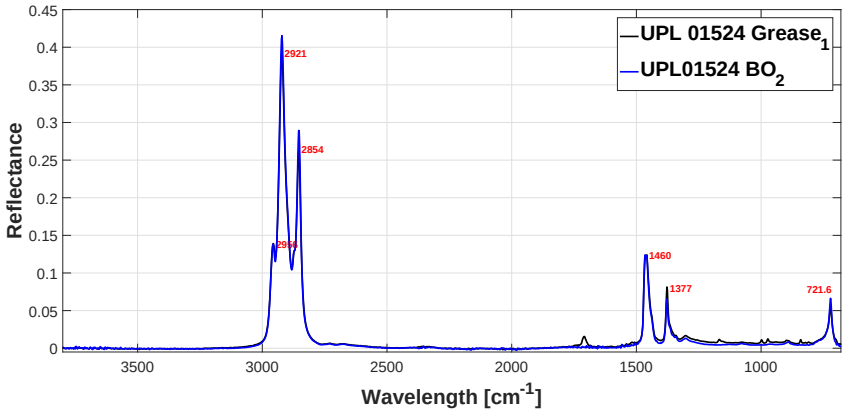


(b) Thickener

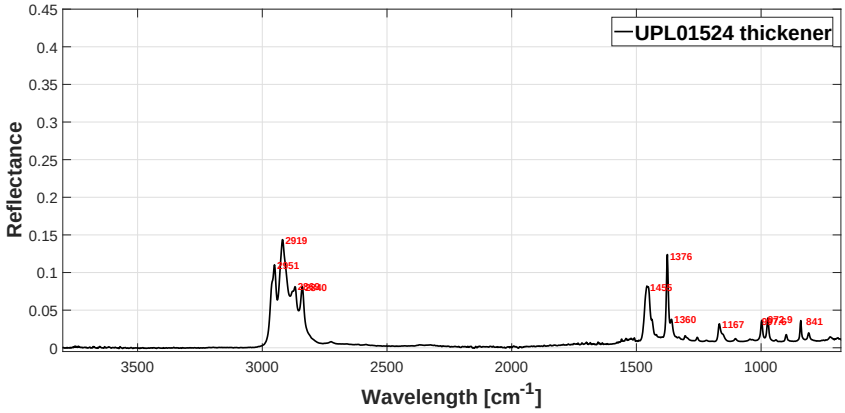
Figure 3.8: ClayM FTIR Spectra

Of all the tested greases, PPAO its the more distinct. This grease is not only formulated with a different type of thickener but also with a different type of base oil, a synthetic oil. PPAO grease, base oil and thickener spectra are shown in Figure 3.9 , the main aspects concerning these spectra are list bellow:

- The existence of isotactic polypropylene in the grease is detected at approximately 1330, 1303, 1167, 998, 973, 940, 841 cm^{-1}. Those peaks are only seen in the grease and thickener spectra. [49];
- The broad band present in the LiM and CaLiM thickeners around 3300 cm^{-1} is not seen on the PP thickener, considering PP is not a soap thickener.
- The band around 3000-2800 cm^{-1} is also present on the base oil, thickener and grease, since the asymmetric C-H stretch of CH_2 and CH_3 molecules are also present, though its reflectance value is not so high on the thickener [44];
- The CH_2 and CH_3 groups present in the base are responsible for the peaks at the following wavelengths [cm^{-1}]: 2956, 2921, 2854,1460,1377,721. [44; 45].



(a) Grease and Base oil



(b) Thickener

Figure 3.9: PPAO FTIR Spectra

3.6 Oil bleeding

When subdued to high pressures or deformations, or when rested for a long time, greases releases oil of their matrix, this oil is currently named bled oil. When bled oil exits the thickener matrix, the grease dries up. One of the objectives of this work is to study the friction behaviour of the dried grease and therefore an oil bleeding procedure had to be adopted.

In spite of the existence of many standard processes for oil bleeding - static bleeding processes such as ASTM D1742 pressure bleed or ASTM D6184 cone bleed, or even dynamic bleeding tests, like ASTM D4425 centrifugal oil bleeding - in this work, a non-standard procedure was implemented, a dynamic bleed procedure, very similar to ASTM D4425. This process was implemented by Gonçalves*et al.* [50].

In this process, a given amount of grease is pressurized by the action of centrifugal forces against an 8 μm paper filter sustained by a metallic grid, on a centrifuge cup, rotating at 1000 rpm and at room temperature (about 22ºC). The amount of grease centrifuged was different for each tested grease, since none of the grease presents the same bleed rate. oils.

In the Figure 3.10, it is presented an elucidative illustration of the oil bleeding apparatus that was used.

The amount of grease to centrifuge was established by a trial and error process:

- Initially, 5 ml of each grease was centrifuged. If the grease reached a dry state, then the sample was collected. This was the case of CaLiM and PPAO;
- If the previous premise was false than the mount of grease to "dry" was reduced.

As a result of this process, the amount dried by cup of LiM was 3 ml and 2 ml for ClayM.

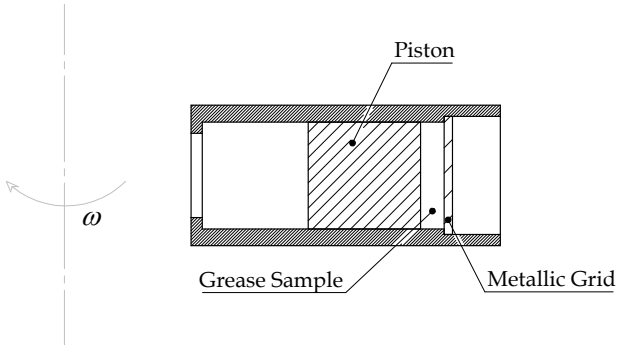


Figure 3.10: Bleeding apparatus

3.7 Surface Roughness Measurements

Surface roughness parameters of the ball and disks used for friction coefficient analysis were measured by a *Bruker's NPFLEX^{TM} 3D Surface Metrology System*. Using white light interferometric technology, this device not only elaborates a full parametrization of surface roughness but also creates three-dimensional images of the surface from which one can evaluate possible surface flaws or imperfections or any incongruity in the shape of the sample.

As stated earlier, this device uses white light interferometry (WLI), which is a non-contact optical profiling system for measuring step heights and surface roughness. This technology would seem to be the ideal technique for roughness measurements, since there's no contact between the measuring device and the surface. Recent developments in both instrumentation and in measurement software for this technique have increased the vertical resolution of these instruments allowing resolutions better than 0.01 nm [51–53]

This technique involves splitting an optical beam from the same source into two separate beams, one of which is passed through or reflected from the object to be measured while the other beam (which serves as reference) ensues a known and invariable optical path, this creates an interference pattern of light and dark fringes and this static fringe image would show differences in distance apart of the reference and sample.

Nevertheless if the objective lens is moved vertically the path length between sample and beam splitter changes and creates a series of moving interference fringes which can be detected by a CCD camera, the objective is to establish the point at which maximum constructive interference occurs (i.e. at which the image is brightest). When this is achieved, the vertical movement of the lens can be meticulously tracked, thus it is possible to create a 3D map of the sample surface [52].

To ensure representativeness of the measurements in relation to the sample several measurements were conducted, a Gaussian type filter was used. For the spheres, eight samples were measured in three randomly chosen positions, the samples area was 480x640 μm^2, with a cutoff of 80 μm. For the three disks, 3 measurements were conducted, with an angle thereabout 120^o between them. The samples section was 2043$\times$2043 μm^2, with a cutoff of 250 μm.

On Table 3.9, the mean values of the roughness parameters measured for each sample are presented.

	Smooth Disk	Intermediate Disk	Rough Disk	Sphere
Ra	0.020	0.147	0.395	0.022
Rq	0.028	0.209	0.573	0.034
$Rz_{(DIN)}$	0.121	0.882	2.370	0.132

Table 3.9: Roughness parameters of each disk and sphere /μm

3.8 Closure

This section was dedicated to the characterization of the tested greases and their base oils and thickeners. These components were chemically identified through FTIR spectroscopy, and their base oil natures or thickener types were entirely discussed.

Base oils physical properties, such as viscosity, and its dependence with pressure and temperature, or density, were also calculated.

The roughness of the test specimens was also studied, in order to better understand its influence on the friction behaviour of greases. All these measurements will be important in the following chapters.

An oil bleeding process was also mentioned. This process was used to extract bled oil from the grease in order to analyse the friction behaviour of dried greases, showing increased thickener content.

All experimental procedures regarding these measurements or procedures were utterly addressed.

Chapter 4

Film Thickness of fully flooded grease lubricated contacts

4.1 Introduction

Understanding the phenomena which govern lubricant film formation is of utmost relevance for the design of machine elements. Most mechanisms involve contact of several elements, whence wear might be produced and where extreme pressures are generated, thus lubricants show up as a valuable mean for both wear and tension attenuation by generating a lubricant film that separates both contact surfaces. Still, these mechanism are not entirely understood, particularly for grease lubrication.

Lately, there has been an increasing interest in studying and comprehending the mechanisms behind grease lubrication, in order to improve grease formulation and optimize machine elements which use grease as lubricant, such as rolling bearings. Several models [2; 3; 6; 54] have been proposed for grease lubrication. The most accepted view states that grease acts like a sponge for the base oil, supplying a controlled amount of oil to the contact which forms a lubricant film. As grease is mechanically worked by the over-rolling action, it releases bled oil to the contact track, maintaining the film. Besides, few authors refer that greases generate a thicker lubricant film than their respective base oil, in fully flooded conditions [10; 55; 56]. This model covers grease lubrication at high speeds but it's not verified at low speeds. Evidence suggests that both the bled oil and thickener lumps cross the EHL contact, and both contribute to the development of lubricant film at low speeds [10; 56].

Cann *et al.* performed several grease film thickness measurements on a ball-on-disk device and concluded that grease film thickness, (h_G), may be treated as the sum of two components: a static and a dynamic film component, ($h_G = h_R + h_{BO}$). The static film is due to a layer adsorbed on the surfaces whether or not there's movement (residual layer - h_R), while the dynamic component is due to the elastohydrodynamic effect, like predicted by the EHL equations (typical oil film - h_{BO}). Residual films of thickness around 6 nm to 80 nm were found, consisting of significant amounts of thickener [4].

Cann [4] also wrote that the thickener will not enter the contact at higher speeds but will be pushed to the sides of the contact, which means that at moderate to high speeds, the film thickness can be calculated using the standard EHL film thickness equations, using the base oil viscosity as the viscosity of the active lubricant in the contact.

More recently, film thickness behaviour at ultra-low speeds was investigated [5] and thickener contribution to film thickness formation at low speeds was addressed again.

4.2 Experimental procedure

EHD2 is a device produced by *PCS Instruments* which measures the lubricant film thickness in the contact formed between a 19.05 mm diameter steel ball and a rotating glass disk, using optical interferometry. The contact is illuminated by a white light source directed down a microscope through a glass disk and then on to the contact. Part of the emitted light is reflected from a Cr layer deposited on the glass disk and part travels through the SiO_2 layer and through the fluid film, being reflected back from the steel ball. Then the two light paths are recombined, forming an interference image which is passed into a spectrometer and high resolution black and white CCD (charge-coupled device) camera. The resulting image is captured by a video frame grabber and analysed by the control software to determine the film thickness. Normally the system measures the wavelength of the light returned from the central plateau of the contact and hence calculates the central film thickness.

The apparatus is presented on Figure 4.1.

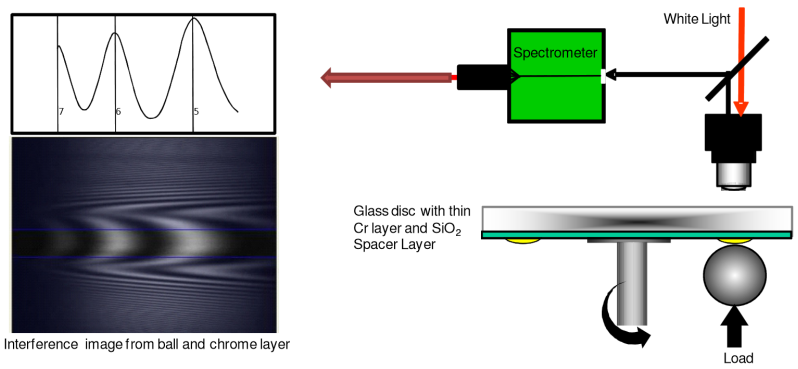


Figure 4.1: EHD2 device

Before each test, both the ball and disk are clean with petroleum ether so that any kind of contaminations that could interfere with the process were removed. The tests started with a heating stage where the lubricant was heated until temperature stabilization is achieved, this stage was 20 minutes long. Afterwards, the disk's spacer layer thickness is measured at the defined track radius, in order to set the zero film thickness and trigger point.

At this point, the procedure diverges according to the lubricant used. For greases, the entrainment speed was ramped up three times, in a speed range from 10 mm/s to 2 m/s; for the base oils, the entrainment speed was ramped up from 10 mm/s to 2 m/s then it was decreased from 2 m/s back to 10 mm/s, this process was repeated once, so four curves were plotted.

A combined curve that contemplates all measurements was elaborated.

For both grease and oil, it was defined a constant Slide-to-Roll ratio and also a constant load. Table 4.1 contains the test conditions used.

Fully flooded conditions were ensured for both oil and grease. To ensure such conditions were accomplished in the grease test, a grease scoop was used to confirm that grease was sent back to the contact track.

	Ball	Disk	Units
Radius - $R_{x,y}$	9.525	∞	mm
Ra	≤ 20	5	nm
Material	AISI 52100	Glass	-
Young Modulus - E	207	64	GPa
Poisson coefficient - ν	0.29	0.20	-
Load - F	50		N
Entrainment speed - U_0	$0.01 \rightarrow 2$		m/s
Slide-to-Roll Ratio - SRR	5		%
Temperature - T	40; 80; 110		ºC
Equivalent Young Modulus - E^*	≈ 51.8		GPa
Maximum Hertzian Pressure - p_0	≈ 0.66		GPa
Hertzian half-width - a	≈ 190.7		μm

Table 4.1: Ball-on-disk test conditions for film thickness measurements

4.3 Base oil film thickness

4.3.1 Introduction

In the interest of comprehending greases lubricant film formation, a base oil film thickness analysis must be performed, therefore both experimental and theoretical analysis were available.

Several equations can predict oil film thickness [57–59], which only differ in the method used to relate viscosity and density with temperature and pressure. One of the most popular equations that expresses pressure and temperature influence on viscosity is the Roelands law. Evidence says that this equation might not be suitable for high pressure-viscosity values [60]. Notwithstanding, Hamrock *et al.* equation was deducted using Roelands law [33] and considering the lubricant to be compressible [61].

In this work, the Hamrock and Dowson equation, equation (4.1), was used to draft film thickness prediction, a thermal correction coefficient ϕ_T was included to take into consideration lubricant shear heating at the contact inlet [62]. Equation (4.2) and equation (4.3) present the parameters ϕ_T and L, correspondingly.

$$h_{0c} = \phi_T \cdot 1.165 \cdot \frac{\left[\eta_0 \left(U_1 + U_2\right)\right]^{0.67} \cdot \alpha^{0.53} \cdot R_x^{0.464}}{F_n^{0.067} \cdot E^{*0.073}} \tag{4.1}$$

$$\phi_T = \left[1 + 0.1\left(1 + 14.8 V_e^{0.83}\right) L^{0.63}\right]^{-1} \tag{4.2}$$

$$L = \frac{\beta \cdot \eta_0 (U_1 + U_2)^2}{k} \tag{4.3}$$

In spite of its accuracy for Newtonian fluids, Hamrock's equation largely overestimates film thicknesses for non-Newtonian fluids as shear-thinning effects are not included [62], for this type of fluid shear deformation influence on viscosity must be taken into account.

4.3.2 Specific film thickness

An additional parameter involving film thickness was used, in the upcoming section, that is worthy to refer forthwith. The specific film thickness, Λ [63], is a criterion often used to evaluate the lubrication regimen a contact is operating on. Specific film thickness relates the lubricant film thickness and the surfaces roughness, low Λ values mean that a boundary lubrication is running on the contact, while an high specific film thickness means that the contact is under full film lubrication.

$$\Lambda = \frac{h_{0c}}{\sigma} \tag{4.4}$$

$$\sigma = \sqrt{\sigma_1^2 + \sigma_2^2} \tag{4.5}$$

Table 4.2 shows the characteristic Λ values for each lubrication regime, for typical machine elements. Withal, Figure 4.2 shows the correlation between friction and specific film thickness, and also typical values for COF under the multiple lubrication conditions.

	Bearings	Gears
Full Film	$\Lambda \geqslant 3,0$	$\Lambda \geqslant 2,0$
Mixed Film	$1,0 < \Lambda < 3,0$	$0,7 < \Lambda < 2,0$
Boundary Film	$\Lambda \leqslant 1,0$	$\Lambda \leqslant 0,7$

Table 4.2: Characteristic Λ values for each lubrication regime

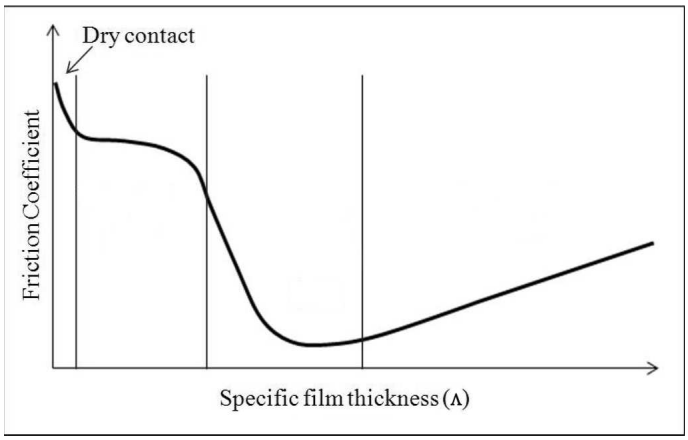


Figure 4.2: Stribeck curve.

4.3.3 Results

As referred above, four base oils were tested, three of these are mineral oils and the remaining is a synthetic oil, a polyalphaolefin. The tests were performed according to the procedure previously discussed , under three operating temperatures: 40, 80 and 110°C.

Figure 4.3 presents the experimental results obtained for these base oils, from which the following conclusions might be taken:

- For 40°C, the base oil which generated a thicker lubricant film was ClayM base oil, followed by CaLiM, LiM and PPAO, respectively. PPAO form a very thin film when compared with the remaining base oils;
- For 80°C, the base oil that presented a higher film thickness was ClayM base oil, followed by LiM , CaLiM and, finally, PPAO, respectively. The relative difference between the film thickness generated by the mineral oils and the synthetic one has been reduced;
- For 110°C, ClayM was, once again, the base oil which presented the highest film thickness, followed by LiM, CaLiM and at last PPAO. The difference between PPAO and the mineral oils film thickness has diminished when compared to the previous temperature;

Since testing conditions were the same, it is expectable that the differential parameter in the lubricant film formation will be the lubricant's viscosity and pressure-viscosity. ClayM presents the highest dynamic viscosity of the four base oils on test, it also presents a high pressure-viscosity coefficient, therefore it presents the highest film thickness. The dynamic viscosity values are shown on Table 3.2 and the pressure-viscosity values are presented on Table 3.8.

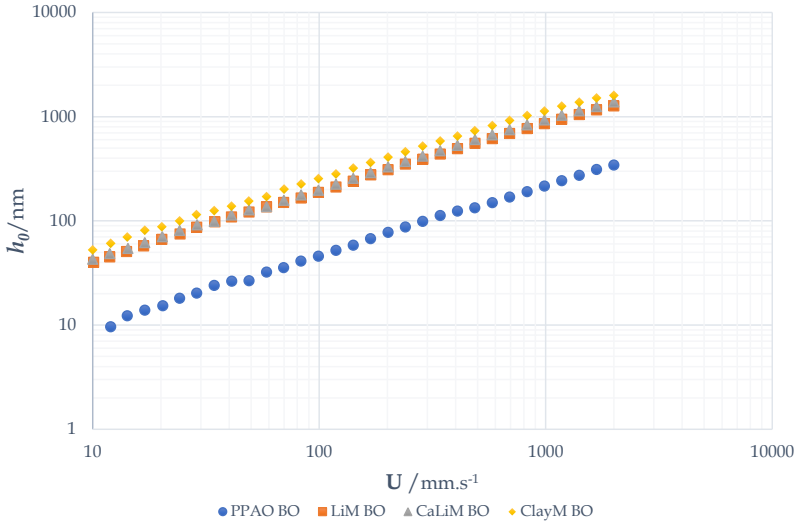
Figure 4.4 shows the comparison between the experimental measurements and the Hamrock and Dowson solution. For the four base oils, the film thickness measurements were corroborated by the results obtained using the Hamrock and Dowson equation, although some slight deviations might be observed for some base oils at certain operating temperatures. Thus an optimization of the pressure-viscosity coefficient was performed.

Van Leeuwen [64] and Gonçalves [65] used film thickness measurements to inversely calculate pressure viscosity, which seems to be the suitable way to determine α when high pressure viscosity measurements are not available. Yet, this method was disapproved by Krupka *et al.* [66] and Kudish *et al.* [67] who showed that pressure-viscosity values obtained with this process could differ depending on the geometry used for the film thickness measurements.

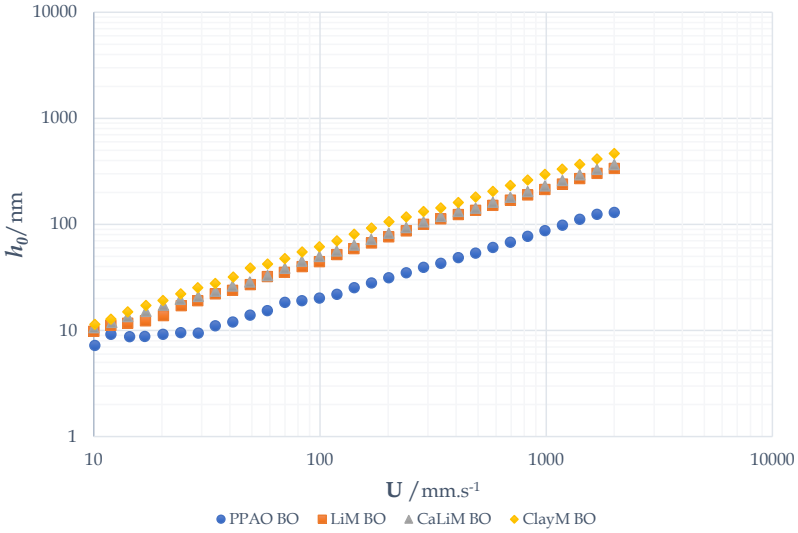
Nevertheless, a similar approach to Gonçalves' method was chosen, and pressure-viscosity was optimized to match the experimentally measured and the analytically calculated film thicknesses of each base oils. The optimization procedure was based on equation (4.6).

$$\frac{h_{exp}}{h_{H\&D}} \propto \left(\frac{\alpha_{opt}}{\alpha_{Gold}}\right)^{0.53} \tag{4.6}$$

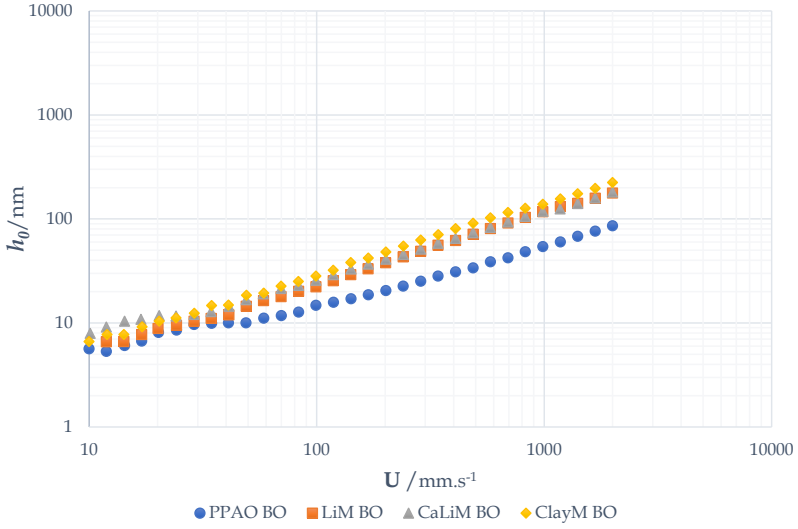
This optimized α was obtained for each measurement point, the mean value was taken as the final solution. Table 4.3 show the optimized pressure-viscosity for each base oil and for each operating temperature.



(a) T = 40°C

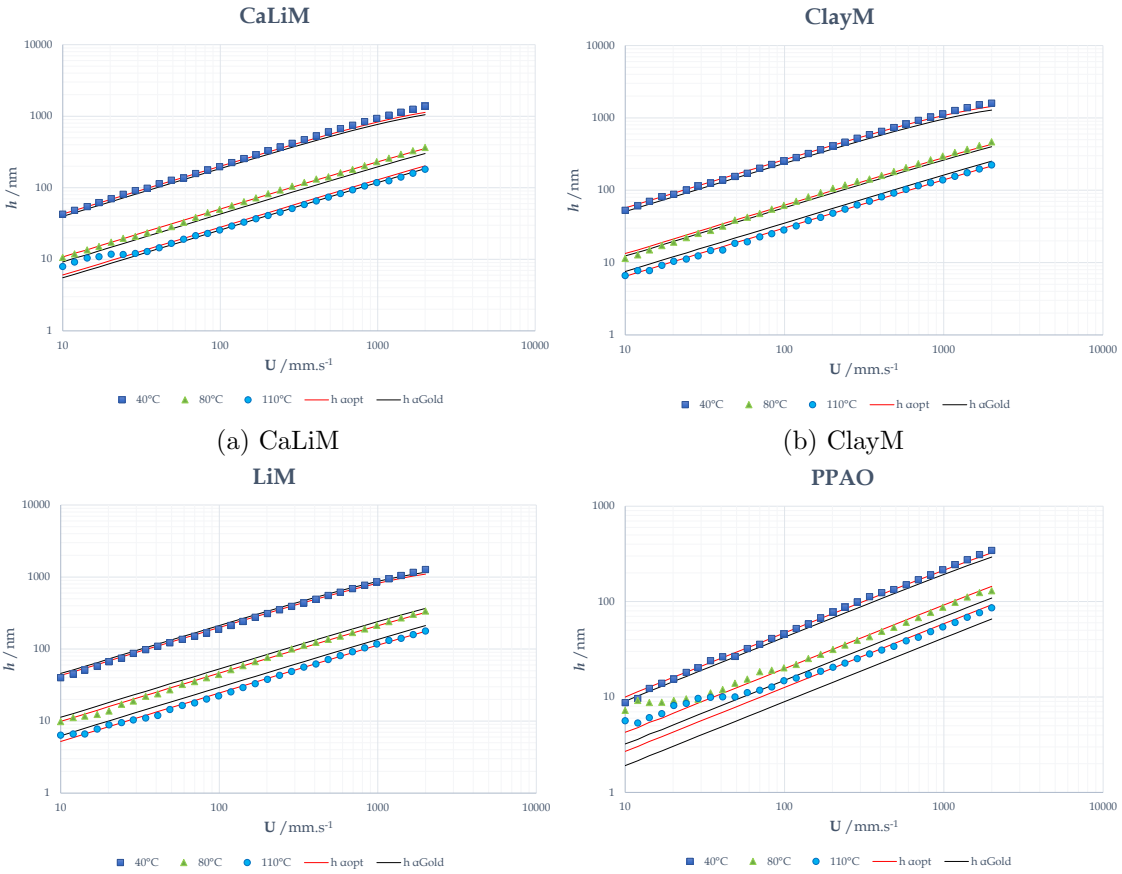


(b) T = 80°C



(c) T = 110°C

Figure 4.3: Base oils film thickness measurements



(a) CaLiM (b) ClayM

(c) LiM (d) PPAO

Figure 4.4: Base oils film thickness measurements

	T	LiM	CaLiM	ClayM	PPAO
α_{opt}	40°C	19.7	24.8	28.1	15.0
	80°C	13.3	22.2	20.3	17.6
	110°C	10.9	17.7	12.1	18.0

Table 4.3: Optimized Pressure-viscosities /Pa^{-1} $\times 10^{-9}$

4.4 Grease film thickness

4.4.1 Introduction

EHL theory is well defined for fully flooded oil lubricated contacts [57–59], the same doesn't apply to grease lubricated contacts since their viscosity is dependent of shear deformation. Yet, there's some studies which suggest how grease lubrication mechanisms operate. It was found that thickener passes through rolling EHL contacts and contribute to film formation [10; 11]; other studies suggest that film thickness depends on the thickener structure [55], while others state that base oil viscosity also plays a key role in lubrication [2] and it is consensual that grease form an higher film thickness than their respective base oils [12; 68].

As one can see a lot has been developed on the matters of grease lubrication in the past few years.

At this moment, it is understood that grease may indeed lubricate the contact during the initial phase of operation but that it will also act as a reservoir, releasing lubricant either by bleeding, shear, or shear-induced bleeding [69]. The result is that the active lubricant will ultimately have a different rheology than bulk grease. Unfortunately, there is no consensus in the scientific literature regarding the rheological properties of the active lubricant.

Regarding the film thickness of lubricating greases, the initial fully flooded film thickness, before starvation occurs, has been modelled by some authors assuming the initial thickness to be proportional to the thickener concentration. Hurley [70] developed an empirical formula regarding this matter. Nevertheless other authors believe that grease rheological properties should be used as input variables, developing a model for fully flooded grease lubricated contacts [54; 71]. The Herschel-Bulkley and Bingham rheological models are the most commonly used non-Newtonian models.

Yang and Qian [7] using the Bingham rheology model, demonstrated that the conventional EHL theory could be used for grease film thickness calculation if the grease's viscosity at high shear rates was used instead of the base oil viscosity. Other researchers developed simple models for film predictions of grease under fully flooded conditions.

4.4.2 Results

Four greases with different base oils and thickeners were tested, at three operating temperatures: 40°C, 80°C and 110°C. It is observable that grease lubrication clearly shows a distinct behaviour, comparing to oil lubrication. Grease clearly shows two regions: a plateau region, where film thickness is approximately constant (depending on grease formulation it can decrease when the entrainment speed raises or it can be constant) and an EHL region, where the grease shows an "oil-like" behaviour. In this work, the film thickness at which the EHL starts is called plateau film thickness.

Figure 4.5 shows the results obtained in these film thickness measurements, from which the ensuing conclusions were made:

- At 40°C, greases composed by mineral base oils show a elastohydrodynamic behaviour, the same doesn't apply for PPAO, whose film thickness increases as the entrainment speed decreases, which is typical in grease lubrication when a low specific film thickness is verified. Some authors believe that this almost constant film

thickness is formed when lumps of thickener cross the contact [10; 11]. PPAO has a plateau film thickness of 132,17 nm, this regime ends when entrainment speed reaches 0.141 m/s. On the EHL phase, ClayM and CaLiM show the highest film thicknesses, followed by LiM and PPAO;

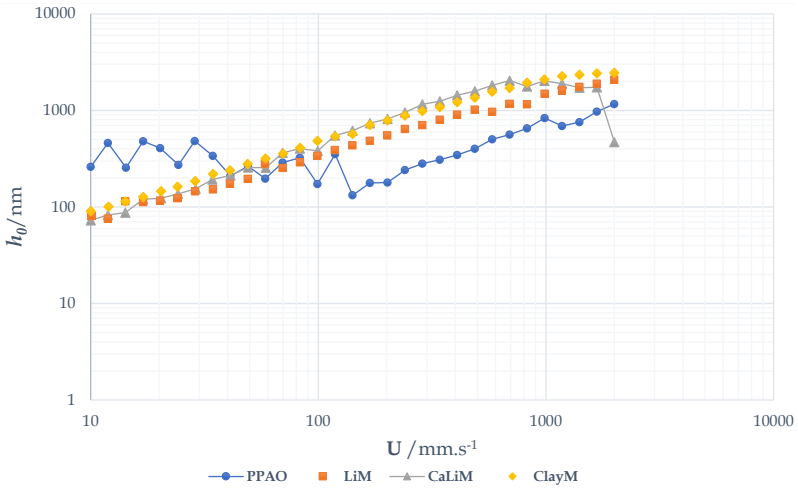
- At 80°C, PPAO shows the same behaviour previously described at low speeds and CaLiM shows a film thickness plateau, also at low speeds. PPAO shows a film thickness of 138.10 nm, finishing when entrainment speed reaches 0.693 m/s. CaLiM has a plateau film thickness of 81.06 nm, this plateau ceases when entrainment speed reaches 0.05 m/s. In the EHL region, CaLiM shows a thicker lubricant film, followed by ClayM, LiM and PPAO, respectively;
- At 110°C, only ClayM does not show a "plateau" region. PPAO has the higher mean film thickness at the low speed region, 123.25 nm, ceasing at 0.486 m/s, followed up by CaLiM which present an average plateau film thickness of 89.05 nm, ending when entrainment speed reaches 0.2 m/s, and at last LiM with a plateau film thickness of 29.85 nm, whose plateau region ends ate 0.06 m/s. For the linear zone, CaLiM shows the higher film thickness, followed by ClayM, LiM and PPAO.

Table 4.4 shows the transition speed as well as the plateau film thickness for each grease. From the analysis of these values, it is observable that the plateau film thickness is approximately constant for each grease formulation and independent of the operating conditions. Since, greases show an EHL behaviour after the plateau film thickness is reached the Hamrock and Dowson equation can be used [61] to obtain the transitional entrainment speed for each test:

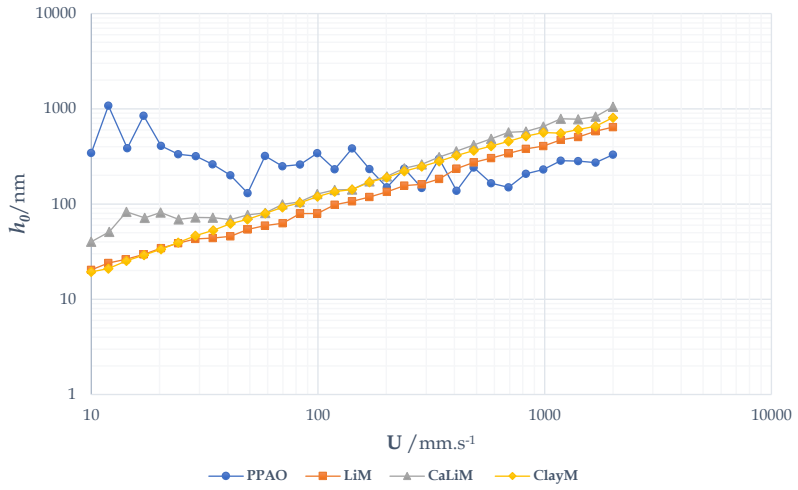
$$U_{tr} = \left[\frac{h_{pl} \cdot F_n^{0,067} \cdot E^{*0,073}}{\phi_T \cdot 1.165 \cdot \eta_0^{0.67} \cdot \alpha^{0.53} \cdot R_x^{0.464}} \right]^{0.67} \tag{4.7}$$

T		LiM	CaLiM	ClayM	PPAO	Units
40°C	h_{pl}	-	-	-	132.17	nm
	U_{tr}	-	-	-	0.141	m/s
80°C	h_{pl}	-	81.06	-	138.10	nm
	U_{tr}	-	0.05	-	0.693	m/s
110°C	h_{pl}	29.85	89.05	-	123.25	nm
	U_{tr}	0.06	0.20	-	0.486	m/s

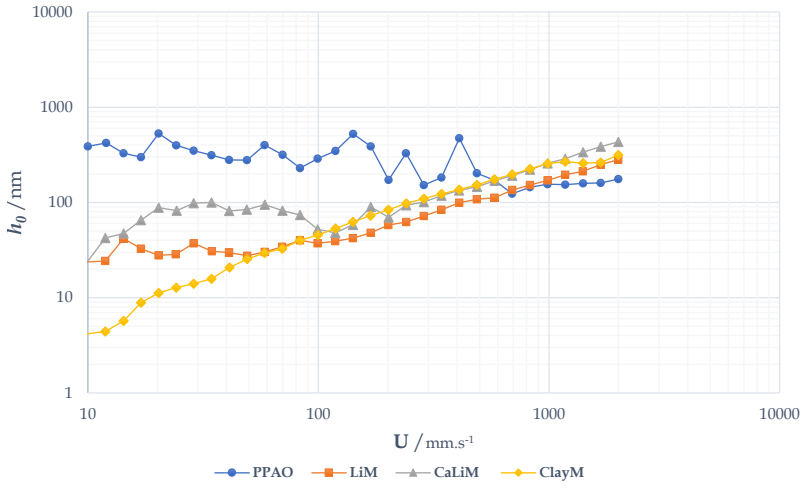
Table 4.4: Plateau thickness and transition speed for each grease



(a) T = 40°C



(b) T = 80°C



(c) T = 110°C

Figure 4.5: Greases film thickness measurements

A comparison between grease and respective base oil film thicknesses was also conducted. This comparison was only executed in the EHL region for greases.

Table 4.5 shows the ratio between grease film thickness and its respective base oil film thickness for each operating temperature.

Greases tend to create a thicker lubricant film than their respective base oil, on fully flooded conditions. The thickener that promoted a greater film thickness increase was the polypropylene thickener. The organophilic clay and the lithium thickener were the thickeners which less contributed to an increase of the film thickness when compared to their base oils.

T	LiM	CaLiM	ClayM	PPAO
40°C	1.748	2.208	1.733	2.944
80°C	1.953	2.638	1.825	2.697
110°C	1.502	2.193	1.645	2.726

Table 4.5: Ratio between grease and base oil film thicknesses $\left(\frac{h_G}{h_{BO}}\right)$

4.5 Closure

Four greases with different formulations, i.e. different base oils and thickeners, were tested on ball-on-disk device, under different operating conditions, in order to better understand what influence the thickener and oil type might have on film thickness formation.

Experimental results show that the thickener has an active role in the generation of a lubricant film, specially at low speeds, as thickener lumps enter the contact increasing film thickness as entrainment speed decreases [5; 72] and reaching a constant value for the Calcium-Lithium grease. At low speeds, the film thickness depends upon the grease formulation, particularly on the thickener type (more specifically on its morphology), since all four greases presented very different plateaus. A high film thickness scatter was observed in this zone, which might be explained by an inconsistency on the thickeners lumps size (larger lumps may enter the contact forming a thicker lubricant film) and these thickener lumps might not enter the contact at all, for lower film thickness values. Referring to each grease in detail:

- PPAO shows a lower film thickness in the EHL region when compared to the other greases, what is a result of the lower viscosity presented by its base oil, however it shows a higher film thickness at lower speeds, which is due to the nature and morphology of its thickener. PPAO also showed little film thickness dependence with temperature, when compared with other greases.
- ClayM does not present a "plateau" zone in the tested conditions, but it presents very high film thickness in the EHL zone. It shows a oil-like behaviour;
- LiM shows a low film thickness at lower entrainment speeds, its plateau zone was only triggered at very high temperatures, also it shows a high film thickness on the EHL region;
- CaLiM shows a low plateau film thickness that can be triggered at low speeds and high temperatures, more than that it shows a high film thickness at the EHL zone. This grease showed great temperature stability for the different test conditions.

More general assumptions might be assessed from this experimental results:

- At low entrainment speeds, the thickener type and morphology seems to govern grease lubricant. Other authors have reported that different thickener morphologies and sizes influence the film thickness in this region [72; 73];
- Plateau film thicknesses seem to be a characteristic of each grease formulation, it might be related to the thickener's dimensions, since there is not a great scattering in the mean plateau film thickness values for the different test conditions;
- Transition entrainment speed changes according to the operating conditions, since it is dependent of the plateau film thickness which is constant, they are related by equation (4.7);
- When the plateau film thickness is reached, the plateau region ceases and the EHL region is achieved. Base oil seems to govern grease lubrication in this region, since the same slope is found on the grease and base oil curves.

Chapter 5

Friction behaviour of fully flooded grease lubricated contacts

5.1 Introduction

Friction behaviour is characterized by the low shear viscosity, the limiting elastic shear modulus and the limiting shear stress the lubricant can endure [74; 75]. For oil lubrication, friction behaviour is well documented [74–76] and two different approaches are taken: one regards experimental data and high pressure rheological measurements [77; 78], while the other adjusts the traction parameters in order to obtain the best numerical fit using traction measurements [79].

When the subject is grease lubrication there's no unanimous consensus regarding the rheological properties of the lubricant film [8; 9] and therefore, its traction behaviour. A great part of experimental measurements on grease lubricated contacts aim to understand lubricant film generation and grease properties, yet only a few works focus on grease traction behaviour.

The understanding of the traction properties of lubricating greases is a key factor on grease formulation and development. Furthermore, the measurement of the coefficient of friction, under distinct testing conditions, leads to a improved understanding of certain aspects that concern grease formulation and performance.

5.2 Introductory notes on Stribeck Curves

In a typical Stribeck curve, the coefficient of friction (COF) is plotted against the Hersey parameter [80], $S = U_0 \cdot \eta \cdot F^{-1}$, where U_0 is the entrainment speed, η the lubricant's dynamic viscosity at the operating temperature and F is the load applied on the contact.

Brandão *et al.* suggested a modified Hersey parameter [76], S_P, in the interest of an improved representation of COF under different operating conditions. This modified and dimensionless parameter grants the possibility to compare lubricants, by normalizing the curves' abscissa, as long as the same geometry, roughness and material are used. S_P parameter considers the lubricant properties, η and α, but also external conditions, F and U_0. This parameter is shown in equation (5.1).

$$S_P = \frac{\eta \cdot U_0 \cdot \alpha^{0.5}}{F^{0.5}} \tag{5.1}$$

In grease lubrication, the greases' properties are generally attributed to the properties of their respective base oils. That is also the case of this work, where the η and α

values of the base oils were also used to represent the S_P parameters of the greases. As aforementioned, both Hersey parameters do not contemplate the geometry, roughness and material effect. Since a very important part of this work is the analysis of roughness influence on the lubricants friction behaviour, roughness must be addressed in order to be able to compare the *COF* of a certain lubricant when measured using surfaces of different roughness.

Plotting friction curves against the specific film thickness requires the calculation of the lubricant's film thickness at the testing conditions. Thus, another parameter was developed in order to address roughness and geometry. The modified Hersey parameter proposed by Brandão was readjusted in order to take into account such variables. This modified parameter, S_{PR}, is presented on equation (5.2).

$$S_{PR} = \frac{\eta \cdot U_0 \cdot \alpha^{0.5}}{F^{0.5}} \cdot \frac{R_x}{Rq} \tag{5.2}$$

where R_x is the equivalent curvature in the direction of rolling, and Rq is the composed roughness of the mating surfaces, $Rq = \sqrt{Rq_1^2 + Rq_2^2}$.

In this work, S_{PR} was not tested in terms of varying geometry, additional measurements will be necessary in the future in order to evaluate whether this effect is properly addressed in this parameter or not.

5.3 Measurement Procedure

EHD2, by *PCS Intruments*, already mentioned in the previous section, allows the measurement of friction coefficients of a lubricant sample, on a ball-on-disk or a roller-on-disc configurations, under multiple conditions by adjusting several parameters like temperature, entrainment speed, load or the Slide-to-Roll Ratio (*SRR*).

In this work, the ball-on-disk configuration was used and the tests were conducted at constant temperature, *SRR* and load, while varying the entrainment speed, from 0.01 m/s to 2 m/s.

The procedure started with a controlled heating step, where the lubricant was conditioned to the test temperature (40, 80 or 110 °C). For the base oils, the entrainment speed was ramped up and later ramped down in the speed range mentioned above, using logarithmic intervals; for greases, the entrainment speed was ramped twice in the same speed range, also using logarithmic intervals. A grease scoop was used in order to force grease back in the contact track. The tests were performed on three disks with distinct surface roughness. The roughness was evaluated using *Bruker's NPFLEX^{TM} 3D Surface Metrology System*, as stated on Chapter 3 . All details concerning the used materials are shown on Table 5.1. Aside from that, all testing conditions are displayed on Table 5.2.

	Ball	Smooth Disk	Intermediate Disk	Rough Disk	Units
Radius - $R_{x,y}$	9.525	∞	∞	∞	mm
Ra	≤ 20	2	100	500	nm
Material			AISI 52100		-
Young Modulus - E			207		GPa
Poisson coefficient - ν			0.29		-

Table 5.1: Test specimens details

Load - F	50 N
Entrainment speed - U_0	0,01 $\rightarrow$ 2 m/s
Slide-to-Roll Ratio - SRR	5 %
Temperature - T	40; 80; 110 ^{o}C
Equivalent Young Modulus - E^*	$\approx$ 113 GPa
Maximum Hertzian Pressure - p_0	$\approx$ 1.09 GPa
Hertzian half-width - a	$\approx$ 146.8 μm

Table 5.2: Test conditions

5.4 Oil Lubricated Contacts - Results

In order to better understand the friction coefficient results it is necessary to know the lubrication regime along the test. The film thickness measurements were carried out in a steel-glass contact and therefore, the equivalent Young modulus has to be corrected in order to use these values in the upcoming section, to present the film thickness curves of steel-steel contact. This correction was performed using Hamrock and Dowson equation (4.1). Assuming that the surface roughness does not affect the film build-up, the surface materials are the only difference between the film thickness tests and the *COF* tests [72]. Thus, it is possible to correct the measured film thickness in order to better represent the film thickness of the steel-steel *COF* tests. So the following proportionality is verifiable:

$$\frac{h_{ss}}{h_{sg}} = \left(\frac{E^*_{sg}}{E^*_{ss}}\right)^{0.073} \tag{5.3}$$

where h_{sg} is the measured film thickness (steel-glass contact), h_{ss} is the film thickness for a steel-steel contact, E^*_{sg} and E^*_{ss} is the equivalent Young modulus for a steel-glass contact and steel-steel contact, respectively.

Since the three disks are made from the same material as the sphere, AISI 52100, the equivalent Young modulus is $E^* = 113$ GPa . Therefore, the proportionality between the measured film thickness and the steel-steel film thickness is:

$$\frac{h_{ss}}{h_{sg}} \approx 0.9442 \tag{5.4}$$

The specific film thickness was then calculated but now considering the composite roughness of the surfaces of the steel ball and of each one of the disks. The Λ *vs.* U_0(m/s) curves are presented on Figures 5.1 to 5.3, for each base oil and for the different operating temperatures. The transition Λ values were $\Lambda_1 = 3.0$, for full film-mixed film transition, and $\Lambda_0 = 1.0$, for the mixed film-boundary film transition, present on Table 4.2

Analysing the smooth disk curves, Figure 5.1, one can conclude the following aspects:

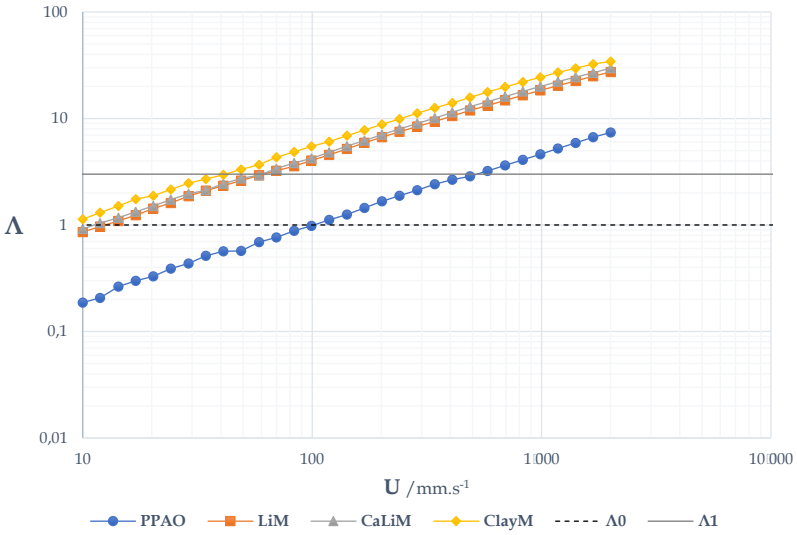
- For 40°C, the mineral base oils are under mixed film lubrication, at low entrainment speeds, and under full film lubrication at high speeds; PAO has a distinct behaviour, for very high speeds it generates a full film lubrication, changing to mixed film lubrication when the entrainment speed decreases, and when it reaches medium to low velocities it reaches boundary film lubrication;
- For 80°C, mineral oils show the three lubrication regimens: full film lubrication for very high entrainment speeds, mixed film lubrication for medium speeds, and boundary film lubrication at low entrainment speeds. PAO is in the mixed film lubrication regimen when entrainment speeds are higher then it reaches boundary film lubrication at medium to low speeds;
- For 110°C, in general, mineral oils are in the full film lubrication at very high entrainment speeds. As speed decreases the regimen changes to mixed film lubrication, and under very low speeds, boundary film lubrication is reached. PAO is in the mixed film lubrication when at high entrainment speeds, but that scenario changes when the entrainment speed decreases, boundary film lubrication is reached.

Addressing now the intermediate disk curves, the following conclusions were taken:

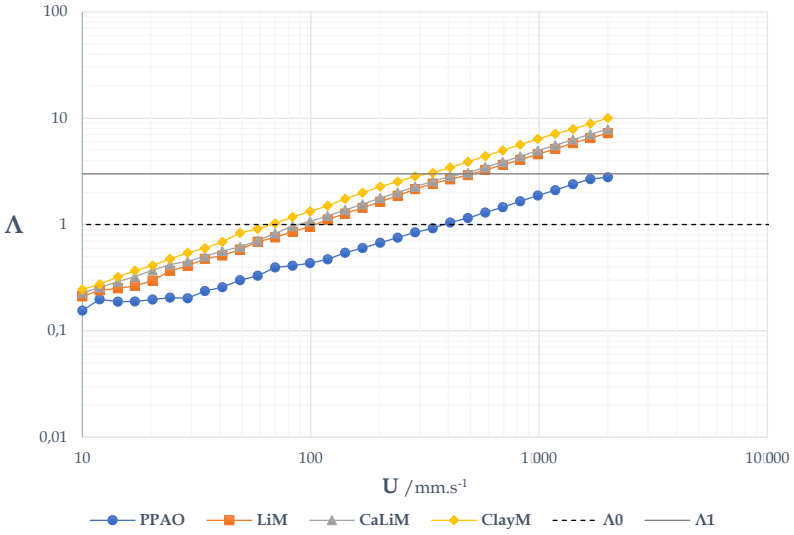
- For 40°C, mineral oils present a full film lubrication when entrainment speeds are very high, slight speed reductions change the regimen to mixed film, and at low speeds the boundary film lubricant is reached; PAO present a mixed film lubrication for very high speeds, but easily reaches boundary film lubrication when entrainment speeds decreases;
- For 80°C, mineral oils are only in mixed film lubrication for very high entrainment speeds, other than that boundary film lubrication is present. PAO is on a boundary film condition no matter what;
- For 110°C, all base oils are on boundary film lubrication.

Targeting the rough disk curves, the following features were inferred:

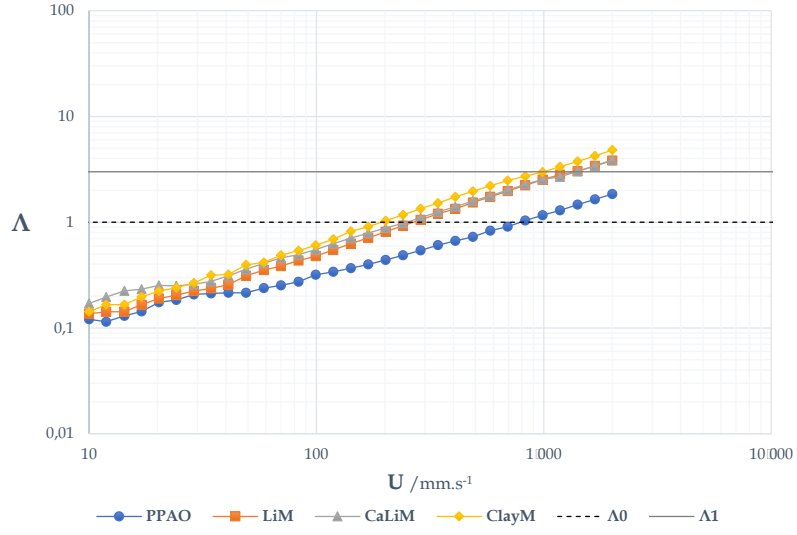
- For 40°C, the full film condition is never reached for mineral base oils, in a matter of fact, boundary film lubrication happens for medium-high entrainment speeds. PAO is on boundary film lubrication;
- For 80°C and 110°C, all base oils are on boundary film lubrication.



(a) T = 40°C

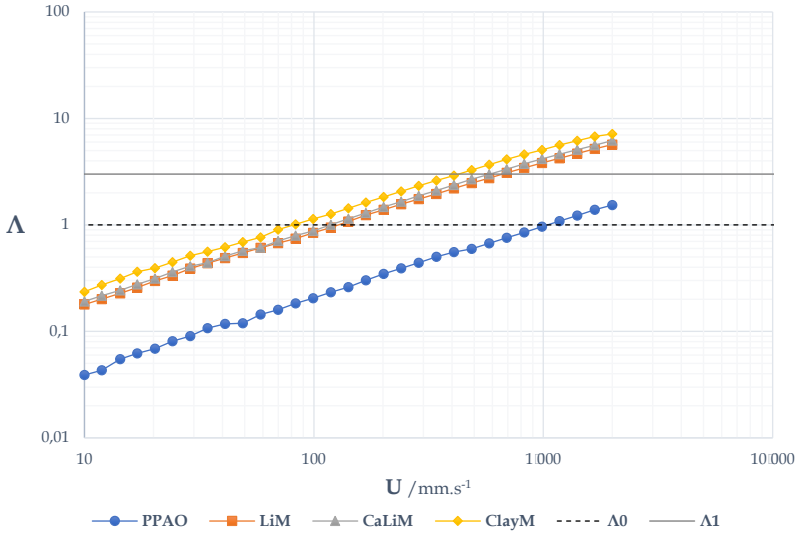


(b) T = 80°C

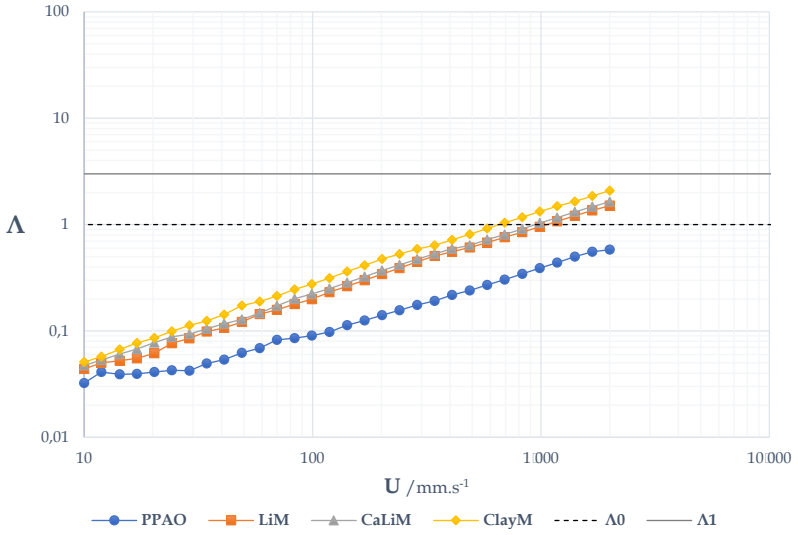


(c) T = 110°C

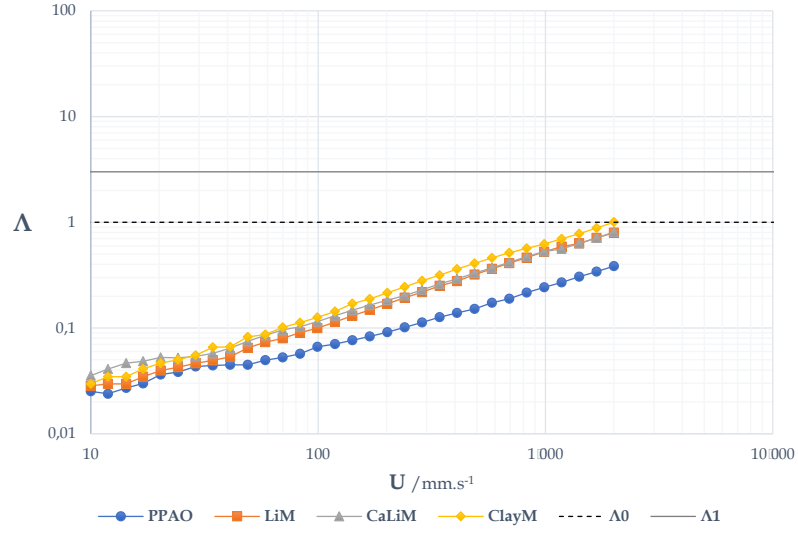
Figure 5.1: Base oils' Specific Film Thickness for the smooth disk (σ = 44 nm)



(a) T = 40°C

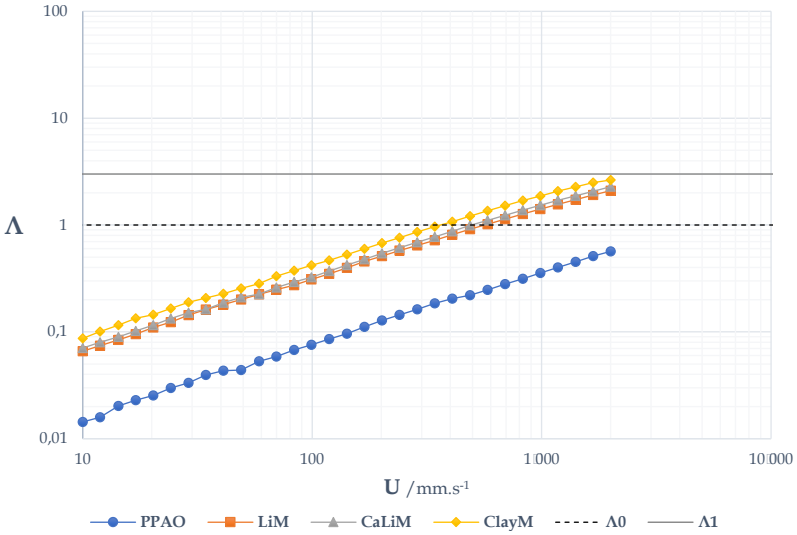


(b) T = 80°C

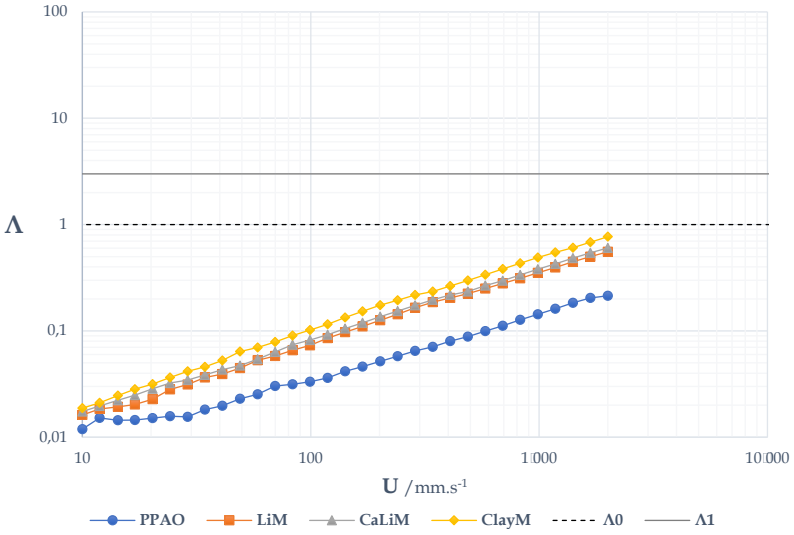


(c) T = 110°C

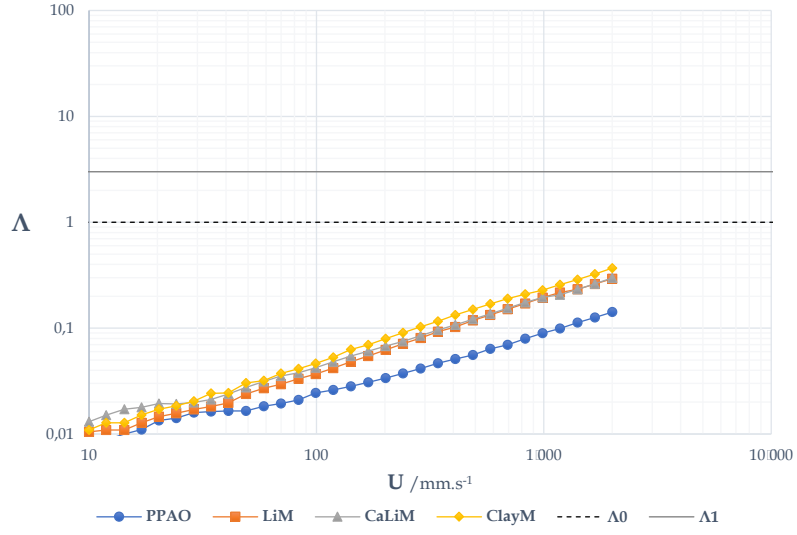
Figure 5.2: Base oils' Specific Film Thickness for the intermediate disk (σ = 212 nm)



(a) T = 40°C



(b) T = 80°C



(c) T = 110°C

Figure 5.3: Base oils' Specific Film Thickness for the rough disk (σ = 574 nm)

Hereupon, the lubrication regimens for each base oil are clearly identified, therefore a more enhanced friction analysis is now viable. *EHD2* output curves are represented against entrainment speed, this kind of configuration doesn't allow for a direct comparison between the different base oils since lubrication regimens might not be the same. With this in mind, this curves were plotted as a function of the specific film thickness. These curves are shown on Figure 5.4. For more detail, these curves are also presented (for each product) on the Appendix.

From the analysis of this figure, it is possible to observe that the coefficients of friction of thr mineral base oils are always higher than those of the synthetic oil, for the same specific thickness, and that mineral oils *COF* is less temperature dependent than the tested PAO's *COF*. In general, for smoother surfaces the tested base oils friction coefficients are related as shown in equation (5.5):

$$COF_{BO\ LiM} > COF_{BO\ CaLiM} > COF_{BO\ ClayM} > COF_{BO\ PPAO} \tag{5.5}$$

According to Brandão *et al.* [81], on full film lubrication, lubricants which present lower pressure-viscosities or higher Viscosity Index (VI) generate lower coefficients of friction. Table 5.3 presents the $\frac{\alpha}{VI}$ ratio for each base oil, with Gold's α, being clear that for higher $\frac{\alpha}{VI}$ values, the lubricant presents higher *COF* values. However, this premiss was not valid for the CaLiM base oil, since the LiM base oil generated higher friction; this facts leads to an important conclusion: α has a more important influence than VI on an oil's friction behaviour.

For rougher surfaces and under mixed/boundary film lubrication this correlation is no longer valid. Instead, the following correlation is observed:

$$COF_{BO\ ClayM} > COF_{BO\ CaLiM} > COF_{BO\ LiM} > COF_{BO\ PPAO} \tag{5.6}$$

As can be observed on Figure 5.4, different base oils show distinct behaviours when confronted with an increase of the composite roughness of the contact, the same applies for temperature as it was aforesaid, these phenomena might be due to the higher shear rates verified in such circumstances, thus, it is appropriate to compare the base oils *COF* dependence with both roughness and temperature. In general, the *COF* decreases when the temperature increases, under full film lubrication, that is with the smooth disk. With the rough disk, mixed film lubrication prevails, and the *COF* increases when the temperature increases. The base oil whose coefficient of friction depends the most on temperature is PPAO, followed by LiM and CaLiM, whose *COF* dependence on temperature is very similar, and finally ClayM. In general, the *COF* increases when the surface roughness increases, for the same operating conditions. However, at 40 °C, the full film regime prevails, and this influence is only observed at low entrainment speeds. In the matter of roughness influence on *COF*, the base oils whose *COF* is less roughness dependent is LiM, followed closely by CaLiM, then ClayM and at last PPAO.

It is also verifiable that for smoother surfaces, *COF* decreases with temperature, but

	T	LiM	CaLiM	ClayM	PPAO
$\frac{\alpha}{VI}$	40°C	219.6	259.6	177.0	9.804
	80°C	164.7	198.0	137.1	81.44
	110°C	147.3	179.9	126.1	74.64

Table 5.3: $\frac{\alpha}{VI}$ ratio /$\text{Pa}^{-1} \times 10^{-12}$.

the same is not applicable for rougher surfaces, in this case, when temperature raises more friction is produced. As temperature raises, the lubricant properties decrease causing also a decrease on lubricant film thickness and consequently Λ decreases, thus, the surfaces start to contact directly and more and more friction is generated. As it was expected, higher surface roughness, also generates higher friction forces, for the same reason explained before, since Λ decreases.

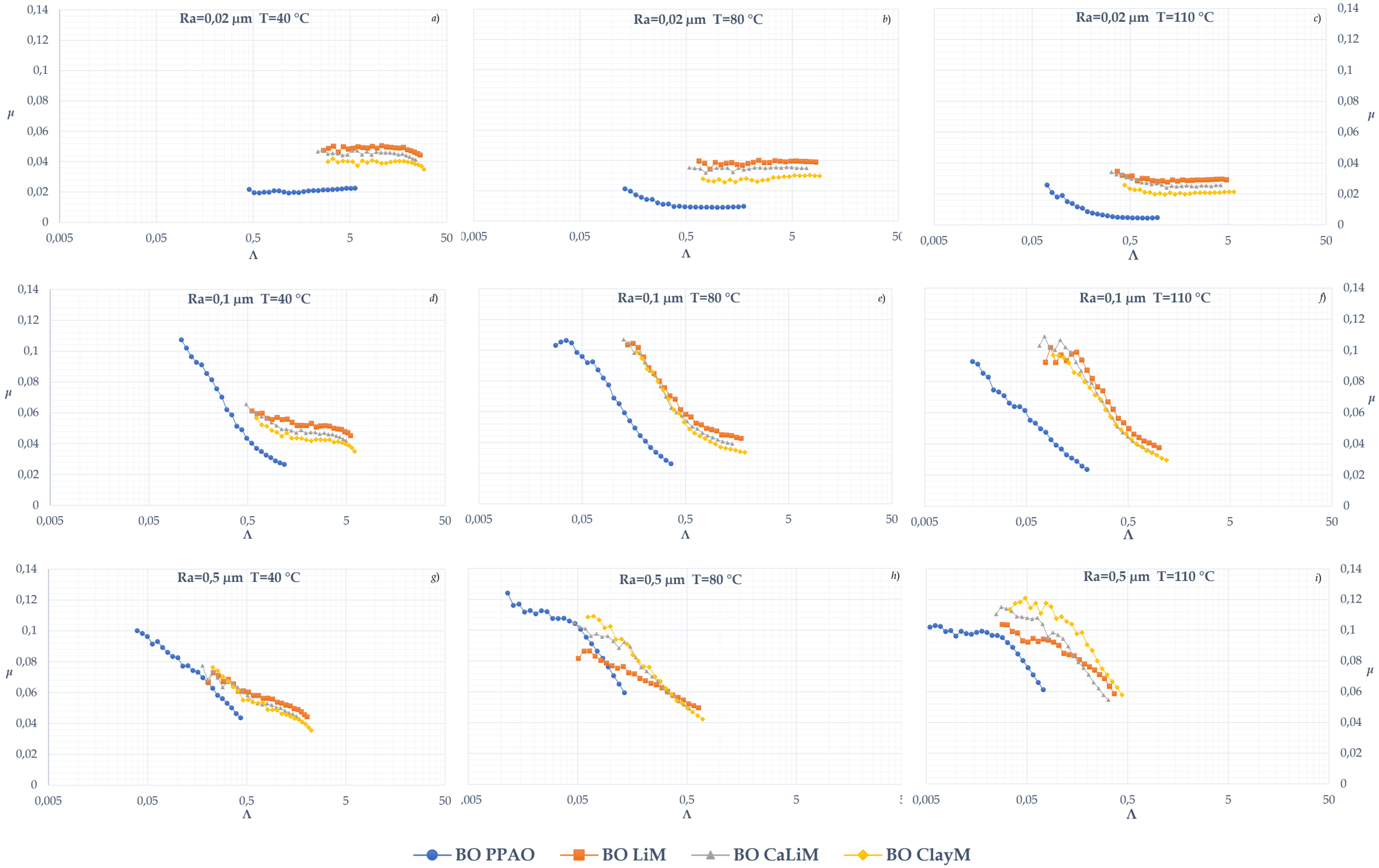


Figure 5.4: Base oils friction measurements

5.5 Grease Lubricated Contacts - Results

In the interest of an improved perception of the friction coefficient results it is necessary to perceive the lubrication regime along each test. The film thickness measurements of each grease at different operating temperatures were corrected to represent the film thickness in a steel ball on steel disc contact.

The specific film thickness was then calculated but now considering the composite roughness of the surfaces of the steel ball and of each one of the disks.
These resulting curves are presented on Figures 5.5 to 5.7, for the smooth (Ra = 20 nm), intermediate (Ra = 100nm) and rough disk (Ra = 500 nm), respectively, and for each base oil, for the different operating temperatures.

Analysing the smooth disk curves, one can conclude the following aspects:

- For 40°C, greases with mineral oils (as their base oils) are always in full film lubrication; PPAO has a distinct behaviour, since it show a plateau region, but still running on full film lubrication;
- For 80°C, again all greases are running on full film lubrication, but for lower speeds greases composed by mineral base oils reach the mixed film regimen. It is noteworthy that both PPAO and CaLiM show a plateau zone at this temperature;
- For 110°C, greases whose base oils are mineral are in the full film regimen for higher entrainments speeds, when it decreases mixed film lubrication takes place, for very low speeds they even reach boundary film. Only ClayM doesn't show a plateau region, at this temperature. PPAO is always under full film lubrication.

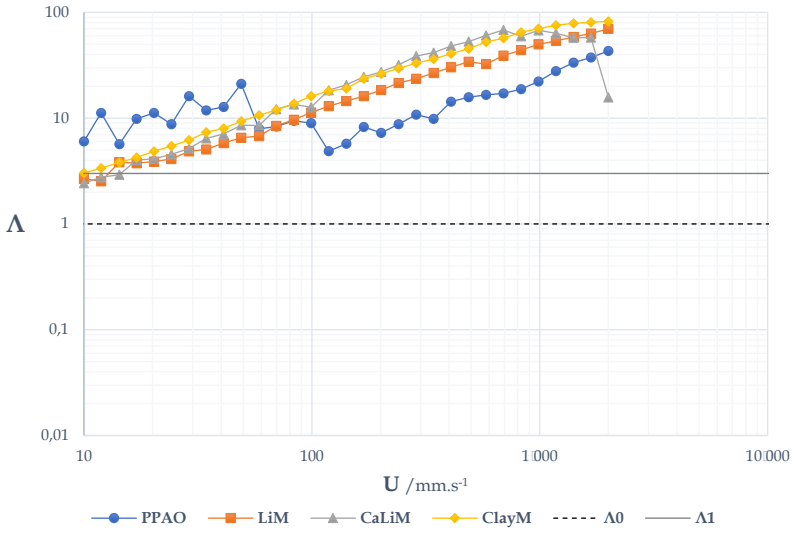
Addressing now the intermediate disk curves, the following conclusions were taken:

- For 40°C, greases including mineral base oils present a full film lubrication at higher speeds, at lower speeds they reach boundary film, at the majority of the speed range they are on mixed film lubrication. PPAO in running on mixed film lubrication for the bigger part of the speed range, except for higher entrainment speeds, where it presents a full film, PPAO also presents a plateau region;
- For 80°C, in general, all greases composed by mineral base oils are on boundary film lubrication until entrainment speeds raises, mixed film lubrication takes place then, ClayM and CaLiM reach to full film when entrainment speeds are very high. PPAO is always on mixed film lubrication, clearly showing a plateau region, also verifiable on CaLiM;
- For 110°C, all grease operate on boundary film lubrication, except for higher speeds, then mixed film lubrication takes place. PPAO shows an untypical behaviour on mixed film regimen and for higher speeds it reaches boundary film lubrication, this is caused by transition between the plateau region and the "linear" region, whereupon, generally, film thickness drops.

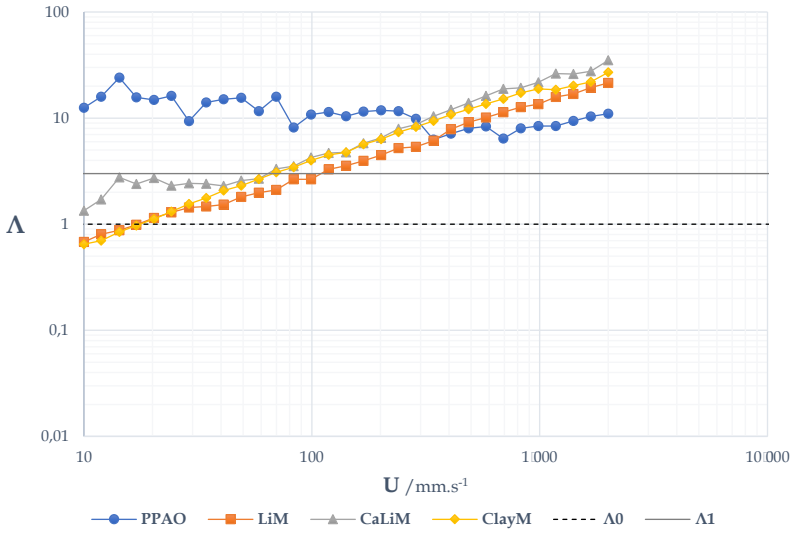
Targeting the rough disk curves, the following features were inferred:

- For 40°C, the full film condition is never reached for any grease, boundary film lubrication takes place when entrainment speeds are low, as velocity raises the regimen changes to a mixed film condition. PPAO is on boundary film lubrication, only reaching mixed film lubrication at very high speeds;

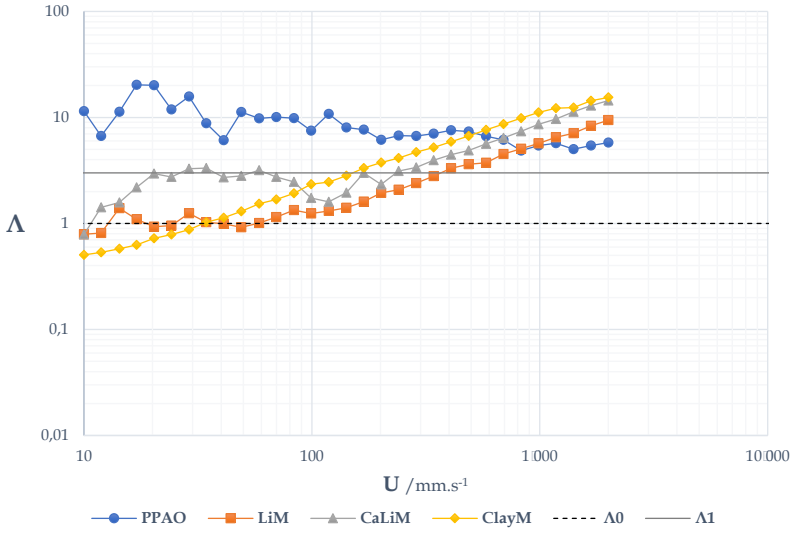
- For 80°C, all greases are on boundary film lubrication, except for CaLiM, which reaches mixed film lubrication for higher entrainment speeds;
- For 110°C, all greases are under boundary film lubrication.



(a) T = 40°C

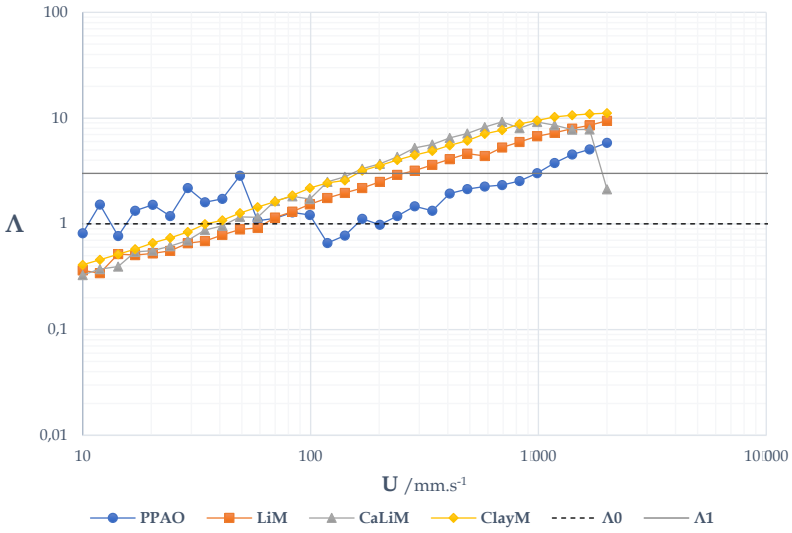


(b) T = 80°C

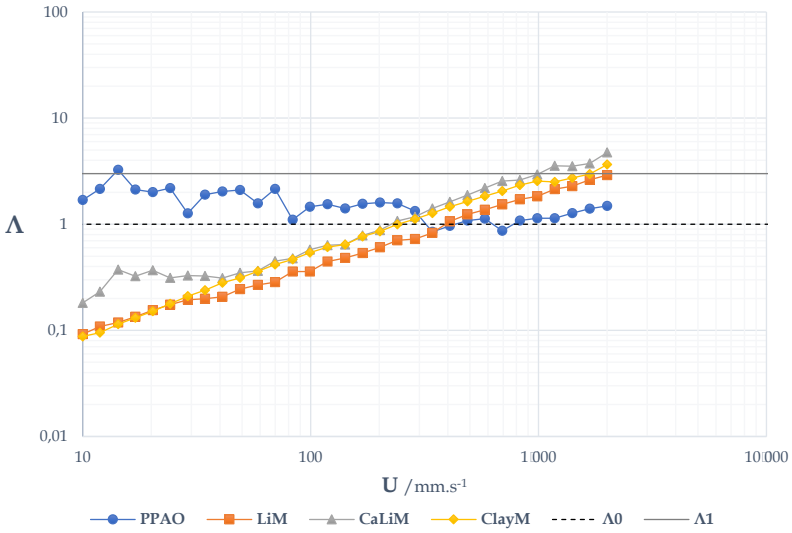


(c) T = 110°C

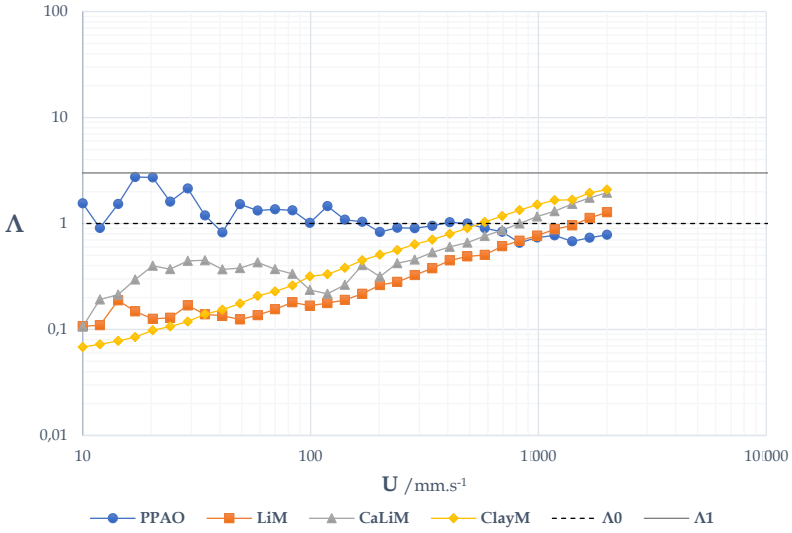
Figure 5.5: Greases Specific Film Thickness - Smooth disk (Ra = 0.02 μm)



(a) T = 40°C

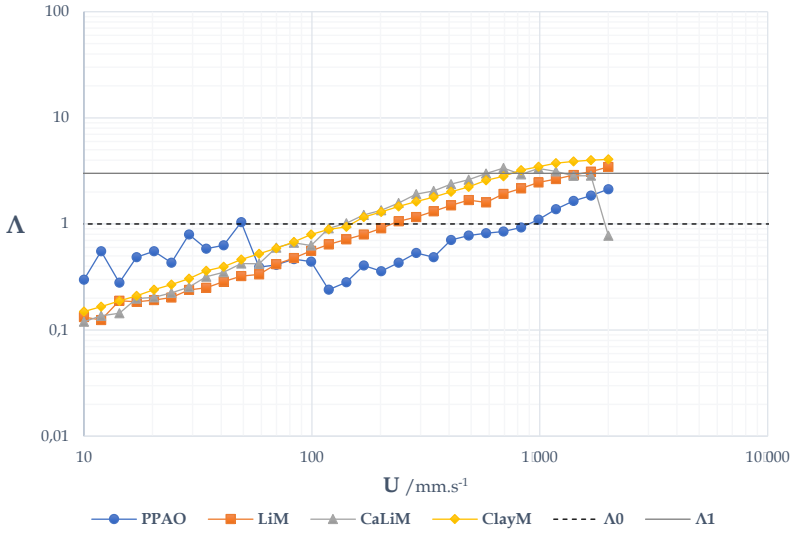


(b) T = 80°C

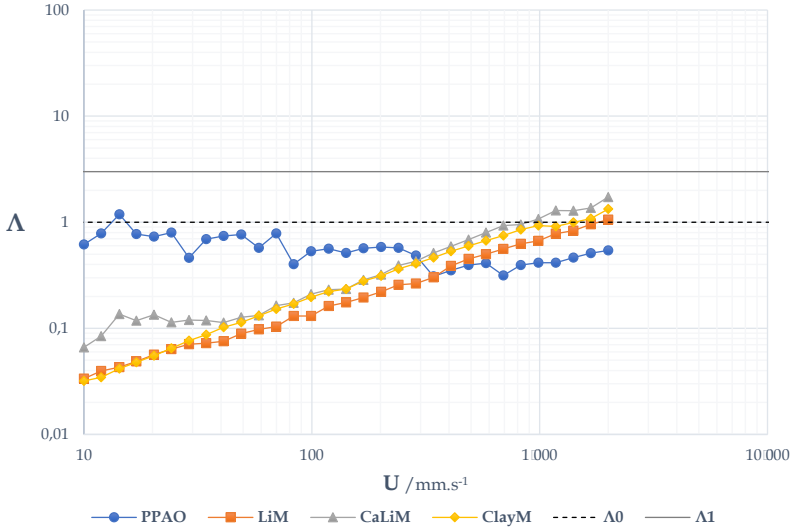


(c) T = 110°C

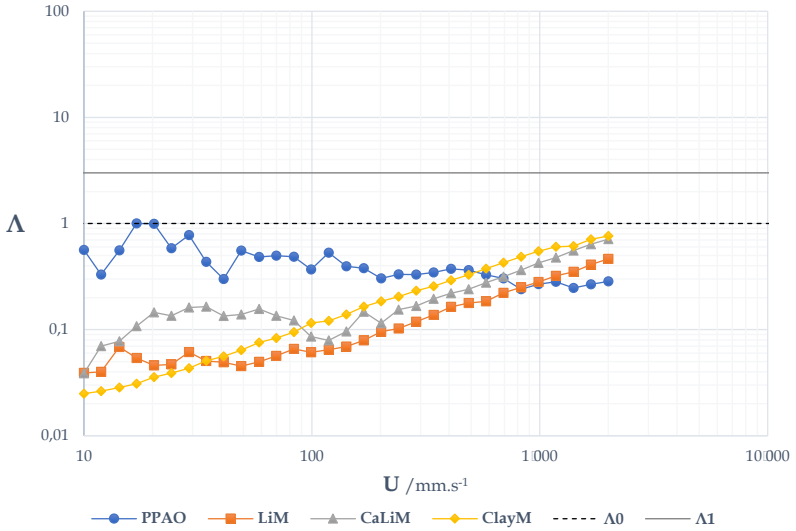
Figure 5.6: Greases Specific Film Thickness - Intermediate disk (Ra = 0.1 μm)



(a) T = 40°C



(b) T = 80°C



(c) T = 110°C

Figure 5.7: Greases Specific Film Thickness - Rough disk (Ra = 0.5 μm)

Since most of grease properties come from their base oils and no grease properties were measured in this work, only the base oil film thickness predictions were used, this means that for a given grease the specific film thickness used was its respective base oil Λ. This procedure was implemented in order to obtain smoother Stribeck curves. The curves are shown in Figures 5.8, and are plotted against the specific film thickness. For more detail, these curves are also presented separately (for each product) in the Appendix.

From the analysis of the smooth disk curves on the top of Figure 5.8, it can be observed that the *COF* of all greases decreases with raising temperature, due to the reduction of film thickness with temperature. Besides the grease which shows lower friction is PPAO, followed by ClayM, then CaLiM and finally LiM. In general,

$$COF_{LiM} \simeq COF_{CaLiM} > COF_{ClayM} > COF_{PPAO} \tag{5.7}$$

As for the intermediate disk, since all greases enter the mixed film lubrication regime, it is expectable to observe an increase on *COF* when the specific film thickness drops, as shown in Figure 5.6. However, PPAO has a distinct behaviour, since its *COF* increases with decreasing entrainment speeds, until it reaches a maximum from which the *COF* drops as the speed decreases (see Figure 5.8 e) and f)). This maximum occurs when the transition to the plateau region is triggered, mentioned in Figure 4.5. This phenomenon was observed with grease CaLiM at 110 ºC (see Figure 5.8 f)).

For this disk, PPAO shows the lowest friction coefficient, followed by CaLiM, that is,

$$COF_{LiM} \simeq COF_{CaLiM} > COF_{ClayM} > COF_{PPAO} \tag{5.8}$$

Regarding the rough disk, all greases enter on boundary film lubrication eventually, plus, in general, ClayM shows the highest *COF*, then LiM, followed by CaLiM, and with PPAO showing the lowest friction coefficient one more time. Again, PPAO and CaLiM show a distinct behaviour when compared with the other two greases, whose *COF* presents a maximum value when the transition to the plateau zone occurs (see Figure 5.8 d)).

As it can be seen this phenomenon is not characteristic of the lubrication regime, since for different contact roughnesses, the transition occurs at different Λ, and is typical of each grease formulation.

As it was observed on the base oils' friction behaviour, for surfaces with lower roughness, grease *COF* decreases with temperature, on the other hand, for rougher surfaces, when temperature raises, grease *COF* raises. As temperature raises, the lubricant properties decrease, which leads to a decrease on the grease's film thickness and, consequently, Λ, thus, the surfaces start to contact directly and more and more friction is generated.

As it was expected, higher surface roughness, also generates higher friction, since Λ decreases. This trend is not observed if the greases plateau film thickness is reached, and the opposite trend occurs.

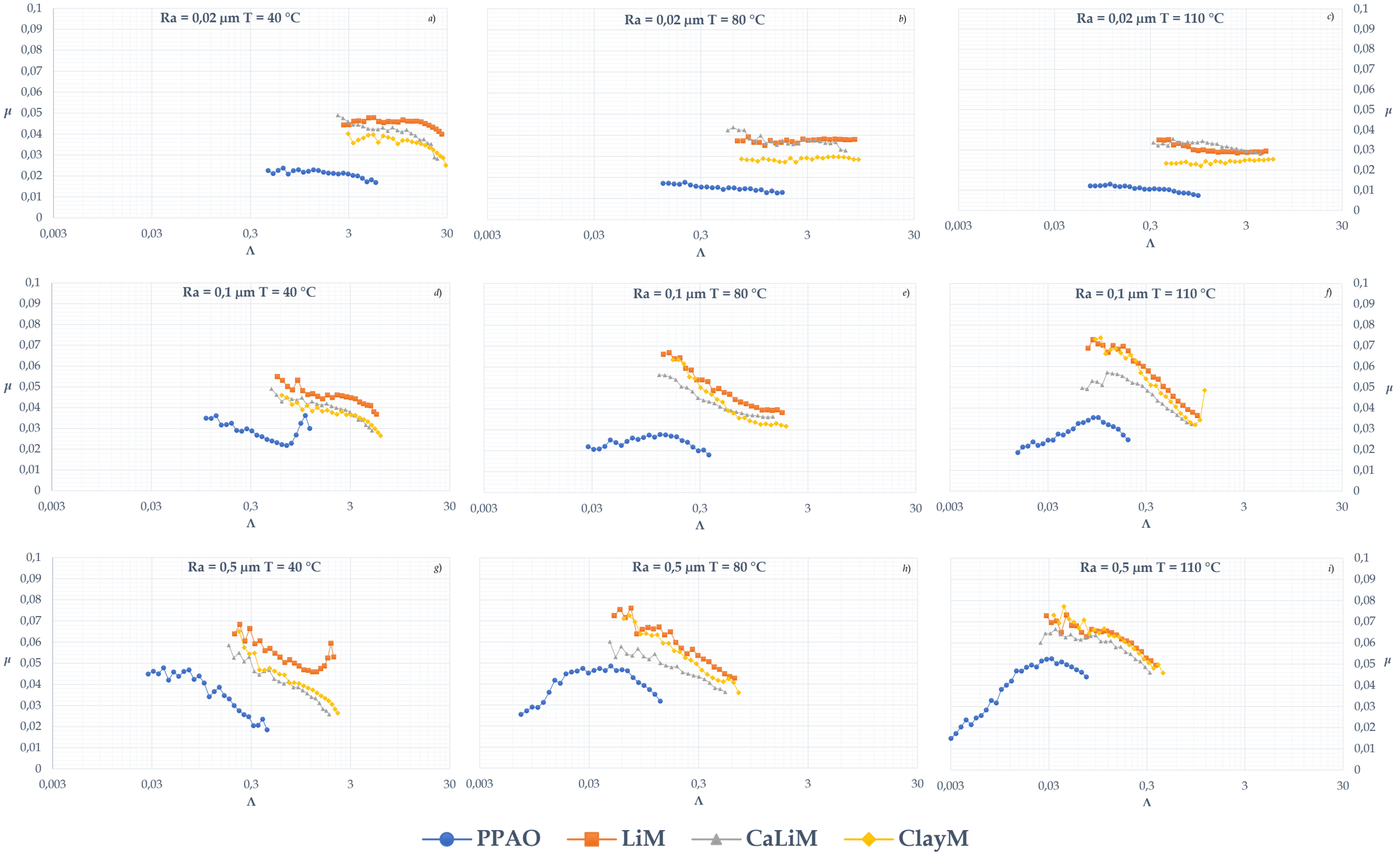
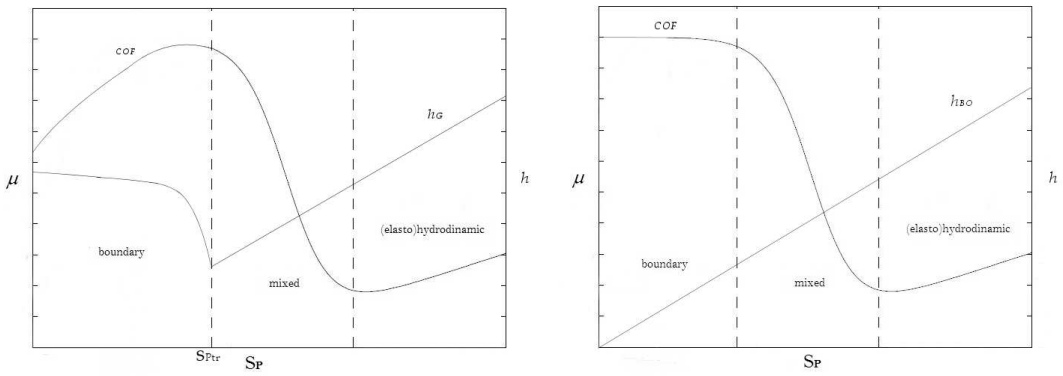


Figure 5.8: Grease friction measurements

To better comprehend this phenomenon, several curves were plotted with distinct variables as abscissa, all presented on Chapter 4. Figure 5.10 shows the Stribeck curves and the grease film thickness, h_G, plotted against S_P, the modified Hersey parameter suggested by Brandão *et al.*.

Analysing Figure 5.10, it is clear that the transition between the grease lubrication region and the EHL region occurs for the same S_P, therefore the transition is a function of the grease properties, probably the thickener dimensions. It is also clear that the maximum COF occurs for the S_P that corresponds to the transition speed, at which the plateau film thickness is reached.

A decrease on COF is observed when the plateau film thickness is reached, this h_{pl} seems to be intrinsic to each grease formulation. This behaviour can be observed on with all disks (Ra = 20 nm, 100 nm, 500 nm), for grease PPAO at all temperatures (see Figure 5.10 j), k), l)), for grease CaLiM at 80 °C and 110 °C, and with grease LiM at 110 °C (see Figure 5.10 e)). For the other greases and temperatures, the plateau film thickness is not observed and this effect just cannot be detected, however the author believes that every grease presents this kind of behaviour, which is illustrated on Figure 5.9. Each grease has an intrinsic plateau film thickness, which is probably related to the thickener's dimensions, for this h_{pl} there is a transition entrainment speed, which depends on the operating conditions as it demonstrated on equation (4.7). If this transition occurs at low entrainments speeds, and therefore low S_P values, the boundary film lubrication regime typical of oil lubrication (constant COF) might occur and two distinct regions are verified on the boundary film lubrication regime, the first where COF is approximately constant and the second where COF decreases, which seems to be the case for CaLiM. As for PPAO, this transition occurs at medium speeds and under the boundary-film condition, COF decreases.



(a) Grease (b) Base oil

Figure 5.9: Stribeck curves

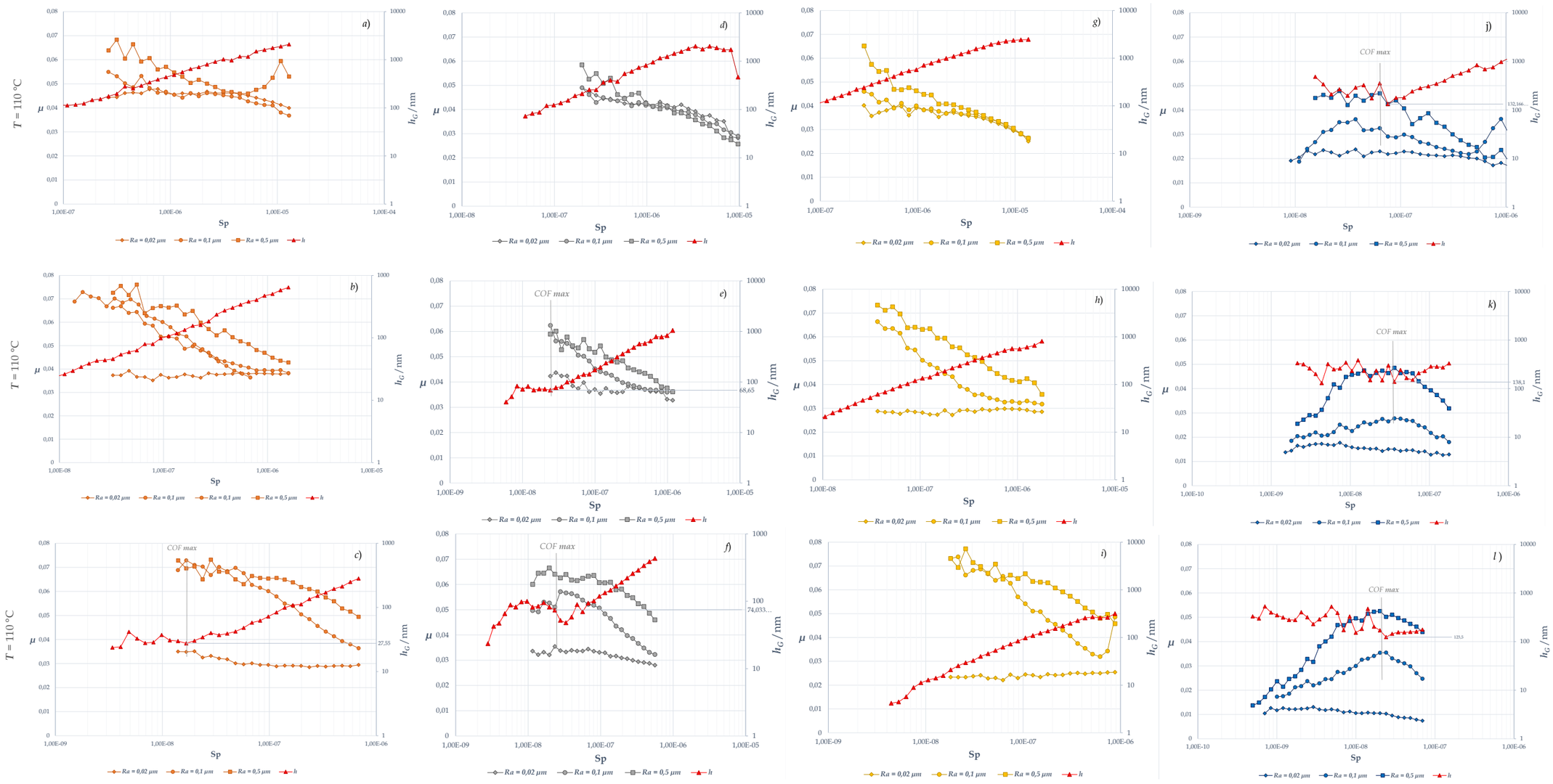


Figure 5.10: Grease Stribeck curve and film thickness

5.6 Grease friction vs Base oil friction

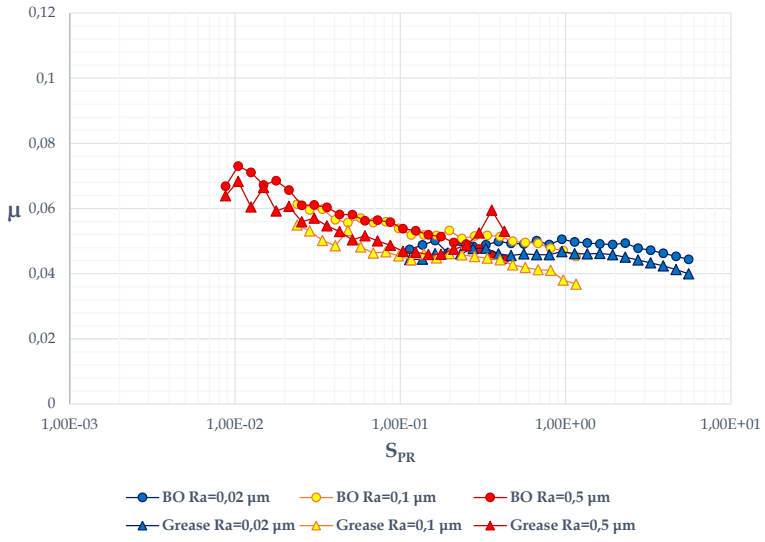
In the interest of an improved comprehension of the friction behaviour of the tested greases, Stribeck curves of both greases and base oils were compared. The curves, measured at different operating conditions, are shown on Figure 5.11 to 5.14. The S_{PR} numbers were calculated using the properties of the base oils.

The analysis of these figures, show that greases always generate lower (or equal) friction coefficients than the corresponding base oils. The reason for this behaviour is due to the fact that greases always generate higher film thickness than their corresponding base oils, as shown in Table 4.5.

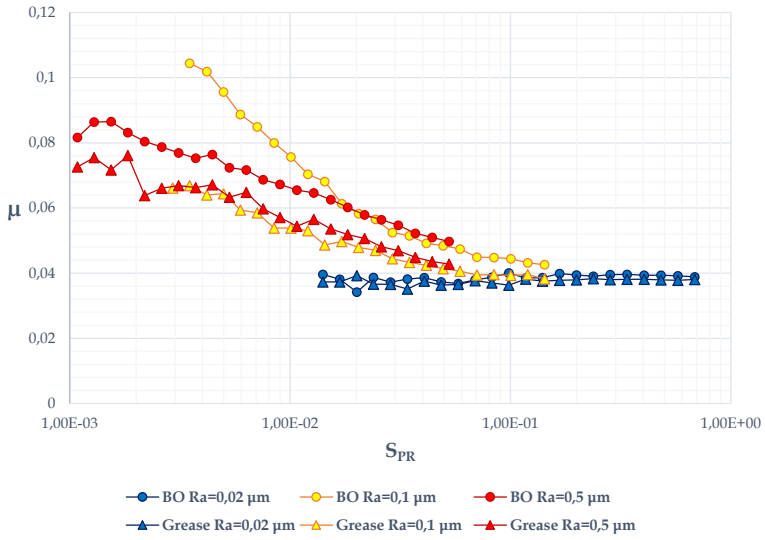
For high values of S_{PR}, that is high speeds or low temperatures, and mainly with the smooth disk (Ra = 20 nm), greases and base oils generate very similar *COF*'s. Although the greases generate higher film thickness, both oils and greases operate under full film lubrication. This is observed in all figures, for the smooth disk case.

As the values of S_{PR} decrease, for lower speeds and higher temperatures, mainly for the intermediate (Ra = 100 nm) and the rough (Ra = 500 nm) disks, greases generate progressively lower *COF*'s than the corresponding base oils. The fact that greases generate higher film thickness than the base oils implies that they operate under higher values of specific film thickness and thus, under less severe mixed or boundary lubrication conditions. This is observed in all cases with the intermediate and rough disks.

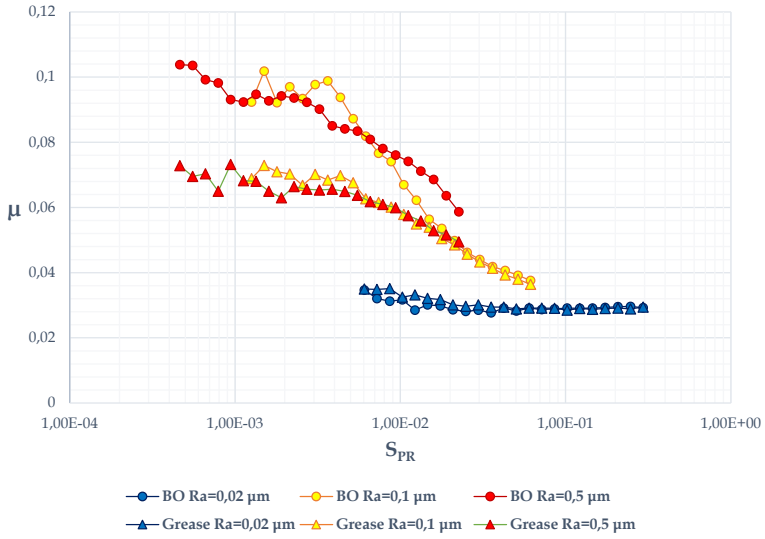
Finally, as the values of S_{PR} decrease more the grease film thickness also decreases. If the plateau film thickness is reached, the grease behaviour modifies and the grease *COF* decreases as S_{PR} also decreases. In this case the *COF*'s generated by the greases are significantly lower than those generated by the base oils, as shown in Figures 5.12 and 5.14, at 80 ^{o}C and 110 ^{o}C.



(a) T=40°C

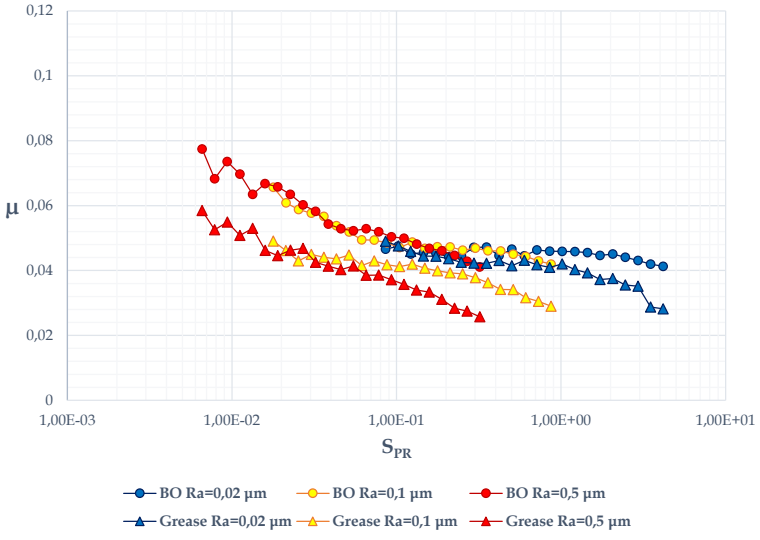


(b) T=80°C

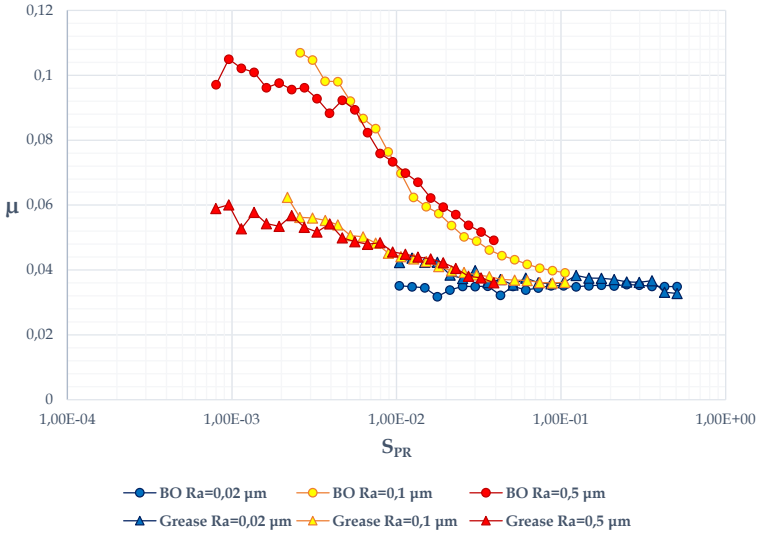


(c) T=110°C

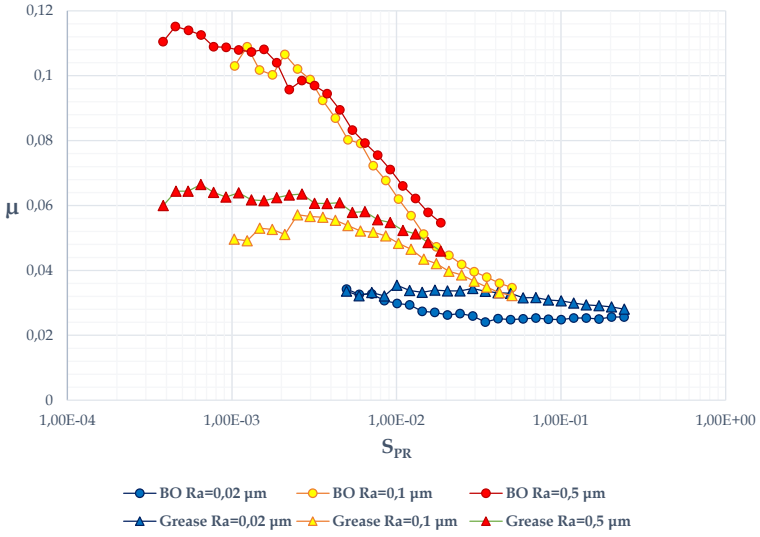
Figure 5.11: LiM - Base oil vs Grease



(a) T=40°C

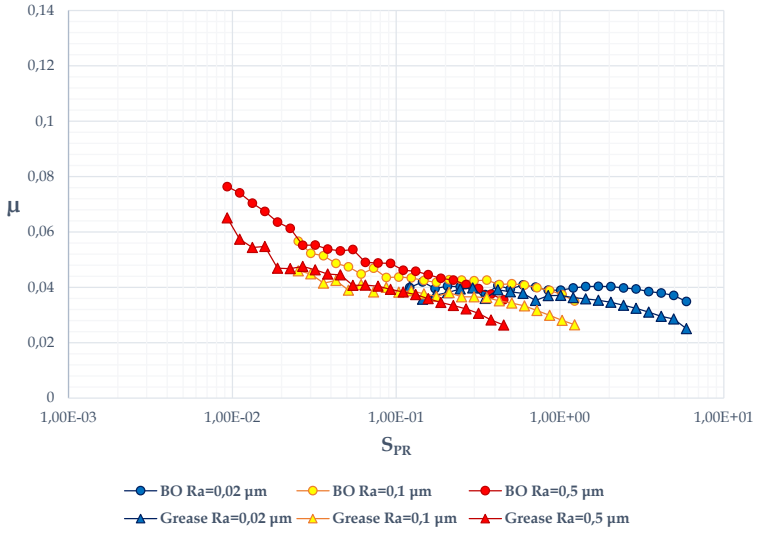


(b) T=80°C

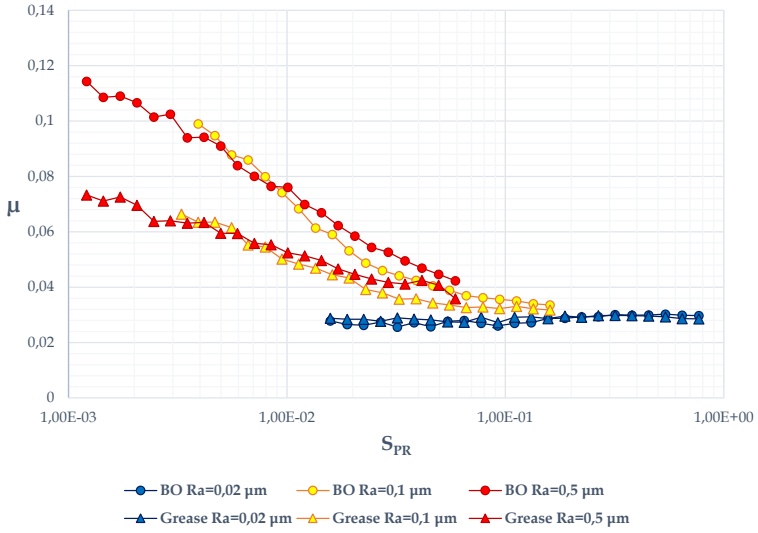


(c) T=110°C

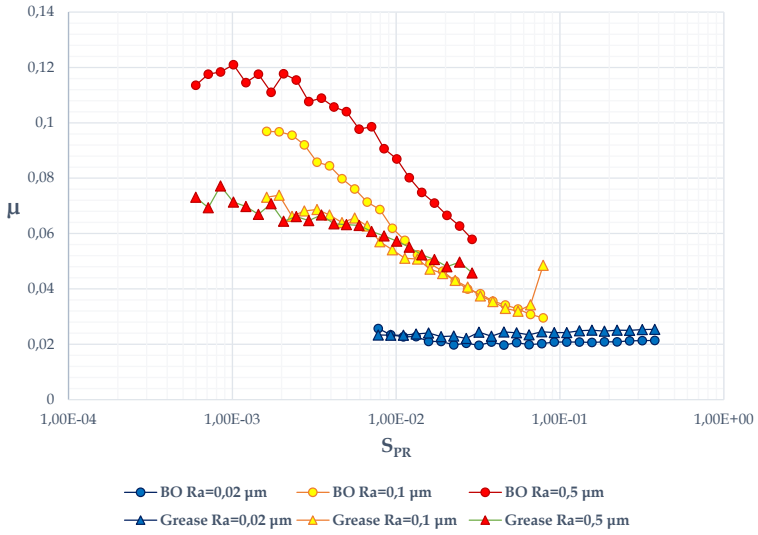
Figure 5.12: CaLiM - Base oil vs Grease



(a) T=40°C

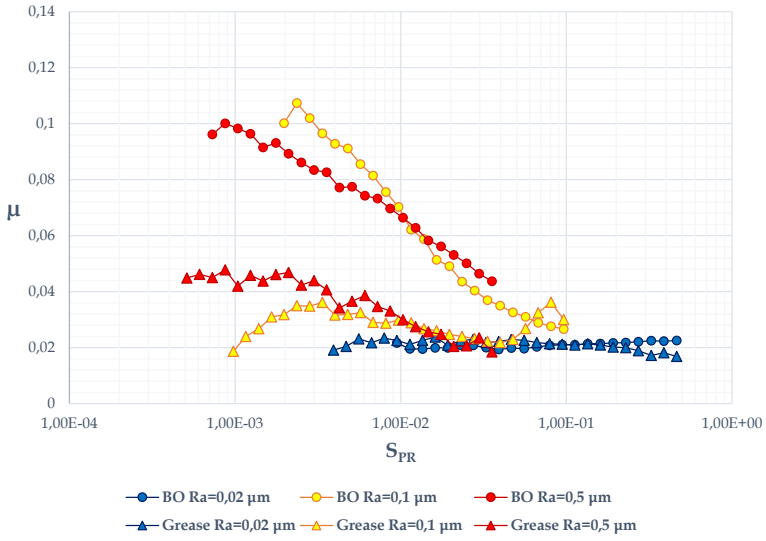


(b) T=80°C

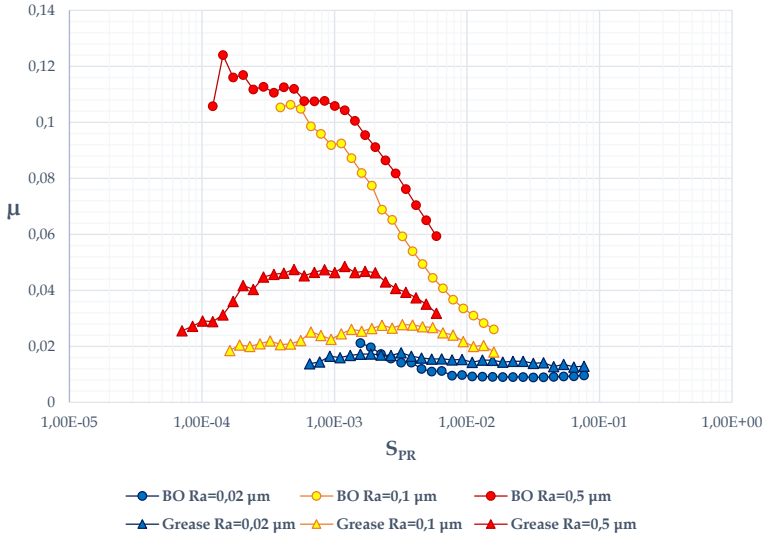


(c) T=110°C

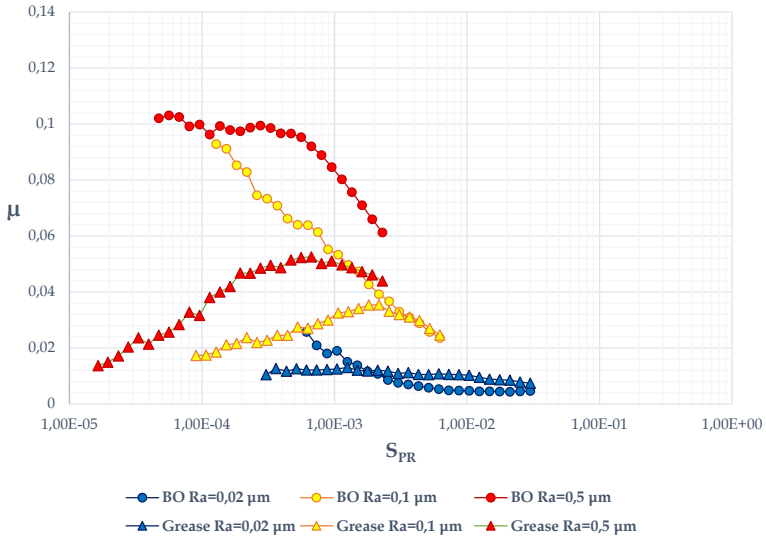
Figure 5.13: ClayM - Base oil vs Grease



(a) T=40°C



(b) T=80°C



(c) T=110°C

Figure 5.14: PPAO - Base oil vs Grease

5.7 Grease friction vs Dry Grease friction

As it was explained on Chapter 3, a bleeding procedure was performed for each grease in order to extract the maximum amount of bled oil. The volume of bled oil extracted from each grease depends on the amount of thickener of the grease, which could vary from grease to grease, on the type of thickener and on the strength of the bond between the thickener and base oil.

The procedure used in this section was the same used for the standard greases.

Figures 5.15 to 5.18 shows the traction curves of each grease, in a dry and normal state, plotted against the entrainment speeds, while Figure **??** shows the traction curves of every grease.

From the analysis of Figures 5.15 to 5.18, we can surmise that a dry grease friction behaviour depends on the thickener type, since grease with distinct thickeners had very different performances. Greases with a soap thickener - LiM and CaLiM - showed a specific trend on their friction behaviour, which diverged from ClayM, composed by an organophilic clay thickener, and PPAO, whose thickener was a polymer.

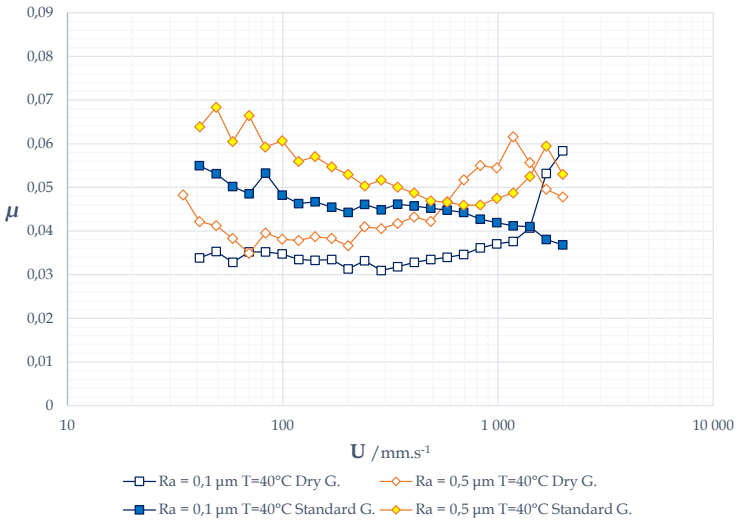
In the case of CaLiM and LiM greases, their dried grease presented a lower friction coefficient when compared with the standard grease, but for higher entrainment speeds lubricant starvation occurs and the *COF* raises drastically, reaching higher *COF* values than the standard grease. This lower *COF* might be due to a thicker lubricant film generated inside the contact. Once the dry greases leave the contact track, causing starvation, it scarcely returns to the track, due to its lack of mobility.

The dried ClayM grease also generates slightly lower friction than the standard grease. However, as the speed increases severe starvation occurs, together with a significative increase of the *COF*. The entrainment speed at which starvation occurs increases as the operating temperature also increases.

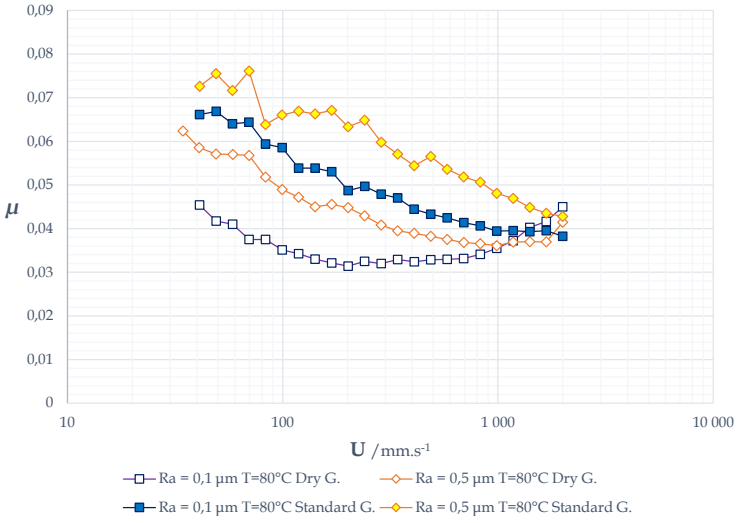
With regard to PPAO dry grease, it presents a slightly lower *COF* when compared to the standard grease, in mixed film condition, but when the entrainment speed decreases and both entered the plateau region, the standard grease showed a significantly lower *COF*. This might be due to a thicker lubricant film of the dried grease lubricated contact, when both greases are on mixed film lubrication, and thicker film will be beneficial since the lubrication is mainly conducted by the base oil, whose viscosity is small. However, when the plateau region is reached an higher film thickness will only generate higher friction forces, since there's more mass to move.

Figures 5.19 to 5.20 compare the dried grease when lubricating the intermediate and rough disks, respectively. In the case of the intermediate disk, dried grease ClayM and LiM generate the highest *COF*'s. PPAO and CaLiM generate similar *COF*, until the dried grease CaLiM enters into starvation, and its *COF* increases drastically.

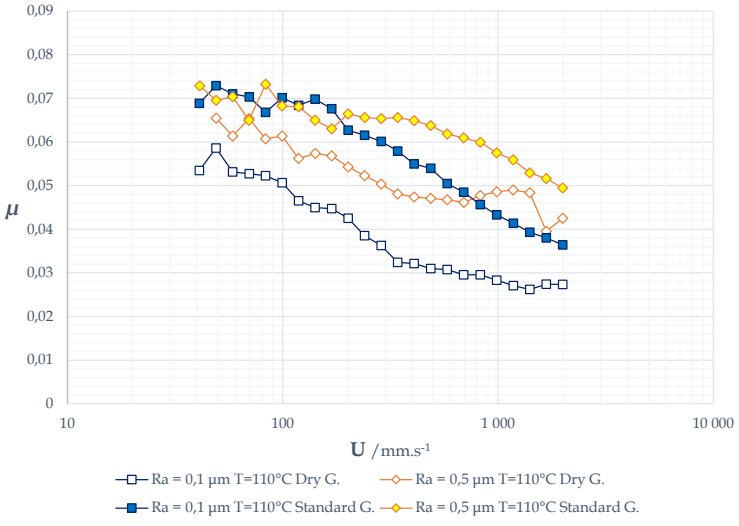
In the case of the rough disk, the scatter of *COF* is very significant, mainly at 40 ^{o}C. Dried grease PPAO and CaLiM have similar *COF*'s until grease CaLiM enters into starvation and its *COF* increases significantly.



(a) T=40°C

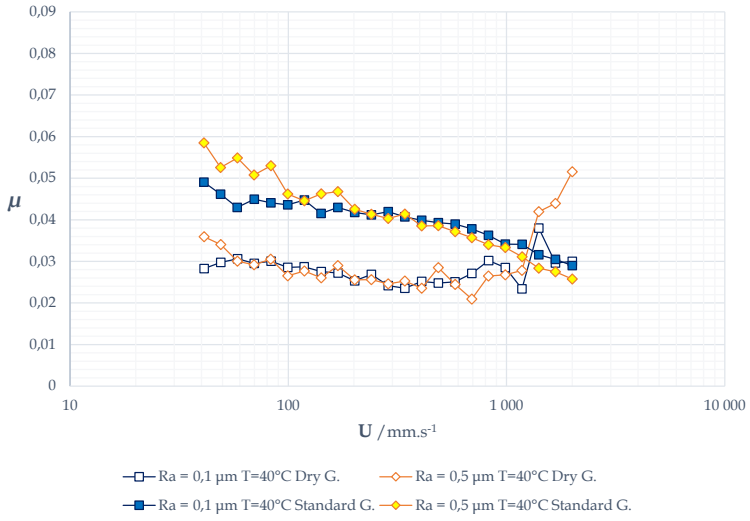


(b) T=80°C

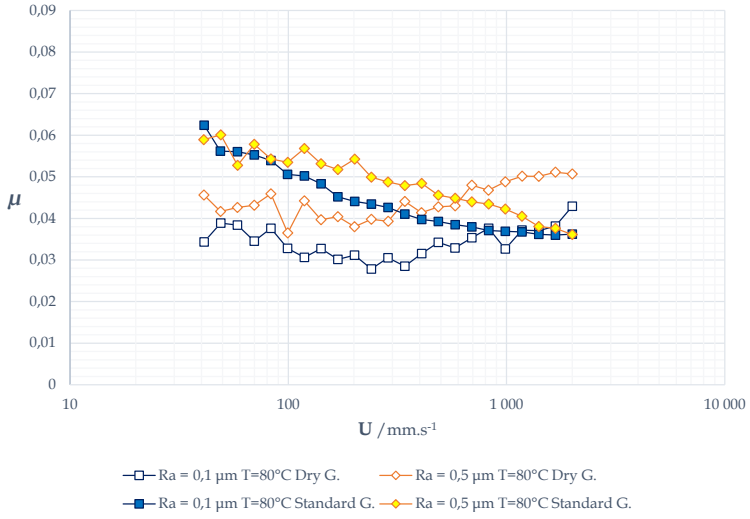


(c) T=110°C

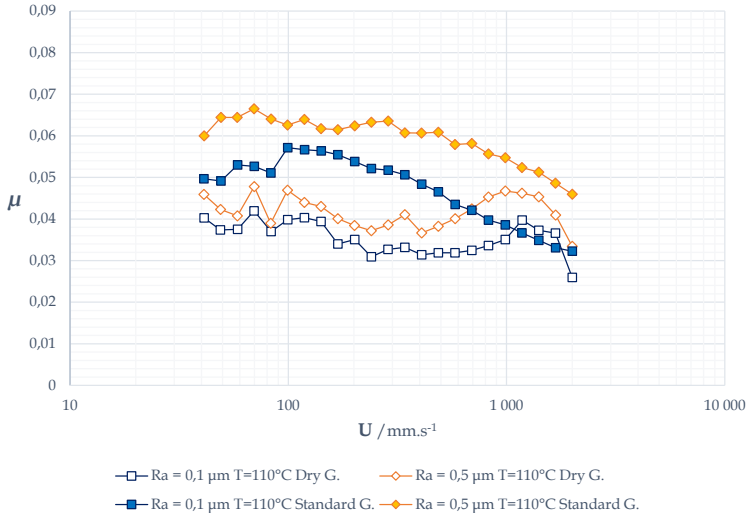
Figure 5.15: LiM - Dry vs Standard Grease



(a) T=40°C

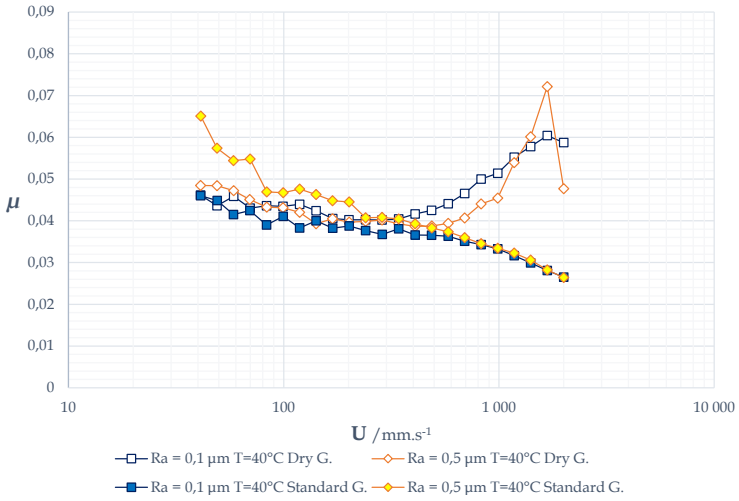


(b) T=80°C

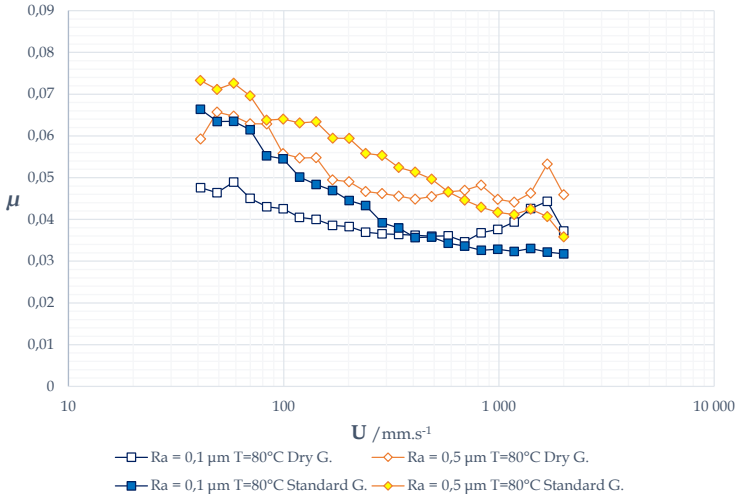


(c) T=110°C

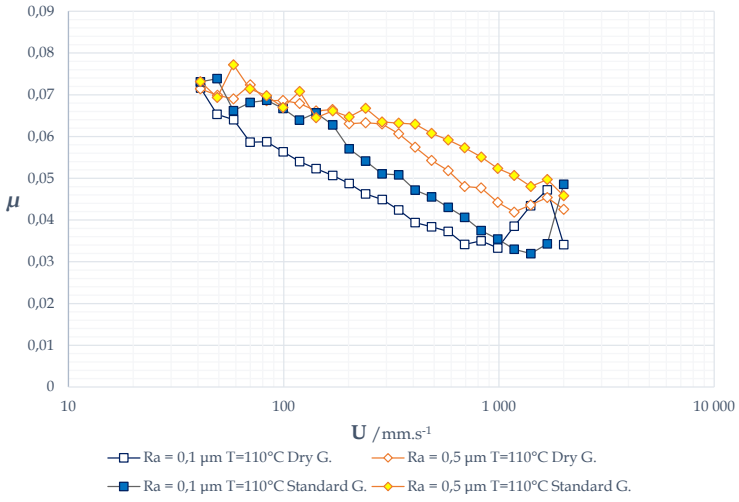
Figure 5.16: CaLiM - Dry vs Standard Grease



(a) T=40°C

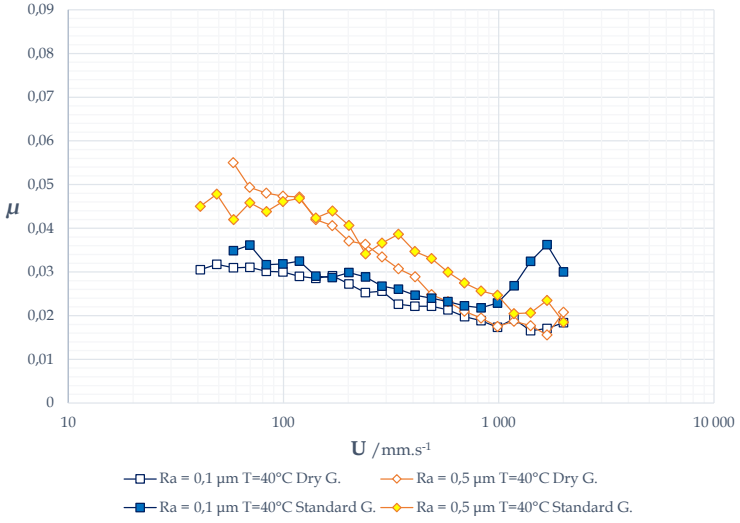


(b) T=80°C

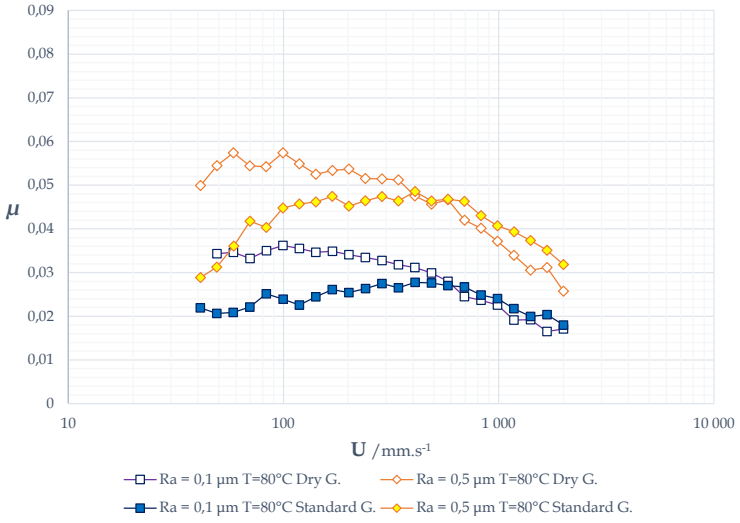


(c) T=110°C

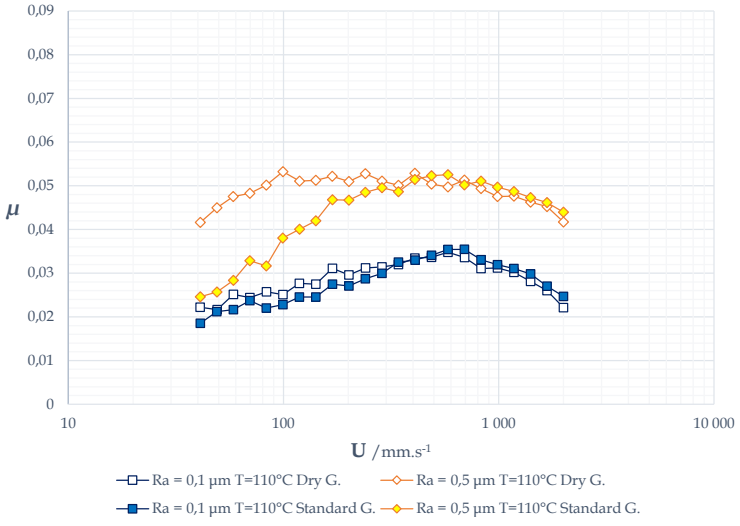
Figure 5.17: ClayM - Dry vs Standard Grease



(a) T=40°C

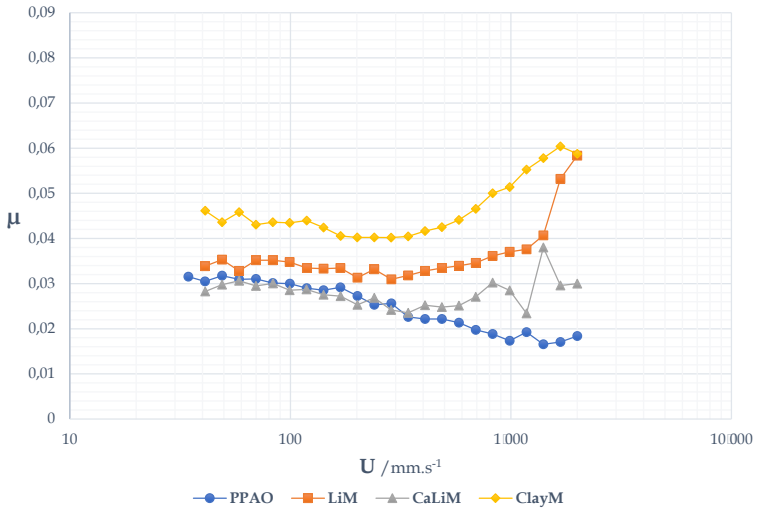


(b) T=80°C



(c) T=110°C

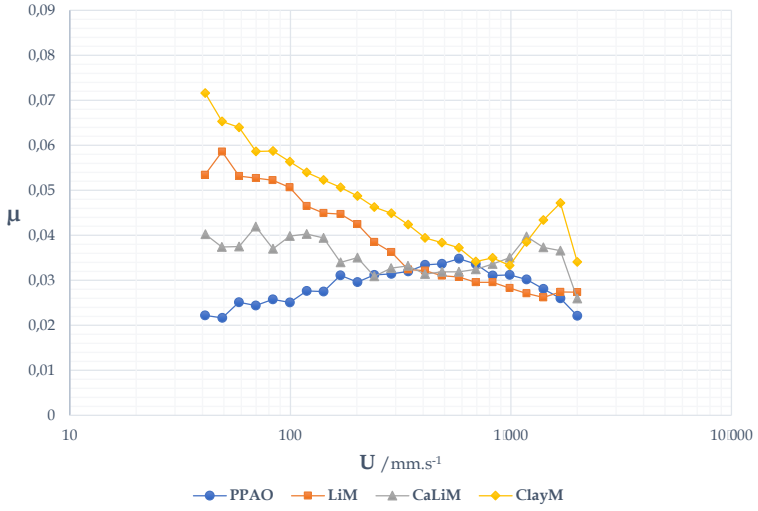
Figure 5.18: PPAO - Dry vs Standard Grease



(a) Ra=0.1 μm T=40°C

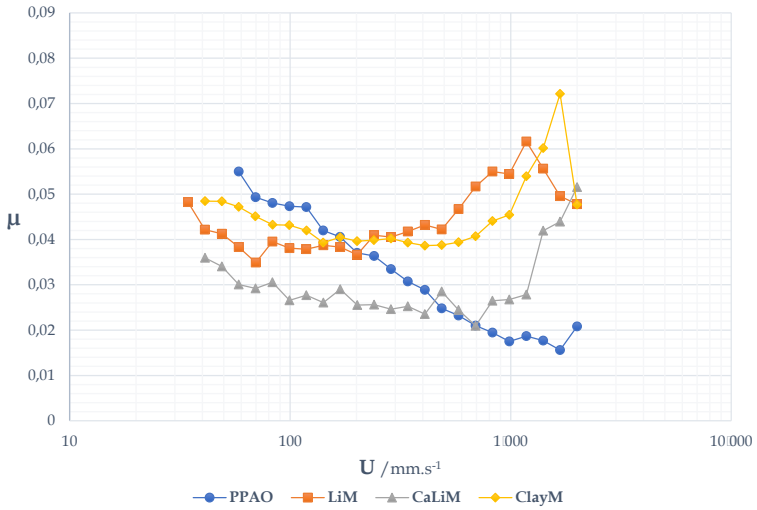


(b) Ra=0.1 μm T=80°C

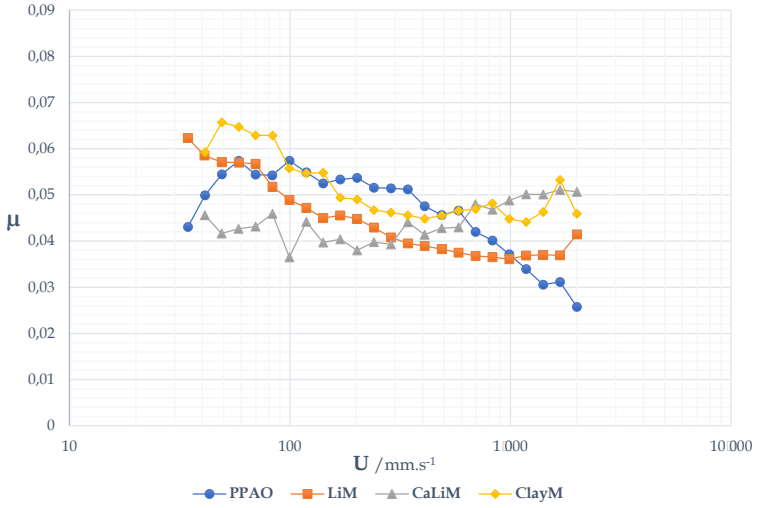


(c) Ra=0.1 μm T=110°C

Figure 5.19: Dry Greases traction curves for the intermediate disk (Ra=0.1 μm)



(a) Ra=0.5 μm T=40°C



(b) Ra=0.5 μm T=80°C



(c) Ra=0.5 μm T=110°C

Figure 5.20: Dry Greases traction curves for the rough disk (Ra=0.5 μm)

5.8 Closure

Traction and Stribeck curves were elaborated with four differently formulated greases, under fully flooded conditions.

The traction measurements were performed using three disks with distinct roughnesses, in order to cover all three lubrication regimens. Thickener and base oil influences on the greases friction behaviour were observed. It was also possible to identify certain grease characteristics which are attributed to certain types of thickener.

PPAO presented the lowest traction coefficient, while LiM had the higher *COF* values, in general. This difference might be explained by the lower base oil viscosity of PPAO and also by the thickener morphology/type/dimensions, since PPAO showed different results also on the film thickness tests. As for LiM, the thickener morphology/type is responsible for the higher *COF* values it shows, since ClayM, whose base oil presents higher viscosities and therefore higher viscous friction, showed a very different behaviour. This fact indicates that not only the base oil properties and thickener morphology influence the grease friction behaviour but also their interaction.

As expected, the thickener contributes to the increase of the film thickness at low entrainment speeds, which certainly affects the grease friction behaviour, it was possible to observe that when a grease enters the plateau film thickness region, this leads to a reduction of the coefficient of friction as the entrainment speed decreases, with a maximum value in the transition speed, which corresponds to the plateau film thickness mentioned on Chapter 4. This behaviour can be observed either on PPAO or on CaLiM. For LiM and ClayM this phenomenon could not be observed due to their transition speeds and plateau film thicknesses being too low.

It was possible to conclude that calcium-lithium thickened greases show an optimized behaviour both in film thickness and friction, when compared to lithium thickened greases. It was also verifiable that the organophilic clay thickener contributes to a higher film thickness and a better temperature performance. At lower speeds ClayM presented an oil-like behaviour, since its performance was identical to a base oil's. The polypropylene thickener shows great performance with low friction values.

Greases present an optimized friction behaviour when compared to their respective base oils. An exception is observed on full film lubrication, on this lubrication regimen, *COF* depends on the base oil viscosity, since the bled oil lubricates the contact. Oils with high viscosities present higher *COF* values when compared with their respective grease, since the generated viscous friction is higher, on the other hand base oils whose viscosity is lower present an optimized friction behaviour comparing to their respective grease.

When a greases loses bled oil, the friction behaviour is thickener-controlled, this means that the more base oil is lost, the more influence the thickener will have on lubrication.

For LiM and CaLiM, the dry grease showed and improved friction behaviour comparing to the standard grease, which might be justified by these thickener matrixes. Regarding ClayM, both dry and standard greases had identical friction behaviours. As for PPAO, both greases showed identical *COF* values except when the transition to the grease lubrication region occurs, from which the standard grease shows better friction performances.

Chapter 6

Conclusion

6.1 Conclusions

It was possible to observe that the thickener has an active role in the lubricant film formation, specially at ultra low speeds, as thickener lumps may enter the contact increasing the film thickness as the entrainment speed decreases, and reaching a constant value (for the Calcium-Lithium grease). This region depends upon the grease formulation, particularly on the thickener type and the interaction between base oil and thickener. This interaction will depend on the thickener microstructure and on its solubility on the base oil [73]. A high scatter was observed in this region, this might be explained by an inconsistency on the thickeners lumps dimensions (larger lumps may enter the contact, forming a thicker lubricant film) and also if no lumps enter the contact, the film thickness decreases. It was also concluded that the film thickness generated at low speeds seems to be characteristic to each grease formulation since there's not a great scattering in the mean film thickness values for the different test conditions and the transition speed, between the EHL region and the "plateau" region seems to depend on external conditions, like temperature,what suggests that this value might be characteristic of the lubrication regimen, De Laurentis *et al.* [72] concluded the same principle in his work about the influence of grease composition on friction in rolling/sliding concentrated contacts.

Regarding the traction behaviour it was possible to conclude that the thickener contributes to the increase of the film thickness, especially at low entrainment speeds, what leads to a decrease on COF as the entrainment speeds decreases. This decrease on friction creates a maximum value, verified at the transition entrainment speeds between the EHL region and the plateau region.

Greases present an optimized friction behaviour when compared to their respective base oils, except on full film lubrication, on this lubrication regimen COF depends upon the base oil viscosity, oils with high viscosities present higher COF values when compared with their respective grease, on the other hand base oils whose viscosity is lower present an optimized friction behaviour comparing to grease.

When a greases loses bled oil, the friction behaviour is thickener-controlled, this means that the more base oil is lost, the more influence the thickener will have on lubrication. It was possible to conclude that Lithium thickened greases, produce less friction on a dry state, which indicates that higher thickener concentrations might be favorable when using a lithium based grease. It was also observed that the thickener concentration may not be of great importance on clay thickened greases, since both dry and standard grease showed similar friction behaviours. The same was verified for polymer thickened grease, under full and mixed film lubrication, however when this grease is under boundary film lubrication,

a higher thickener concentration increases friction.

An additional parameter was formulated, S_{PR} (5.2), which allows Stribeck curves to be plotted using measurements with different surface roughness. The use of this parameter is more expeditious then using Λ, since less calculus are required.

6.2 Future Work

For future works, greases formulated with different thickener types/morphologies than those addressed in this work must be tested and these thickeners morphology and properties must be studied, in order to perceive the thickener's influence on the grease film thickness build-up and friction behaviour. It would be also appropriate to test greases formulated with the same thickener but with different base oils, in order to understand how the base oil-thickener interaction affects grease lubrication.

S_{PR} has a potential of including geometry effects on the Stribeck curves, however this potential was not tested on this work. This potential has to be further investigated on the future.

A study of how surface indentations influence the film thickness build-up was also initiated, however it was not presented in this work since it was on early stages and no measurements were conducted. This study has to be continued, in the near future.

References

[1] S. Hurley, P.M. Cann, and H.A. Spikes. Lubrication and reflow properties of thermally aged greases. *Tribology Transactions*, 43(1):9–14, 2000. doi: 10.1080/10402000008982305.

[2] P.M. Cann, B. P. Williamson, R. C. Coy, and H. A. Spikes. The behaviour of greases in elastohydrodynamic contacts. *Journal of Physics D: Applied Physics*, 25(1A): A124–A132, 1992.

[3] Walter H. Bauer, Alfred P. Finkelstein, and Stephen E. Wiberley. Flow properties of lithium stearate-oil model greases as functions of soap concentration and temperature. *ASLE Transactions*, 3(2):215–224, 1960.

[4] P.M. Cann. Understanding grease lubrication. *Tribology Series*, 31:573–581, 1996.

[5] Hui Cen, Piet M. Lugt, and Guillermo Morales-Espejel. On the film thickness of grease-lubricated contacts at low speeds. *Tribology transactions*, 57(4):668–678, 2014.

[6] Daming Dong and Xianglin Qian. A theory of elastohydrodynamic grease-lubricated line contact based on a refined rheological model. *Tribology international*, 21(5): 261–267, 1988.

[7] Z. Yang and X. Qian. A solution to grease lubricated ehd film thickness in an elliptical rolling contact. In *ImechE Conference Publication*, volume 1, pages 97–104, 1987.

[8] Xiaobin Lu and M.M. Khonsari. An experimental investigation of grease-lubricated journal bearings. *Journal of Tribology*, 129(1):84–90, 2007.

[9] Yanshuang Wang and Boyuan Yang. An investigation into grease behavior in thermal ehl circular contacts. *Tribology transactions*, 49(3):449–453, 2006.

[10] Henrik Åström, Ove Isaksson, and Erik Höglund. Video recordings of an ehd point contact lubricated with grease. *Tribology International*, 24(3):179–184, 1991.

[11] P.O. Larsson, Roland Larsson, Alexei Jolkin, and Olov Marklund. Pressure fluctuations as grease soaps pass through an ehl contact. *Tribology international*, 33(3): 211–216, 2000.

[12] M. Kaneta, T. Ogata, Y. Takubo, and M. Naka. Effects of a thickener structure on grease elastohydrodynamic lubrication films. *Proceedings of the Institution of Mechanical Engineers, Part J: Journal of Engineering Tribology*, 214(4):327–336, 2000.

[13] Duncan Dowson. *History of tribology*. Addison-Wesley Longman Limited, 1979.

[14] W.F. Parish. *Lubricants*, volume 14. 1929.

[15] Ian M. Hutchings. Leonardo da vinci's studies of friction. *Wear*.

[16] Isaac Newton. Principia (1687). *Translated by Andrew Motte*, 1729, 2004.

[17] Beauchamp Tower. First report on friction experiments. *Proceedings of the institution of mechanical engineers*, 34(1):632–659, 1883.

[18] Osborne Reynolds. On the theory of lubrication and its application to mr. beauchamp tower's experiments, including an experimental determination of the viscosity of olive oil. *Proceedings of the Royal Society of London*, 40(242-245):191–203, 1886.

[19] A. Meldahl. Contribution to the theory of the lubrication of gears and of the stressing of the lubricated flanks of gear teeth. *Brown Boveri Rev*, 28(11):374–382, 1941.

[20] MA Ertel. Hydrodynamic calculation of lubricated contact for curvilinear surfaces. *Proceedings of CNIITMASh*, pages 1–64, 1945.

[21] A.N. Grubin, I. E. Vinogradova, and K. F. Ketova. *Investigation of the contact of machine components*. Central Scientific Research Institute for Technology and Mechanical Engineering, 1949.

[22] Alfred Ivanovich Petrusevich. *Principal Conclusions from Contact-hydrodynamic Theory of Lubrication*. Associated Technical Services, 1951.

[23] Duncan Dowson and Gordon Robert Higginson. *Elasto-hydrodynamic lubrication: the fundamentals of roller and gear lubrication*, volume 23. Pergamon Press, 1966.

[24] James J. Kauzlarich and J.A. Greenwood. Elastohydrodynamic lubrication with herschel-bulkley model greases. *ASLE transactions*, 15(4):269–277, 1972.

[25] B. J. Hamrock and D. Dowson. Isothermal elastohydrodynamic lubrication of point contacts: Part i —theoretical formulation. *International Journal of Solids and Structures*, 41(3-4):223 – 229, 1976. doi: http://dx.doi.org/10.1115/1.3452801.

[26] B. J. Hamrock and D. Dowson. Isothermal elastohydrodynamic lubrication of point contacts: Part ii — elipcity parameter results. *International Journal of Solids and Structures*, 41(3-4):375–383, 1976. doi: http://dx.doi.org/10.1115/1.3452801.

[27] B. J. Hamrock and D. Dowson. Isothermal elastohydrodynamic lubrication of point contacts: Part iii — fully flooded results. *International Journal of Solids and Structures*, 41(3-4):264–276, 1976. doi: http://dx.doi.org/10.1115/1.3452801.

[28] B. J. Hamrock and D. Dowson. Isothermal elastohydrodynamic lubrication of point contacts: Part iv - starvation results. *International Journal of Solids and Structures*, 41(3-4):15–23, 1976. doi: http://dx.doi.org/10.1115/1.3452801.

[29] V. V. Sinitsyn. *The Choice and Application of Plastic Greases*. 1974.

[30] Wilfried Dresel et al. *Lubricants and lubrication*. John Wiley & Sons, 2007.

[31] R.F. Crouch and A. Cameron. 'viscosity-temperature equations for lubricants. *J. Inst. Pet*, 47:307–313, 1961.

[32] ASTM Standard. D341-09: Standard practice for viscosity-temperature charts for liquid petroleum products. *Annual Book of ASTM Standards. West Conshohocken: ASTM International*, 2009.

[33] Cornelis Julianus Adrianus Roelands. Correlational aspects of the viscosity-temperature-pressure relationship of lubricating oils. 1966.

[34] Bernard J. Hamrock and Duncan Dowson. Ball bearing lubrication: the elastohydrodynamics of elliptical contacts. 1981.

[35] Theodore L Bergman and Frank P Incropera. *Fundamentals of heat and mass transfer*. John Wiley & Sons, 2011.

[36] Piet M. Lugt. A review on grease lubrication in rolling bearings. *Tribology Transactions*, 52(4):470–480, 2009.

[37] S. R. Schmid B. J. Hamrock and B. Jacobson. *Fundamentals of fluid film lubrication*. 2nd edition edition, 2004.

[38] B. J. Hamrock and D. Dowson. Elastohydrodynamic lubrication of elliptical contacts for materials of low elastic modulus: Part i - fully flooded conjunctions. *International Journal of Solids and Structures*, 41(3-4):236–245, 1978.

[39] B. J. Hamrock and D. Dowson. Elastohydrodynamic lubrication of elliptical contacts for materials of low elastic modulus: Part ii - starved conjunctions. *International Journal of Solids and Structures*, 41(3-4):92–98, 1978.

[40] International Div. *A&D SV10 User's Manual*. A&D Company, Limited, Tokyo, 2016 edition.

[41] H. Vogel. The law of the relation between the viscosity of liquids and the temperature. *Physikalische Zeitschrift*, 22:645 – 646, 1921.

[42] P. W. Gold, A.Schmidt, H. Dicke, J. Loss, and C. Aßmann. Viscosity-pressure-temperature behaviour of mineral and synthetic oils. *Journal of Synthetic Lubrication*, 18(1):51–79, 2001. doi: 10.1002/jsl.3000180105.

[43] D. J. Carré, R. Bauer, and P. D. Fleischauer. Chemical analysis of hydrocarbon grease from spin bearing tests. *ASLE Transactions*, 26(4):475–480, 1983. doi: 10.1080/05698198308981528.

[44] P. M. Cann and H. A. Spikes. In lubro studies of lubricants in ehd contacts using ftir absorption spectroscopy. *Tribology Transactions*, 34(2):248–256, 1991. doi: 10.1080/10402009108982033.

[45] P.M. Cann, M.N. Webster, J.P. Doner, V. Wikstrom, and P. Lugt. Grease degradation in r0f bearing tests. *Tribology Transactions*, 50(2):187–197, 2007. doi: 10.1080/10402000701261003.

[46] K.D.O. Jackson. A guide to identifying common inorganic fillers and activators using vibrational spectroscopy. *Journal of natural rubber research*, 12(2):102–111, 1997.

[47] W.A. Zhang, D.Z. Chen, H.Y. Xu, X.F. Shen, and Y.E. Fang. Influence of four different types of organophilic clay on the morphology and thermal properties of polystyrene/clay nanocomposites prepared by using the gamma-ray irradiation technique. *European Polymer Journal*, 39(12):2323 – 2328, 2003. doi: http://dx.doi.org/10.1016/j.eurpolymj.2003.08.006.

[48] Jyh Ming Hwu, George J. Jiang, Zong Ming Gao, Wei Xie, and Wei Ping Pan. The characterization of organic modified clay and clay-filled pmma nanocomposite. *Journal of Applied Polymer Science*, 83(8):1702–1710, 2002. doi: 10.1002/app.10093.

[49] Xinyuan Zhu, Deyue Yan, and Yapeng Fang. In situ ftir spectroscopic study of the conformational change of isotactic polypropylene during the crystallization process. *The Journal of Physical Chemistry B*, 105(50):12461–12463, 2001. doi: 10.1021/jp012165f.

[50] David Gonçalves. Polymer greases: Film thickness, friction and thermal degradation, 2016.

[51] F. Gao, R. K. Leach, J. Petzing, and J. M. Coupland. Surface measurement errors using commercial scanning white light interferometers. *Measurement Science and Technology*, 19(1), 2008.

[52] Roy T. Blunt. White light interferometry - a production worthy technique for measuring surface roughness on semiconductor wafers. pages 59–62, 2006.

[53] Robert Windecker and Hans J. Tiziani. Optical roughness measurements using extended white-light interferometry. *Optical Engineering*, 38(6):1081–1087, 1999. doi: 10.1117/1.602154.

[54] James J. Kauzlarich and J. A. Greenwood. Elastohydrodynamic lubrication with herschel-bulkley model greases. *ASLE transactions*, 15(4):269–277, 1972.

[55] R.W.M. Wardle, R.C. Coy, P.M. Cann, and H.A. Spikes. An 'in lubro' study of viscosity index improvers in end contacts. *Lubrication Science*, 3(1):45–62, 1990.

[56] A.R. Wilson. The relative thickness of grease and oil films in rolling bearings. *Proceedings of the Institution of Mechanical Engineers*, 193(1):185–192, 1979.

[57] H. S. Cheng. A numerical solution of the elastohydrodynamic film thickness in an elliptical contact. *Journal of Lubrication Technology*, 92(1):155–161, 1970.

[58] RJ Chittenden, D Dowson, JF Dunn, and CM Taylor. A theoretical analysis of the isothermal elastohydrodynamic lubrication of concentrated contacts. i. direction of lubricant entrainment coincident with the major axis of the hertzian contact ellipse. In *Proceedings of the Royal Society of London A: Mathematical, Physical and Engineering Sciences*, volume 397, pages 245–269. The Royal Society, 1985.

[59] Bernard J. Hamrock, Steven R. Schmid, and B. O. Jacobson. *Fundamentals of fluid film lubrication*. CRC press, 2004.

[60] Scott Bair and Peter Kottke. Pressure-viscosity relationships for elastohydrodynamics. *Tribology transactions*, 46(3):289–295, 2003.

[61] Duncan Dowson and Gordon R. Higginson. *Elasto-hydrodynamic lubrication: international series on materials science and technology*, volume 23. 2014.

[62] P.K. Gupta, H.S. Cheng, D. Zhu, N.H. Forster, and J.B. Schrand. Viscoelastic effects in mil-l-7808-type lubricant, part i: analytical formulation. *Tribology transactions*, 35 (2):269–274, 1992.

[63] T.E. Tallian. On competing failure modes in rolling contact. *ASLE TRANSACTIONS*, 10(4):418–439, 1967.

[64] Harry van Leeuwen. The determination of the pressure—viscosity coefficient of a lubricant through an accurate film thickness formula and accurate film thickness measurements. *Proceedings of the Institution of Mechanical Engineers, Part J: Journal of Engineering Tribology*, 223(8):1143–1163, 2009.

[65] David Gonçalves. Polymer greases: Film thickness, friction and thermal degradation, 2016.

[66] Ivan Krupka, Scott Bair, Punit Kumar, M.M. Khonsari, and Martin Hartl. An experimental validation of the recently discovered scale effect in generalized newtonian ehl. *Tribology Letters*, 33(2):127–135, 2009.

[67] Ilya I Kudish, P Kumar, M Khonsari, M, and Scott Bair. Scale effects in generalized newtonian elastohydrodynamic films. *Journal of Tribology*, 130(4):041504, 2008.

[68] Siu-Yun Poon. An experimental study of grease in elastohydrodynamic lubrication. *Journal of Lubrication Technology*, 94(1):27–34, 1972.

[69] E.R. Booser and D.F. Wilcock. Minimum oil requirements of ball bearings. *Lubrication Engineering*, 9(3):140–143, 1953.

[70] Susan Rebecca Hurley. *Fundamental studies of grease lubrication in elastohydrodynamic contacts.* PhD thesis, Imperial College London (University of London), 2001.

[71] L Bordenet, G Dalmaz, J-P Chaomleffel, and F Vergne. A study of grease film thicknesses in elastorheodynamic rolling point contacts. *Lubrication Science*, 2(4): 273–284, 1990.

[72] Nicola De Laurentis, Amir Kadiric, Piet Lugt, and Philippa Cann. The influence of bearing grease composition on friction in rolling/sliding concentrated contacts. *Tribology International*, 94:624–632, 2016.

[73] IDPN Couronné, P Vergne, D Mazuyer, N Truong-Dinh, and D Girodin. Effects of grease composition and structure on film thickness in rolling contact. *Tribology transactions*, 46(1):31–36, 2003.

[74] N. Fang, L. Chang, M.N. Webster, and A. Jackson. A non-averaging method of determining the rheological properties of traction fluids. *Tribology international*, 33 (11):751–760, 2000.

[75] G.E. Morales-Espejel and A.W. Wemekamp. An engineering approach on sliding friction in full-film, heavily loaded lubricated contacts. *Proceedings of the Institution of Mechanical Engineers, Part J: Journal of Engineering Tribology*, 218(6):513–527, 2004.

[76] José A Brandão, Mathilde Meheux, Fabrice Ville, Jorge H.O. Seabra, and Jorge Castro. Comparative overview of five gear oils in mixed and boundary film lubrication. *Tribology International*, 47:50–61, 2012.

[77] Scott Bair and W.O. Winer. A rheological model for elastohydrodynamic contacts based on primary laboratory data. *ASME, Transactions, Journal of Lubrication Technology*, 101:258–264, 1979.

[78] W.O. Winer. Shear strength measurements of lubricants at high pressure. *Journal of Lubrication Technology JULY*, 101:251, 1979.

[79] KL Johnson and JL Tevaarwerk. Shear behaviour of elastohydrodynamic oil films. In *Proceedings of the Royal Society of London A: Mathematical, Physical and Engineering Sciences*, volume 356, pages 215–236. The Royal Society, 1977.

[80] Richard Stribeck and M Schröter. *Die wesentlichen Eigenschaften der Gleit-und Rollenlager: Untersuchung einer Tandem-Verbundmaschine von 1000 PS*. Springer, 1903.

[81] José Brandão, Mathilde Meheux, Jorge H.O. Seabra, Fabrice Ville, and M.J.D. Castro. Traction curves and rheological parameters of fully formulated gear oils. *Proceedings of the Institution of Mechanical Engineers, Part J: Journal of Engineering Tribology*, 225(7):577–593, 2011.

[82] Charles J. Boner. *Manufacture and application of lubricating greases*. Reinhold, 1954.

[83] A.R. Lansdown. *Lubrication and lubricant selection*. Professional Engineering Pub., 2004.

[84] D ASTM. 288 (1961) annual book of astm standards. *ASTM, West Cinshohocken*.

[85] G.W. Mullett. Grease lubrication of rolling bearings. *Tribology*, 6(1):21–28, 1973.

[86] D. Gonçalves, Beatriz Graça, Armando V. Campos, J. Seabra, Johan Leckner, and René Westbroek. On the film thickness behaviour of polymer greases at low and high speeds. *Tribology International*, 90:435–444, 2015.

Appendix A

Graphic Results

Base Oils Results

Film Thickness

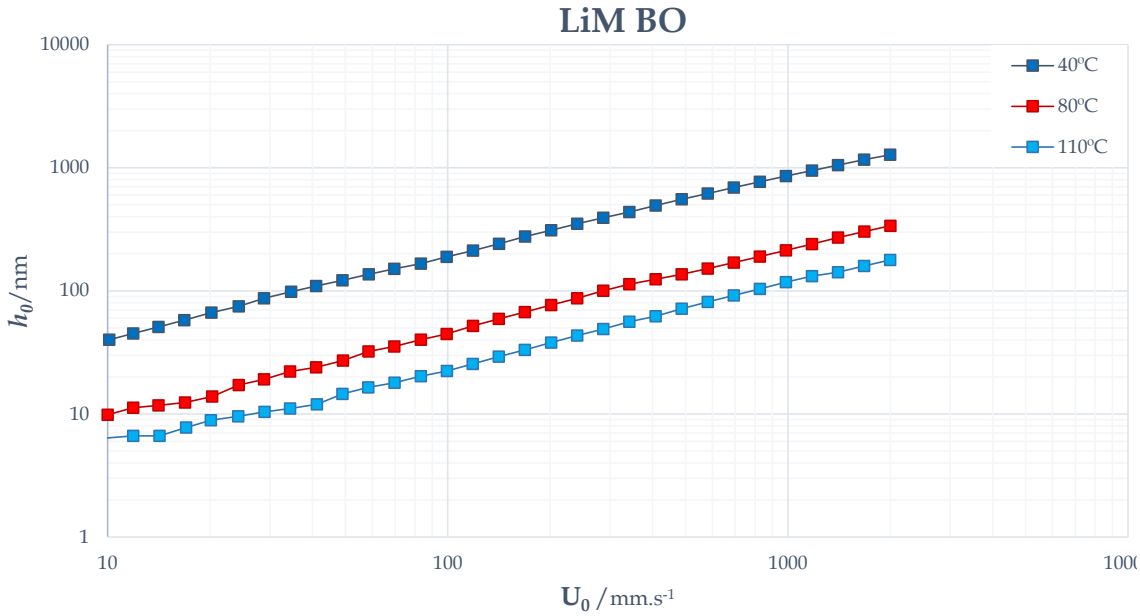


Figure A.1: LiM Base Oil Film Thickness

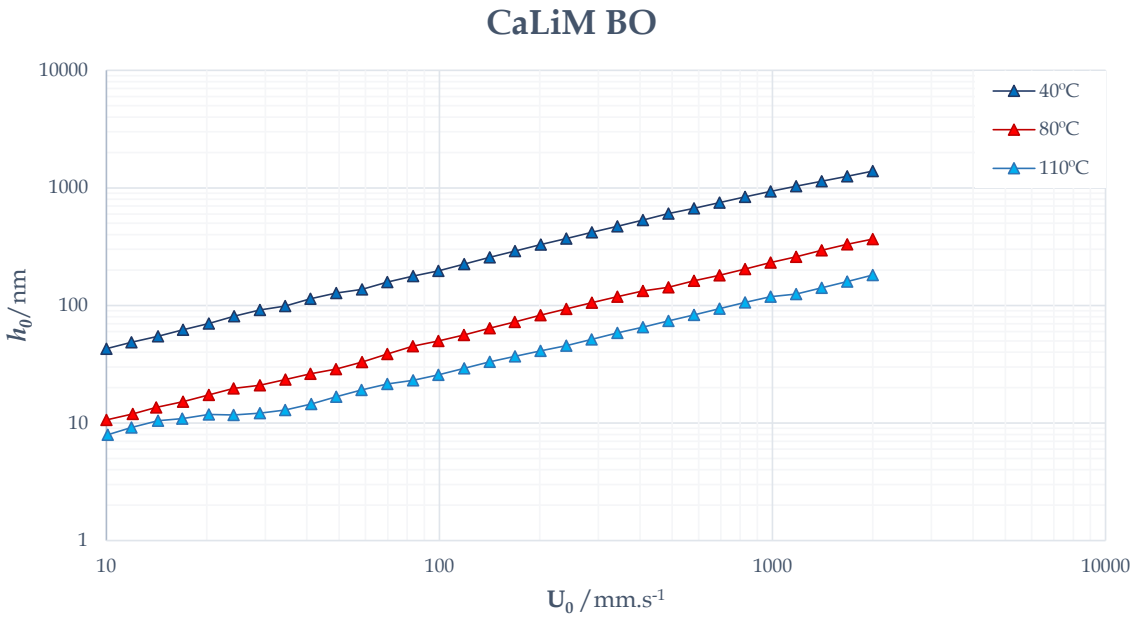


Figure A.2: CaLiM Base Oil Film Thickness

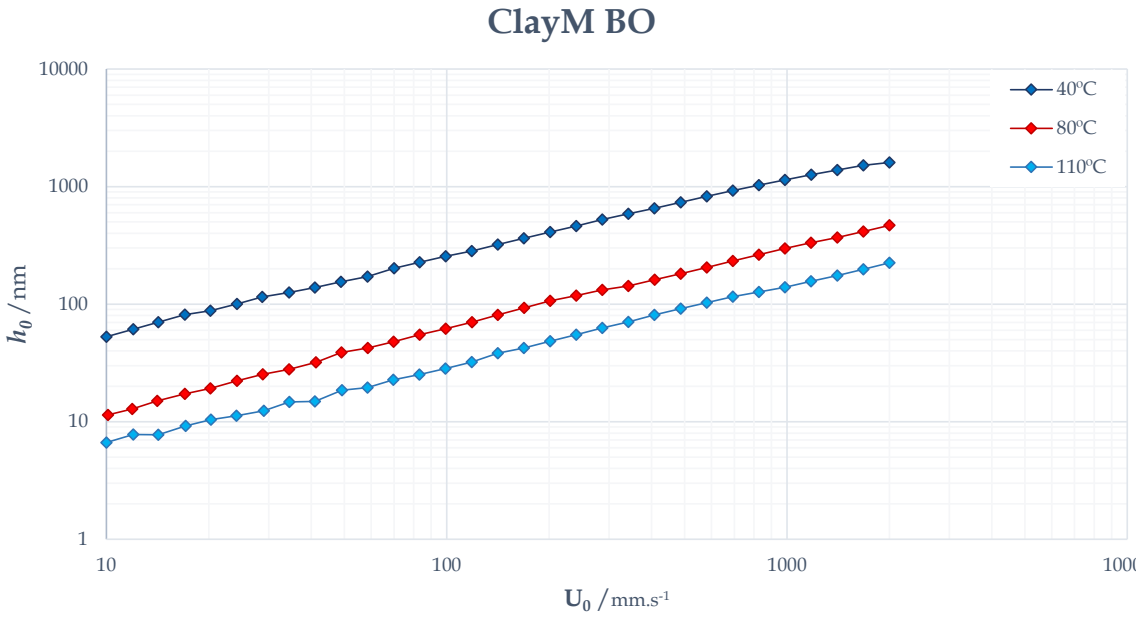


Figure A.3: ClayM Base Oil Film Thickness

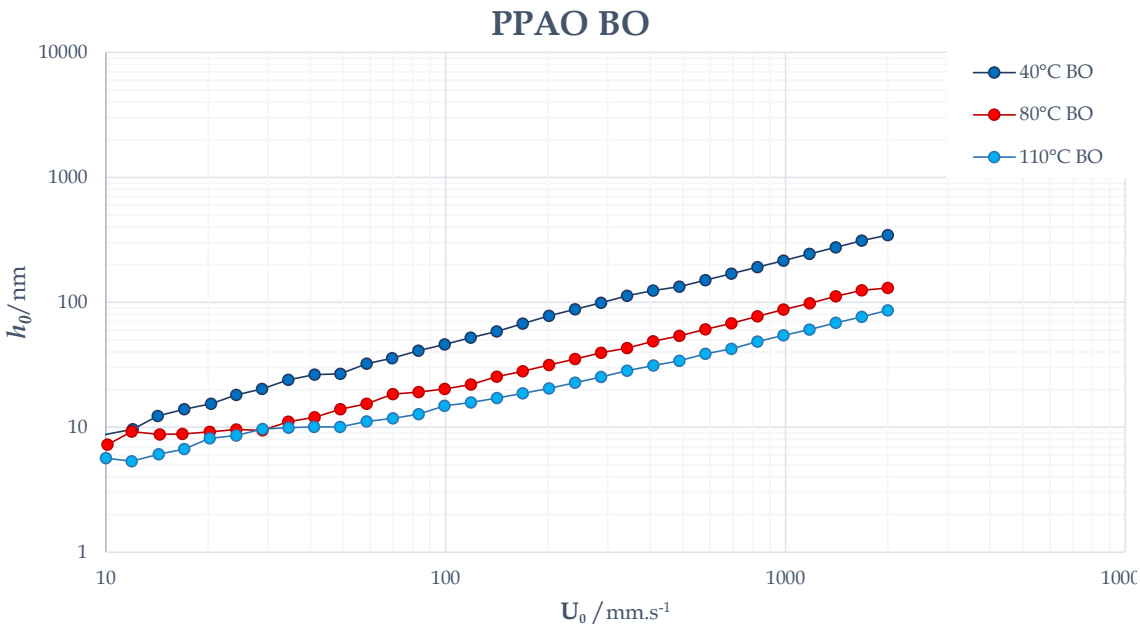


Figure A.4: PPAO Base Oil Film Thickness

Friction Results

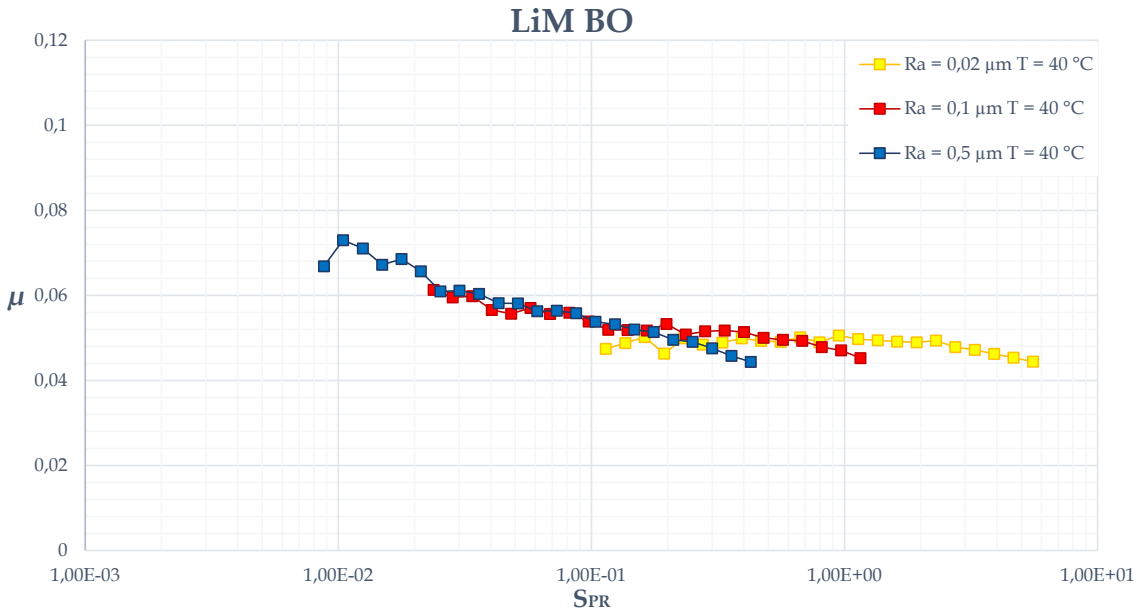


Figure A.5: LiM Base Oil Stribeck Curve T=40°C

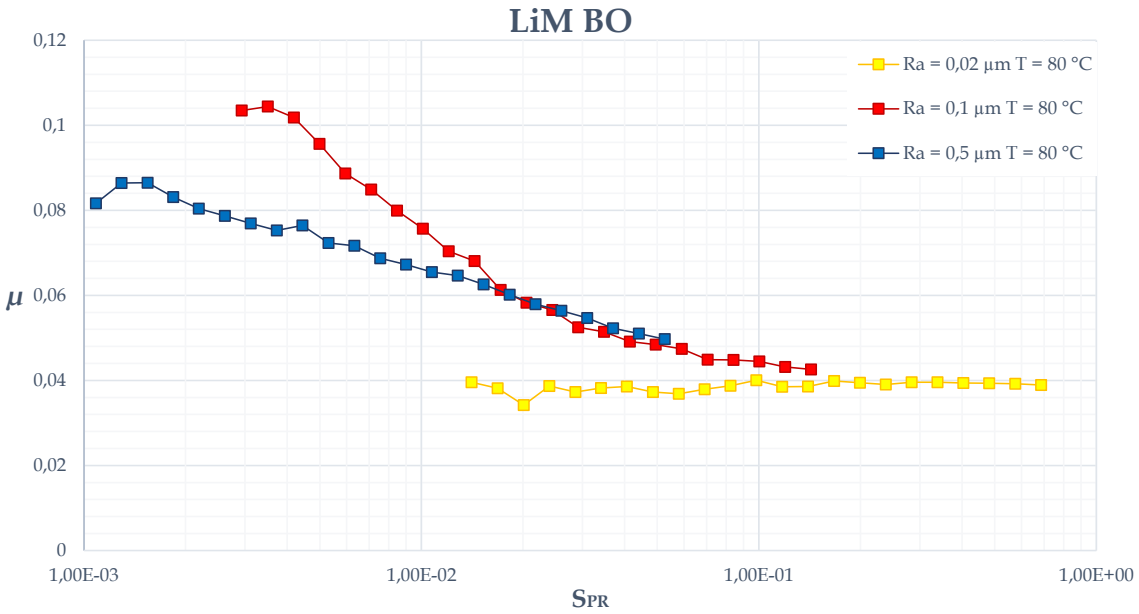


Figure A.6: LiM Base Oil Stribeck Curve T=80°C

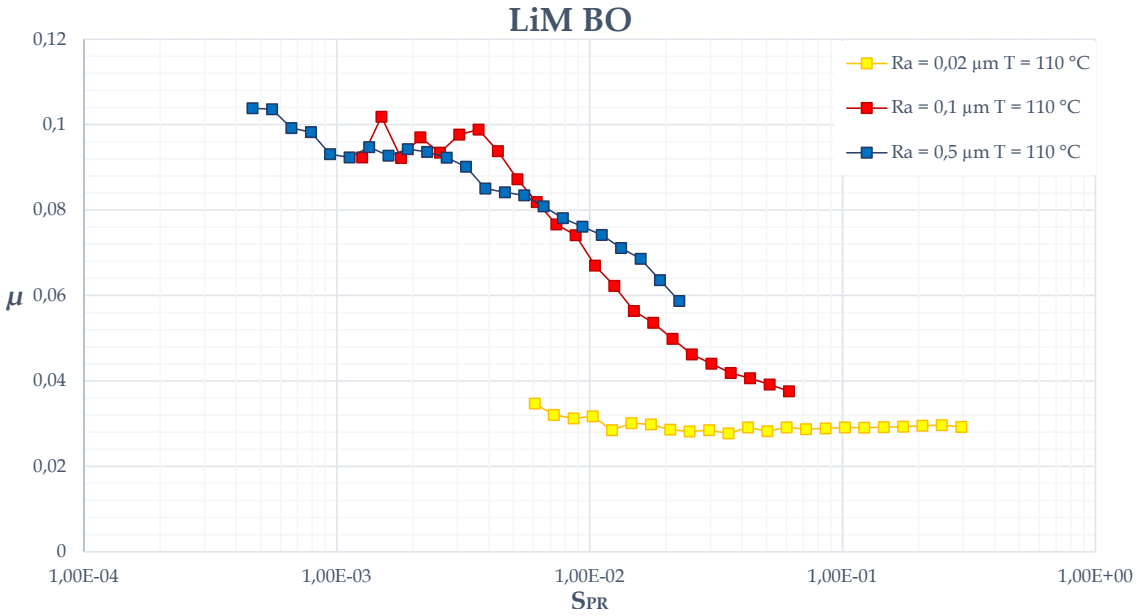


Figure A.7: LiM Base Oil Stribeck Curve T=110°C

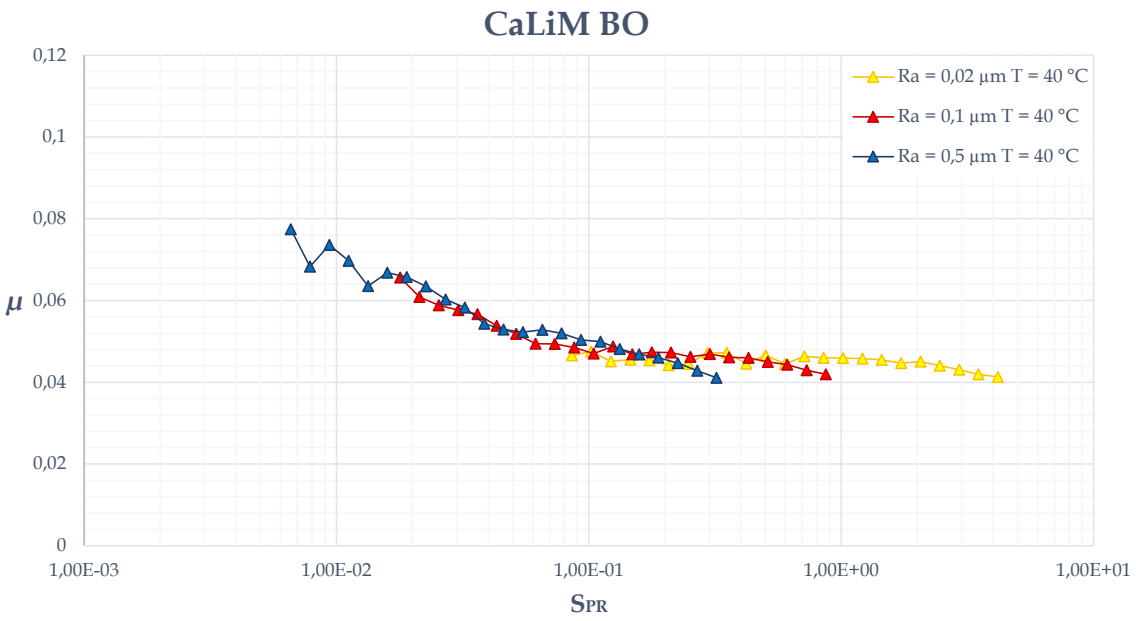


Figure A.8: CaLiM Base Oil Stribeck Curve T=40°C

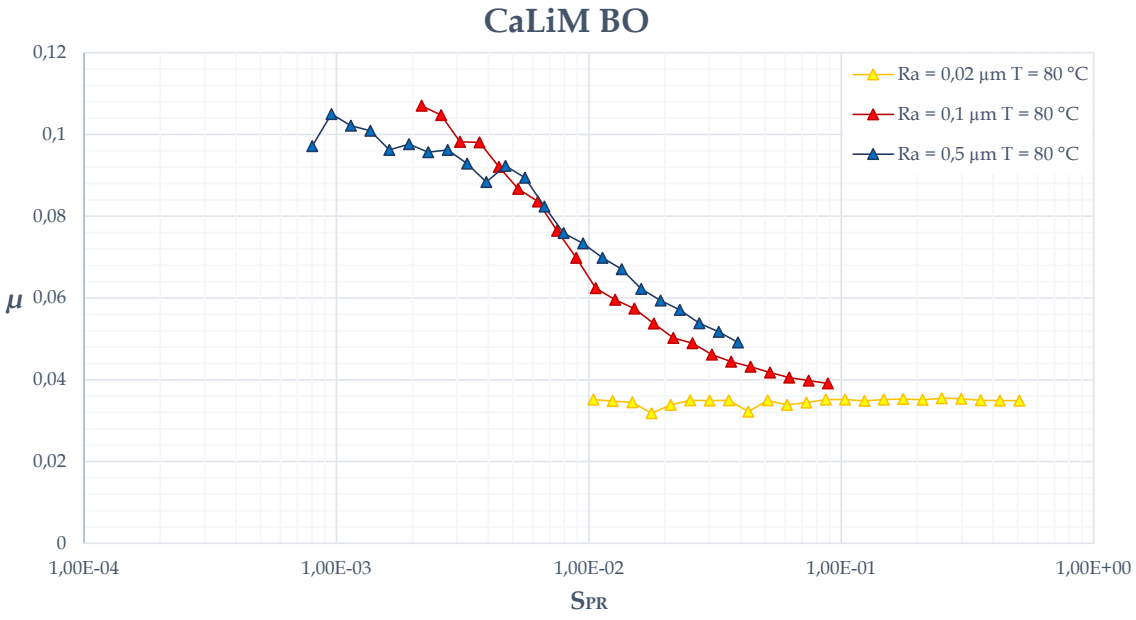


Figure A.9: CaLiM Base Oil Stribeck Curve T=80°C

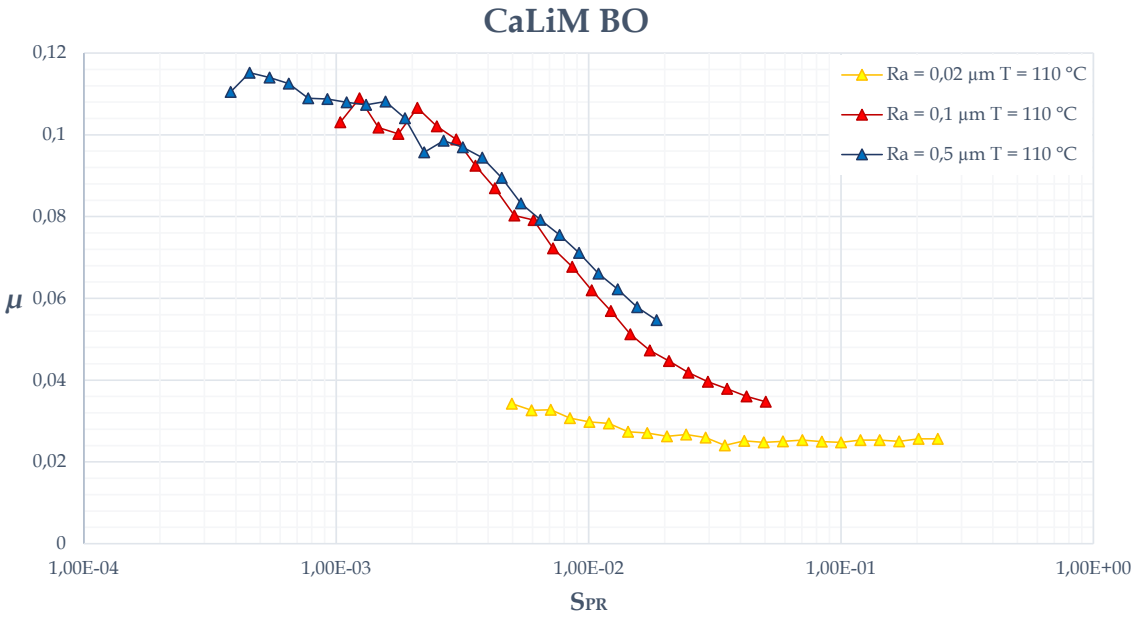


Figure A.10: CaLiM Base Oil Stribeck Curve T=110°C

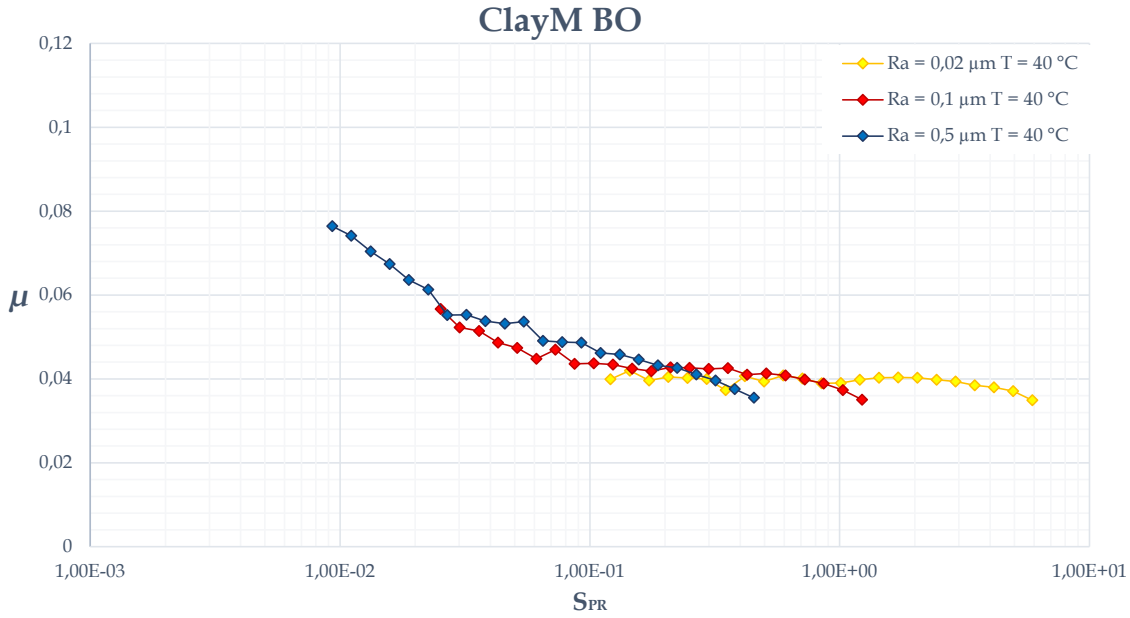


Figure A.11: ClayM Base Oil Stribeck Curve T=40°C

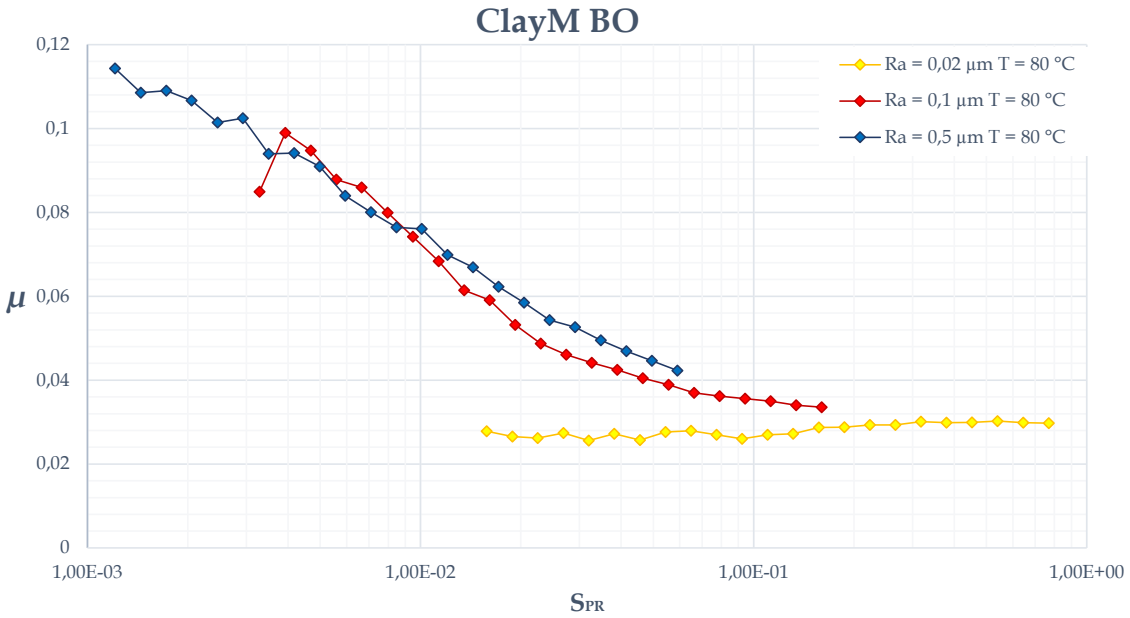


Figure A.12: ClayM Base Oil Stribeck Curve T=80°C

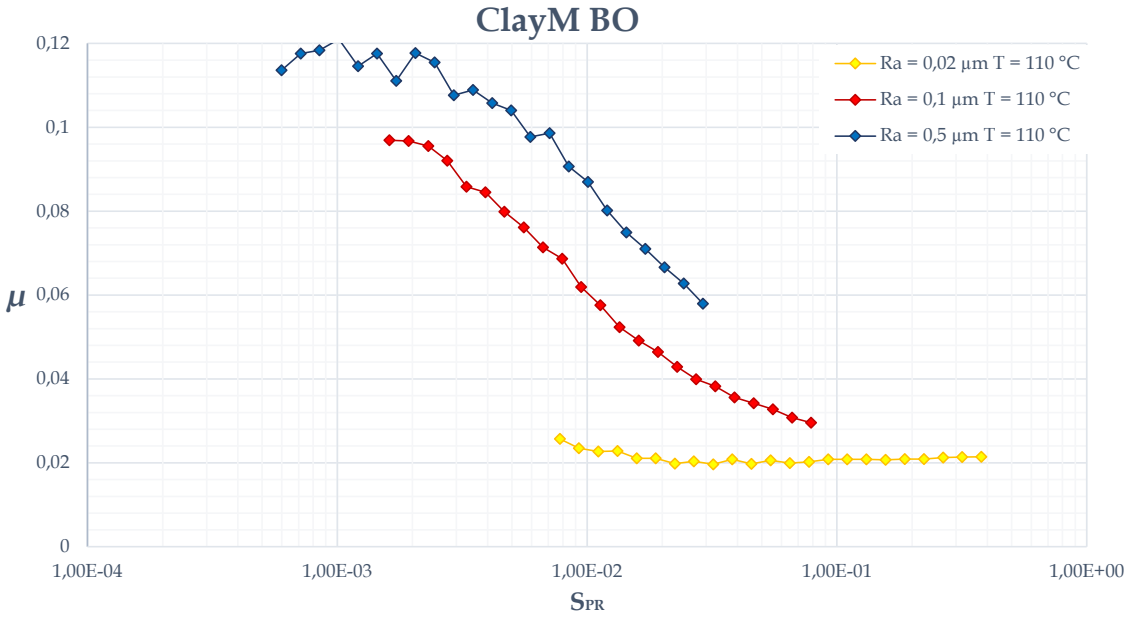


Figure A.13: ClayM Base Oil Stribeck Curve T=110°C

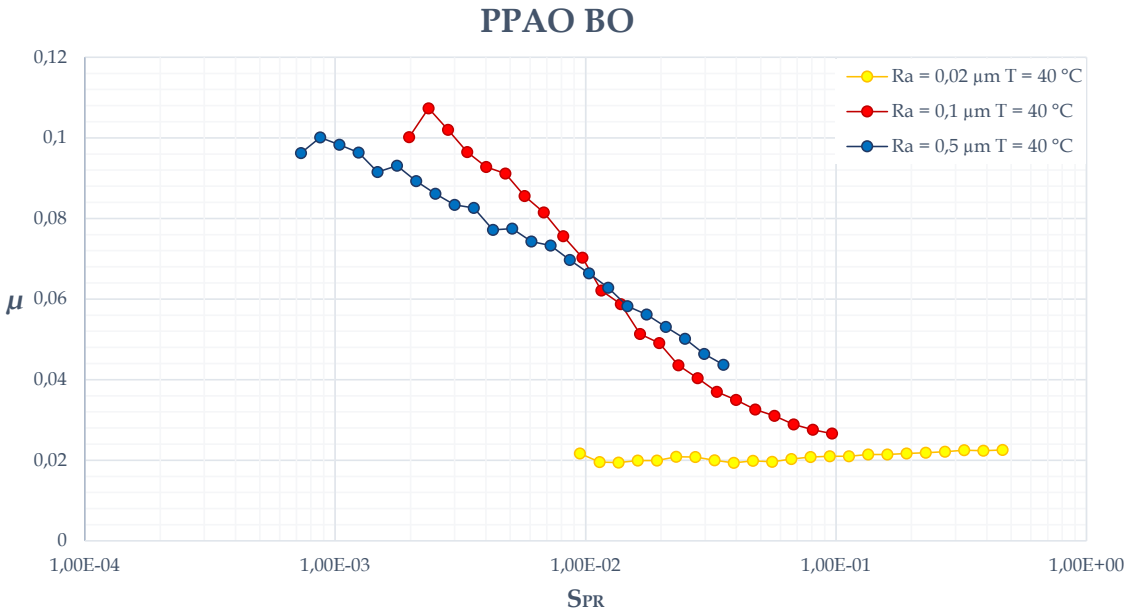


Figure A.14: PPAO Base Oil Stribeck Curve T=40°C

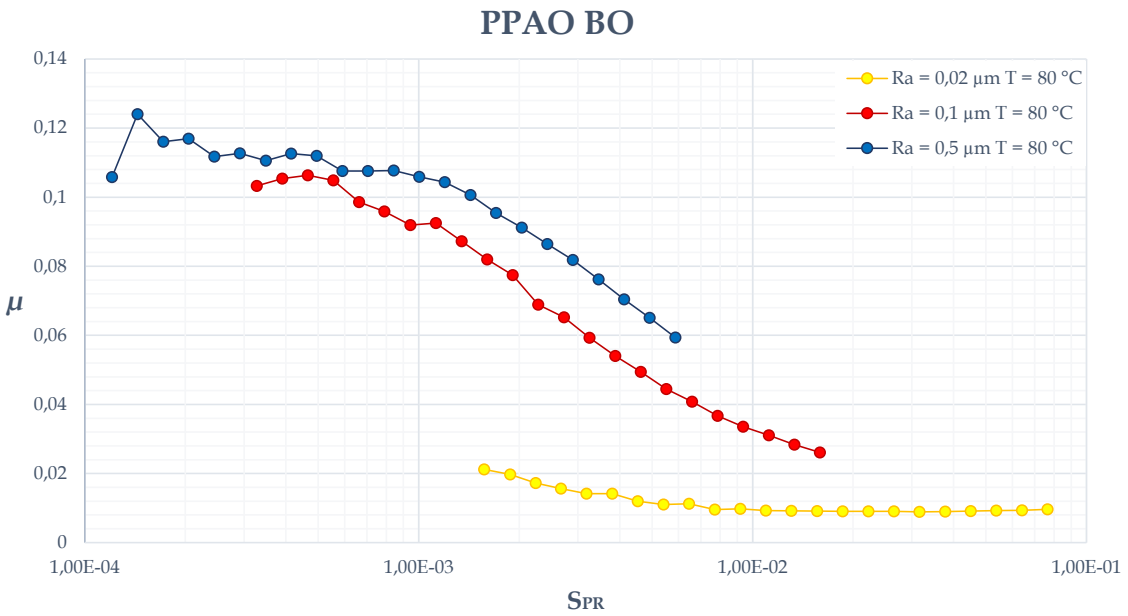


Figure A.15: PPAO Base Oil Stribeck Curve T=80°C

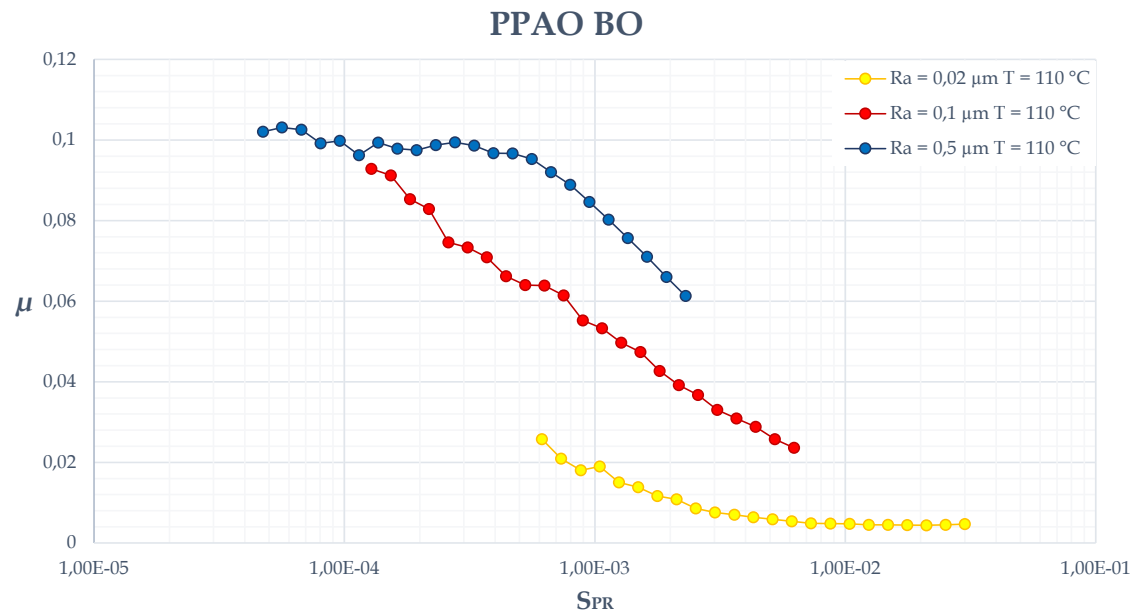


Figure A.16: PPAO Base Oil Stribeck Curve T=110°C

Grease Results

Film Thickness

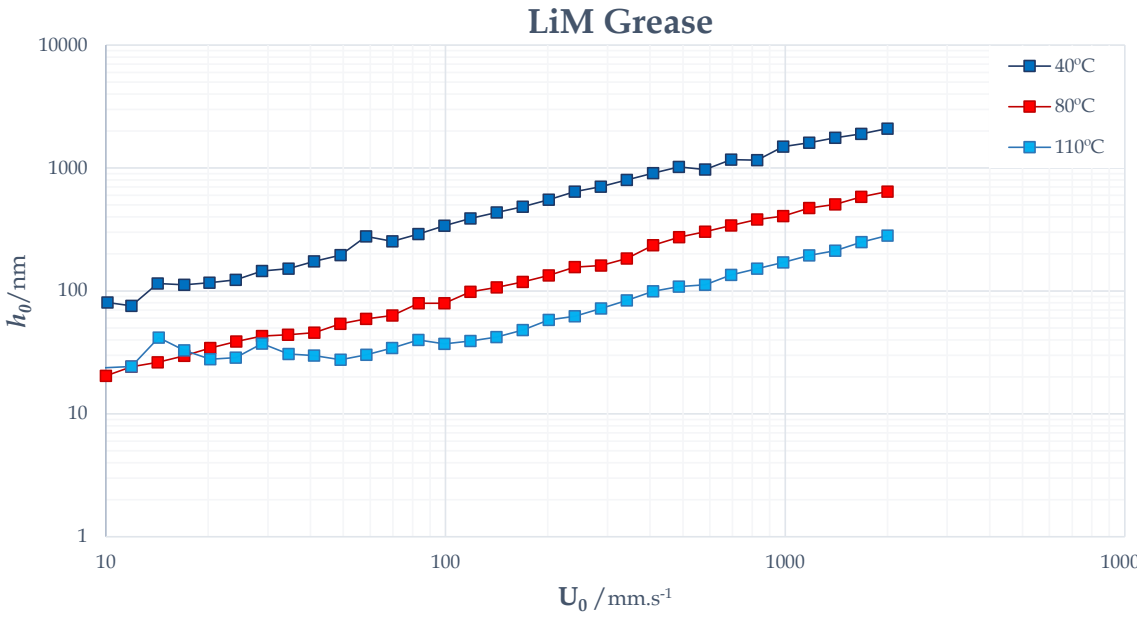


Figure A.17: LiM Grease Film Thickness

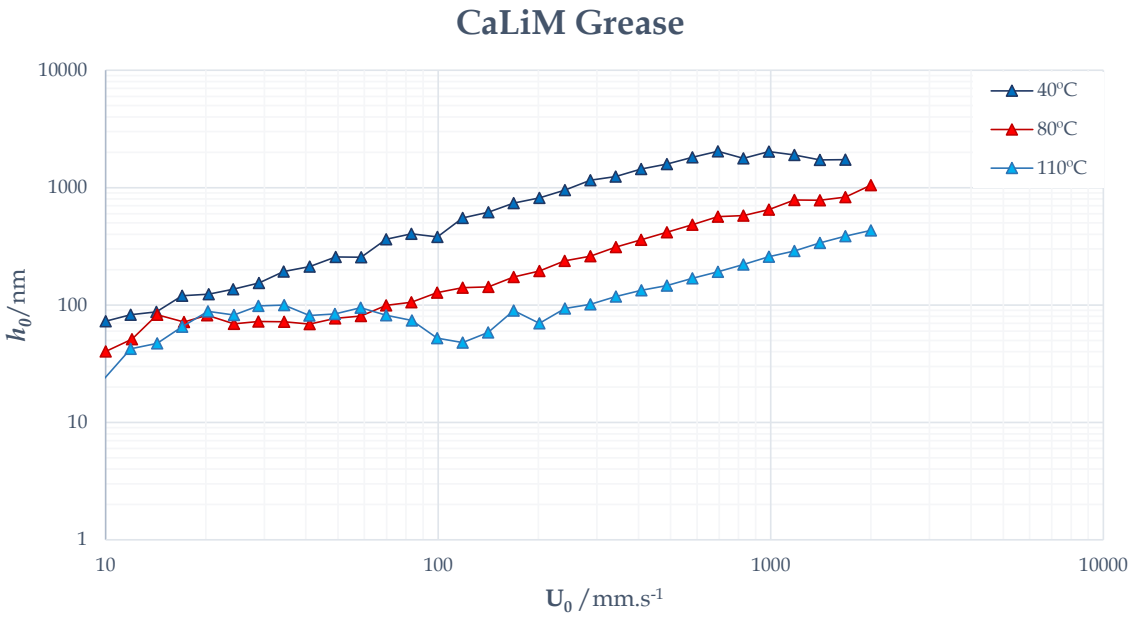


Figure A.18: CaLiM Grease Film Thickness

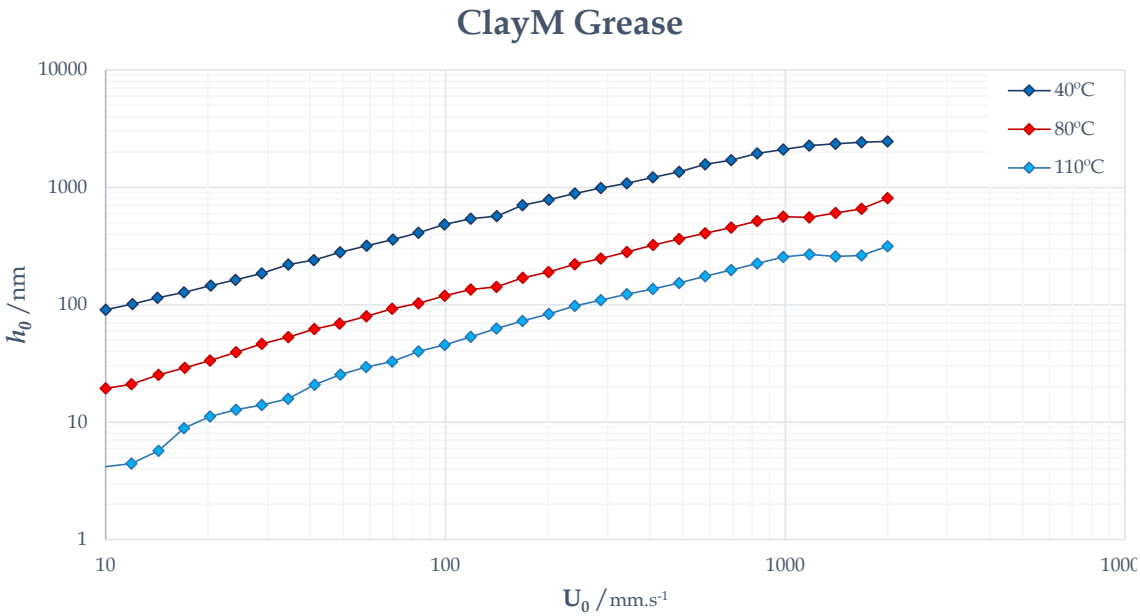


Figure A.19: ClayM Grease Film Thickness

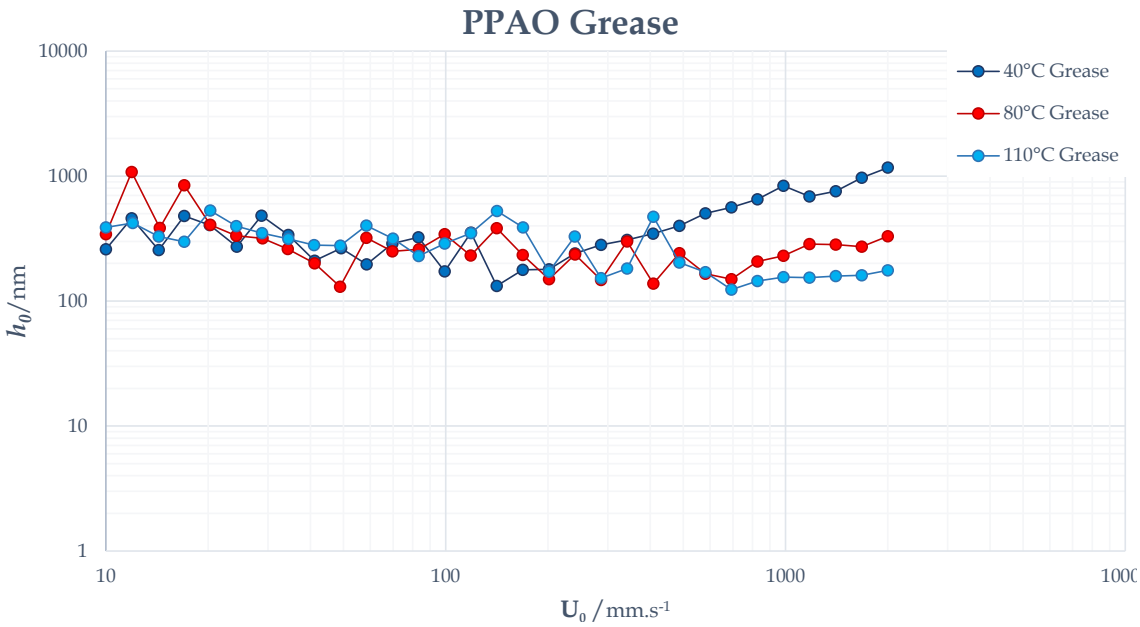


Figure A.20: PPAO Grease Film Thickness

Friction Results

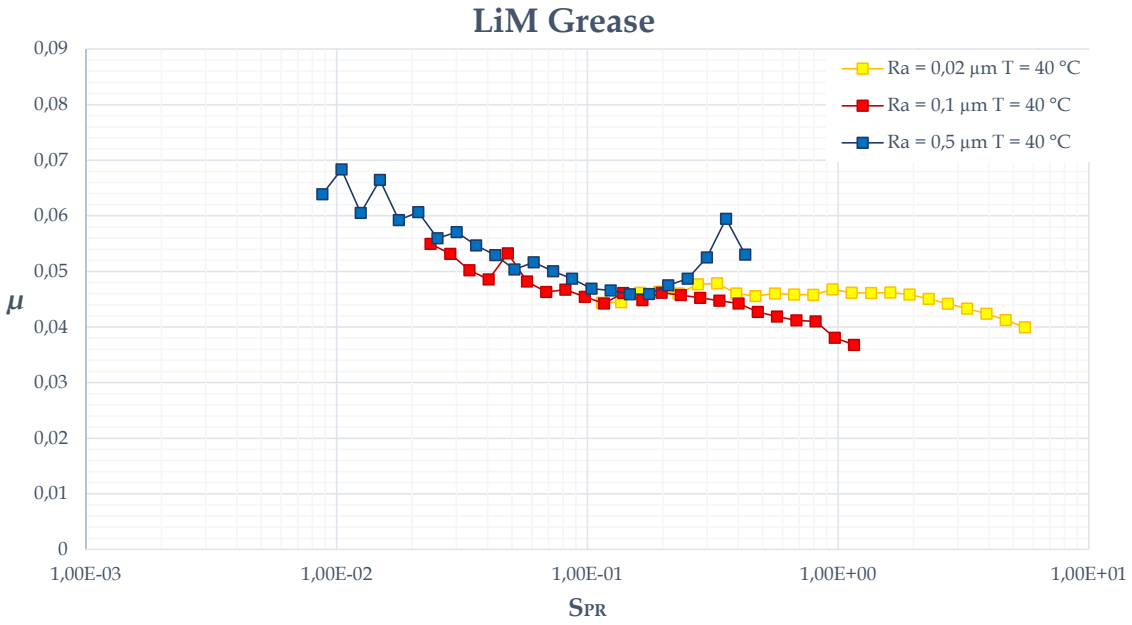


Figure A.21: LiM Grease Stribeck Curve T=40°C

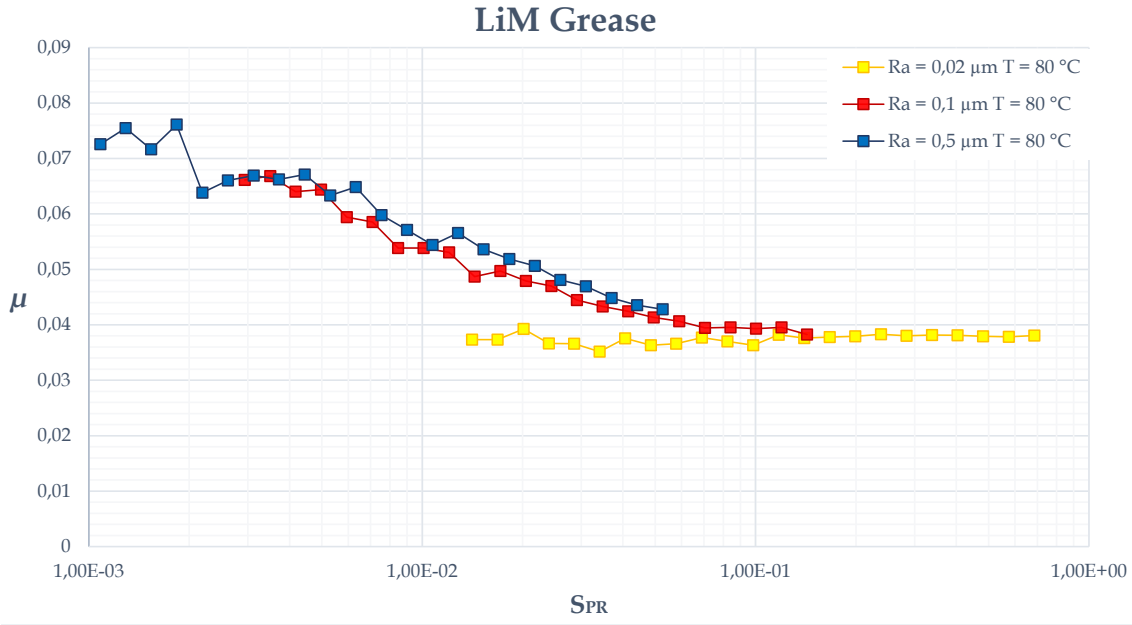


Figure A.22: LiM Grease Stribeck Curve T=80°C

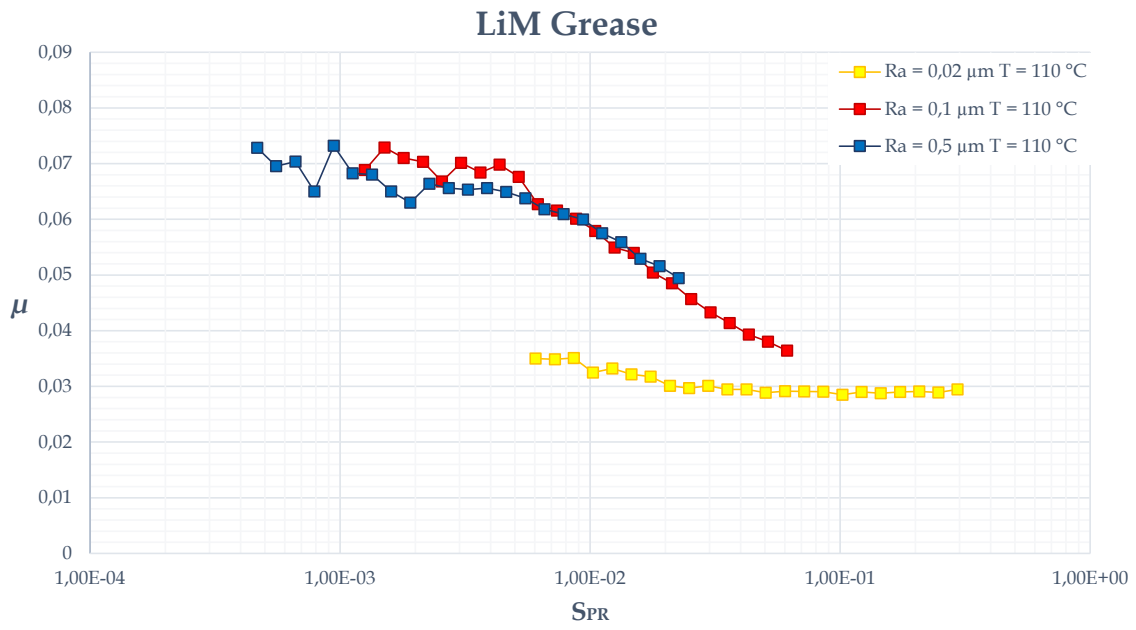


Figure A.23: LiM Grease Stribeck Curve T=110°C

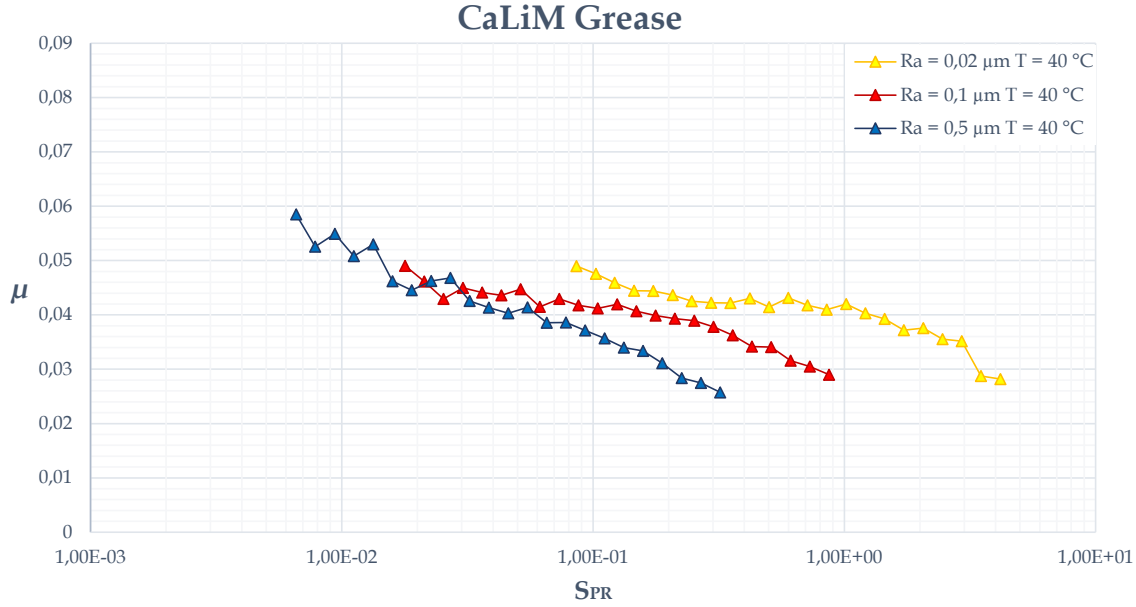


Figure A.24: CaLiM Grease Stribeck Curve T=40°C

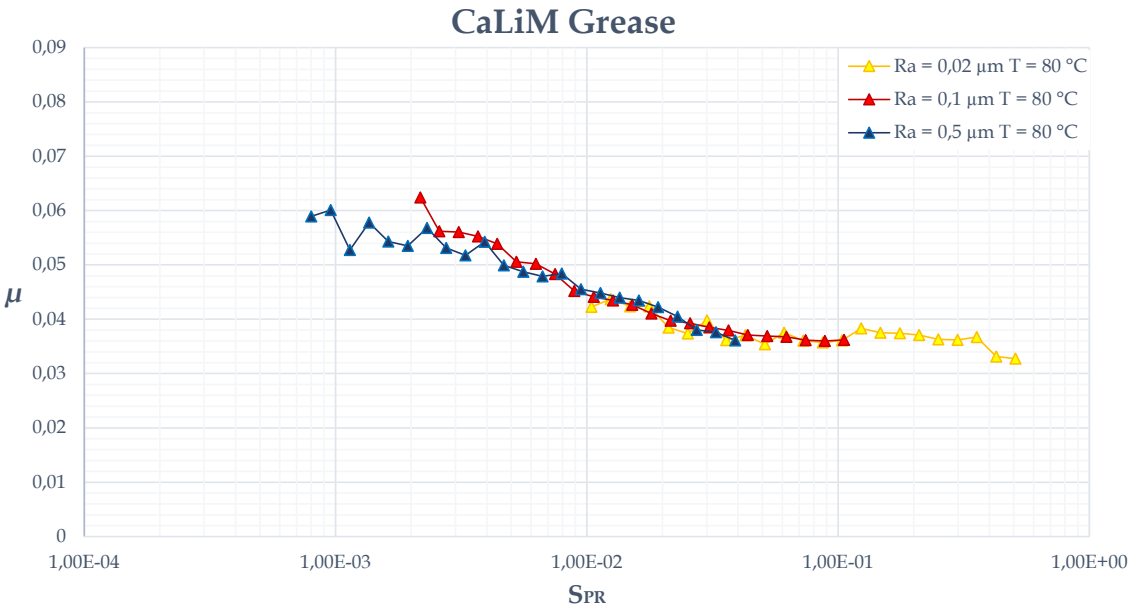


Figure A.25: CaLiM Grease Stribeck Curve T=80°C

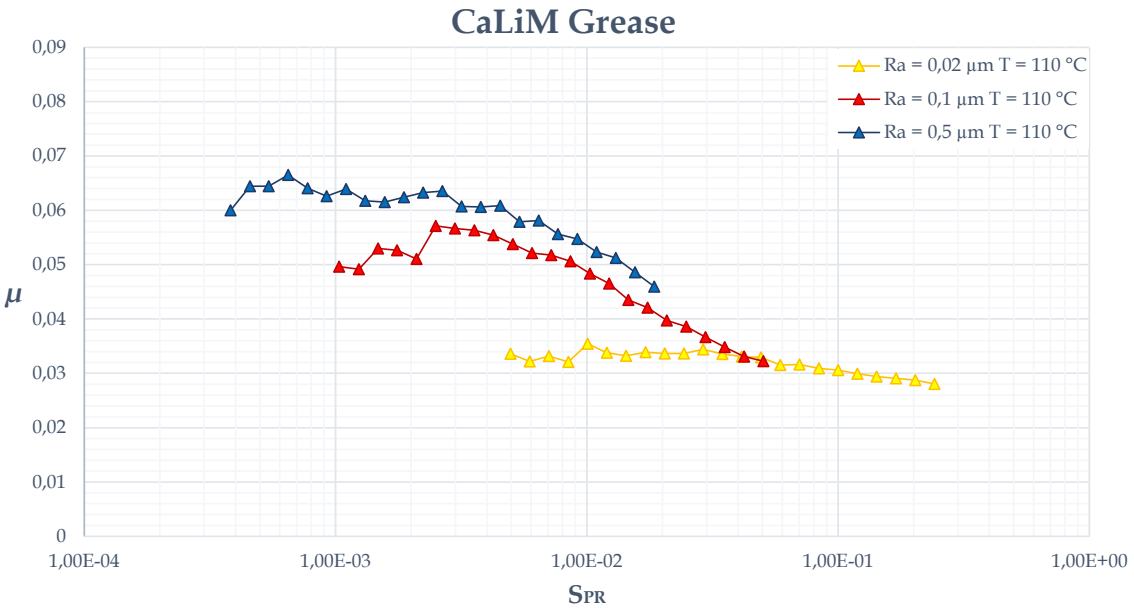


Figure A.26: CaLiM Grease Stribeck Curve T=110°C

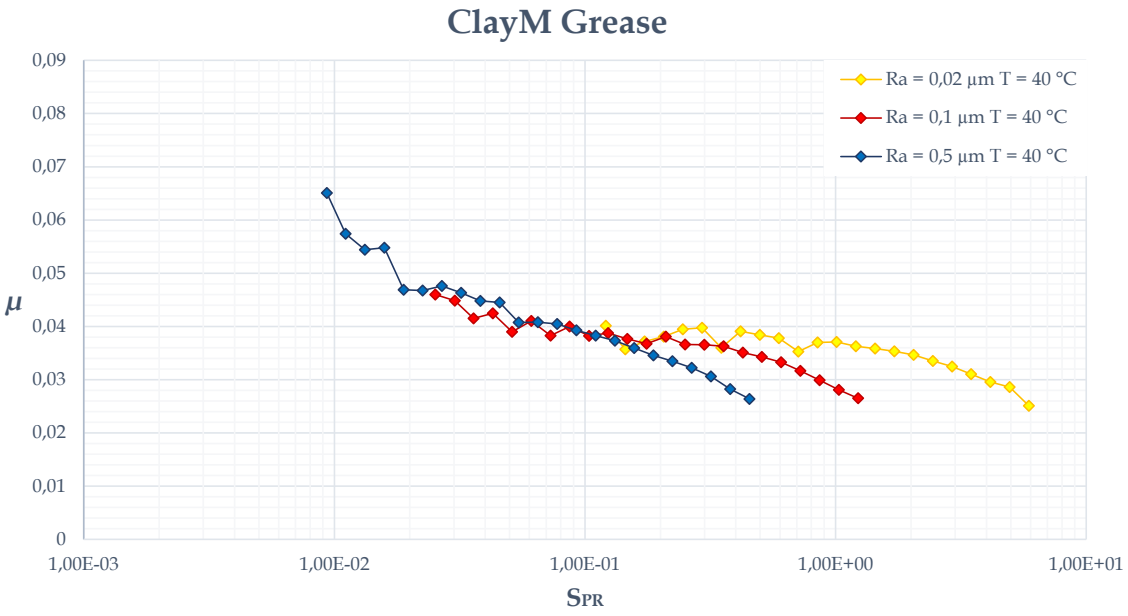


Figure A.27: ClayM Grease Stribeck Curve T=40°C

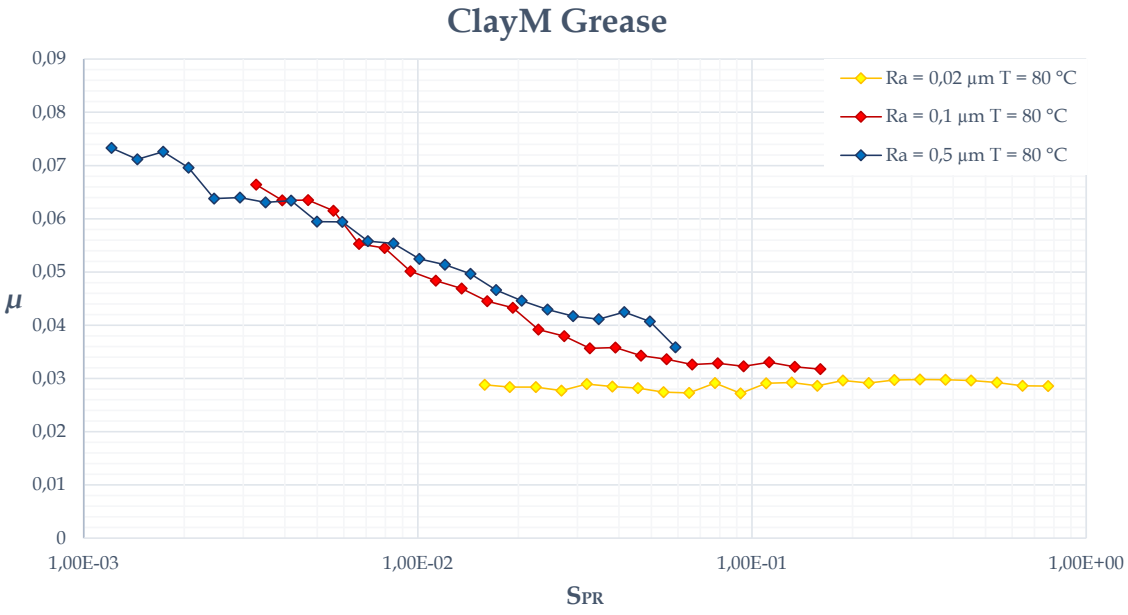


Figure A.28: ClayM Grease Stribeck Curve T=80°C

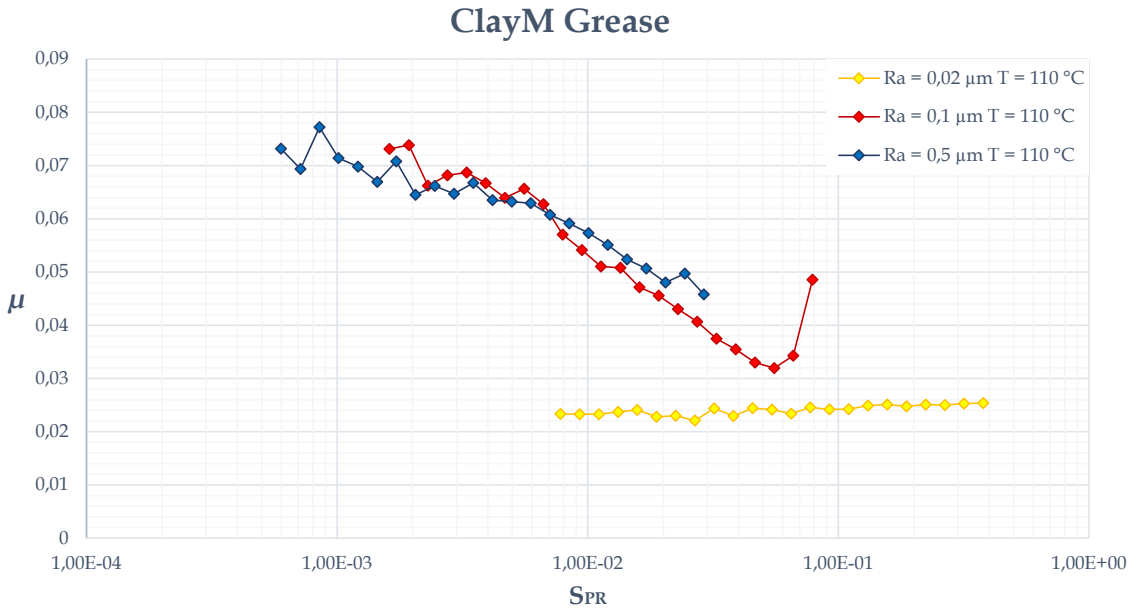


Figure A.29: ClayM Grease Stribeck Curve T=110°C

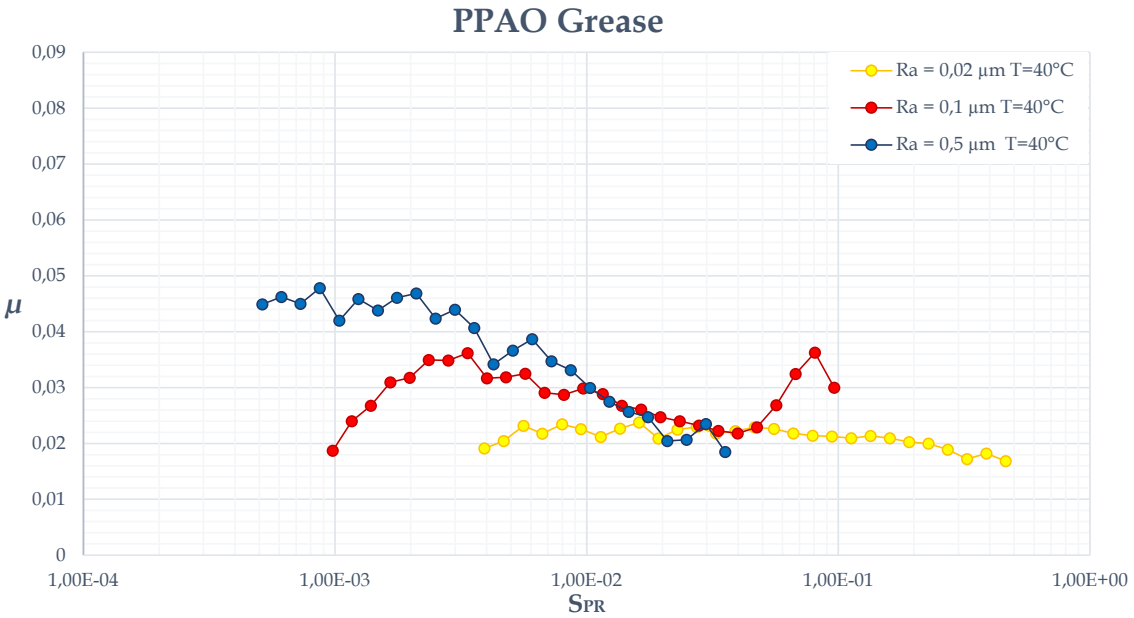


Figure A.30: PPAO Grease Stribeck Curve T=40°C

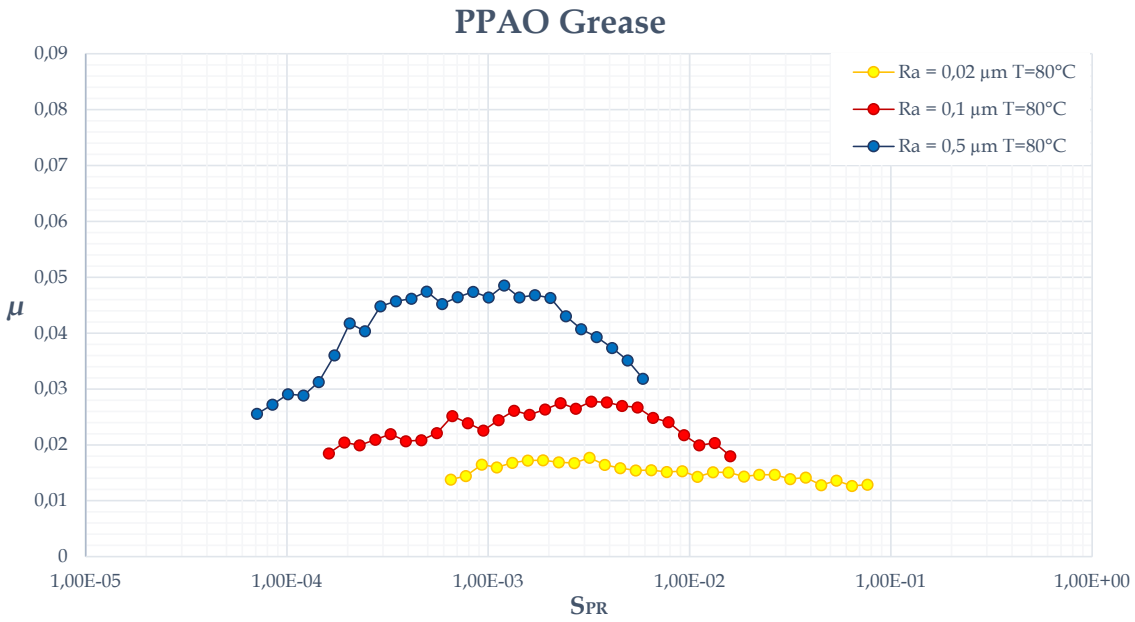


Figure A.31: PPAO Grease Stribeck Curve T=80°C

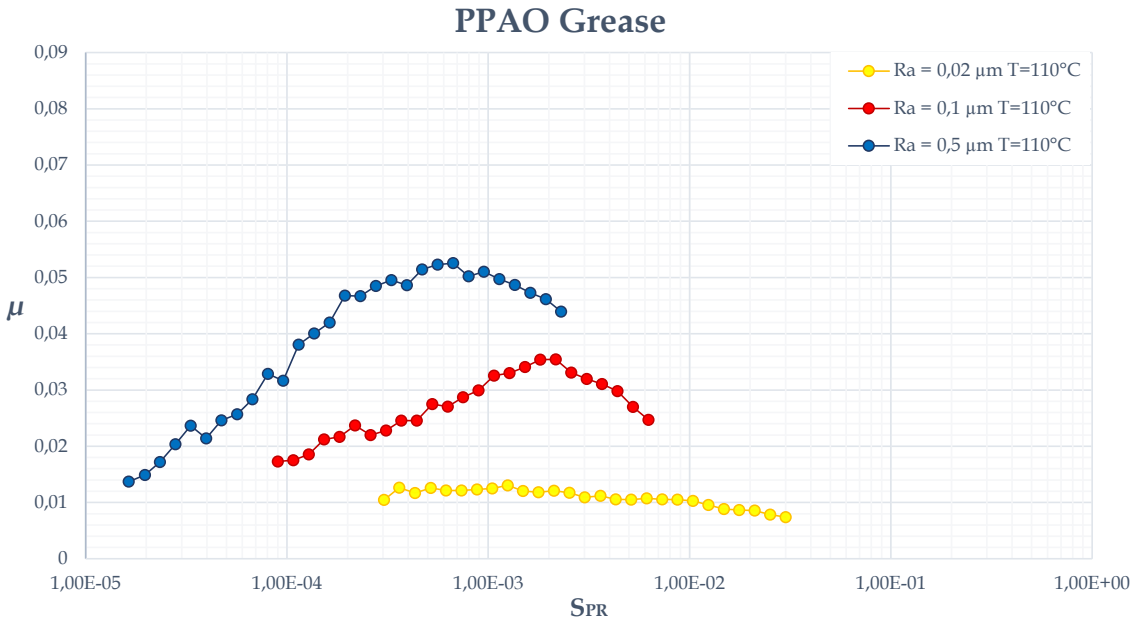


Figure A.32: PPAO Grease Stribeck Curve T=110°C

Dry Grease Friction Results

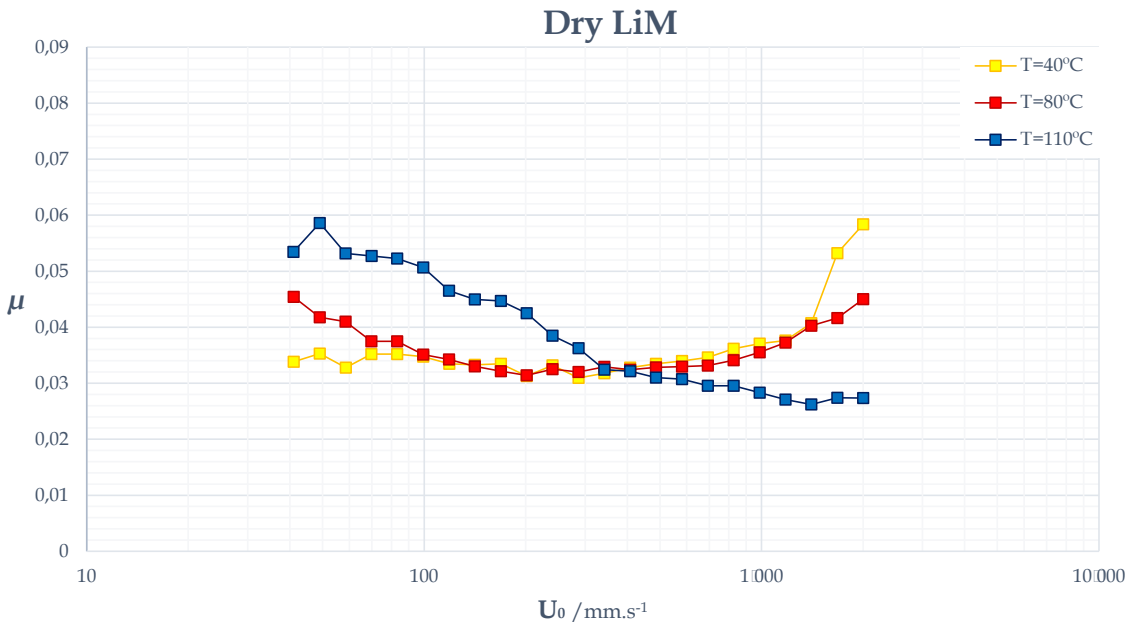


Figure A.33: LiM Dry Grease Stribeck Curve Ra=100 nm

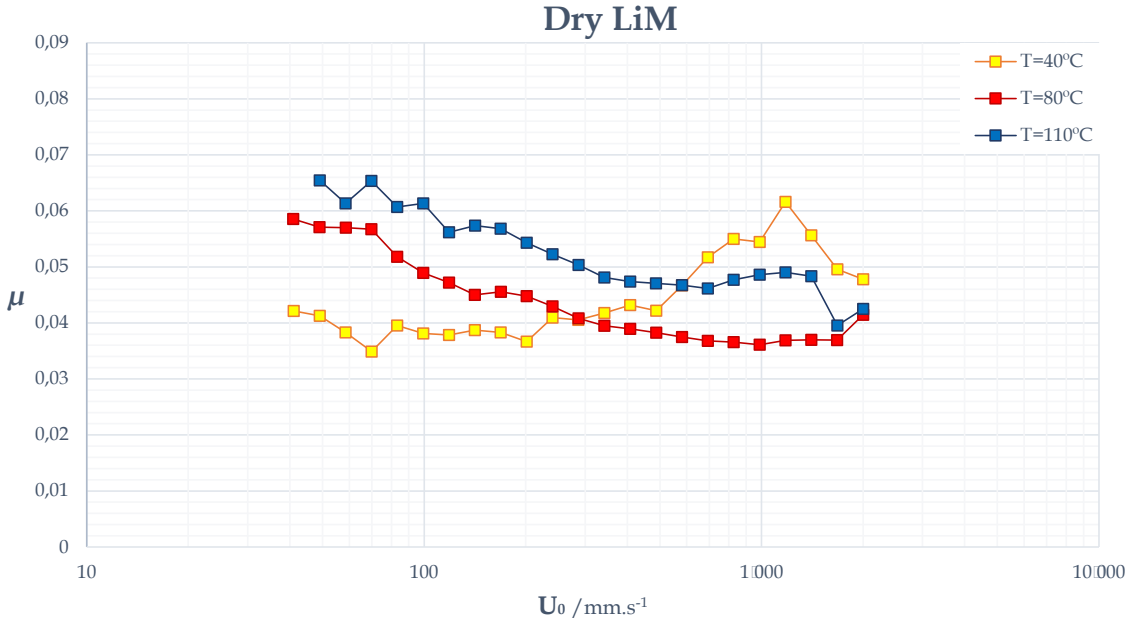


Figure A.34: LiM Dry Grease Stribeck Curve Ra=500 nm

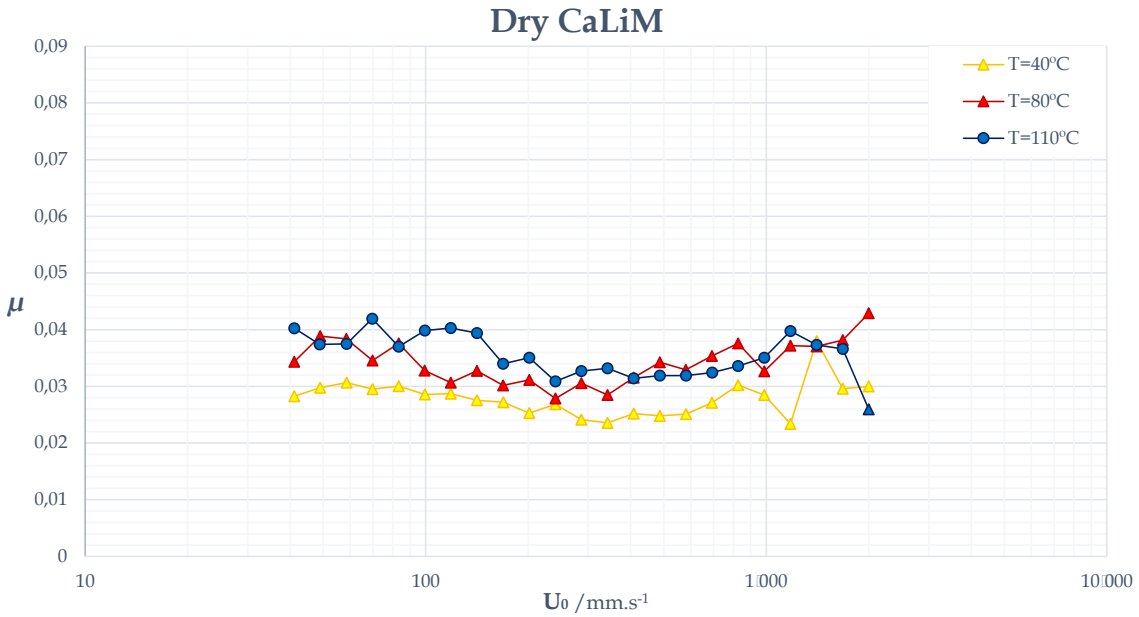


Figure A.35: CaLiM Dry Grease Stribeck Curve Ra=100 nm

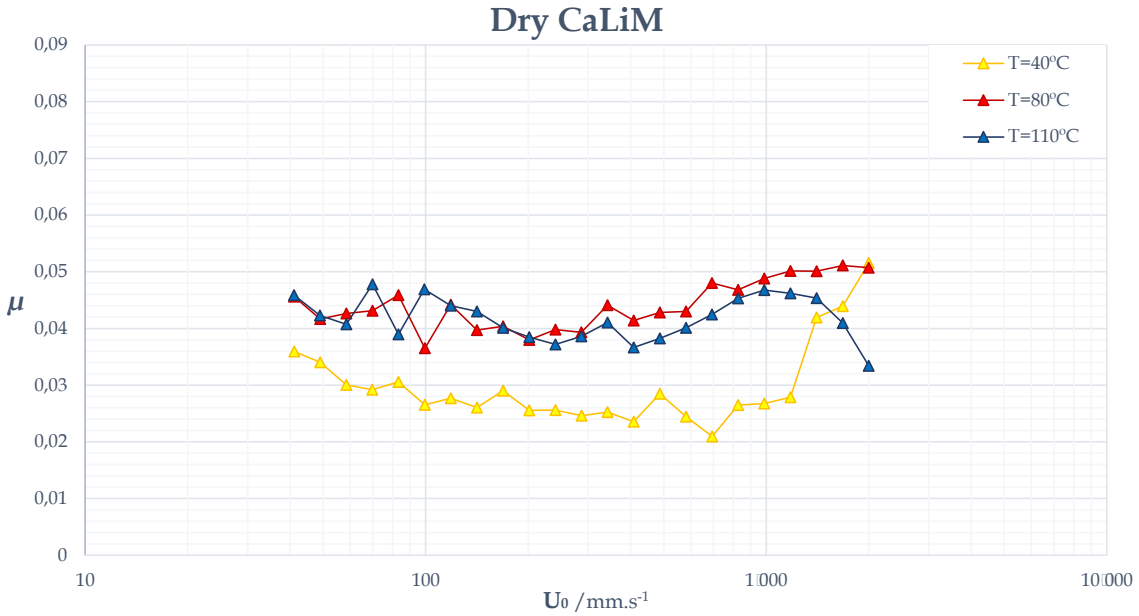


Figure A.36: CaLiM Dry Grease Stribeck Curve Ra=500 nm

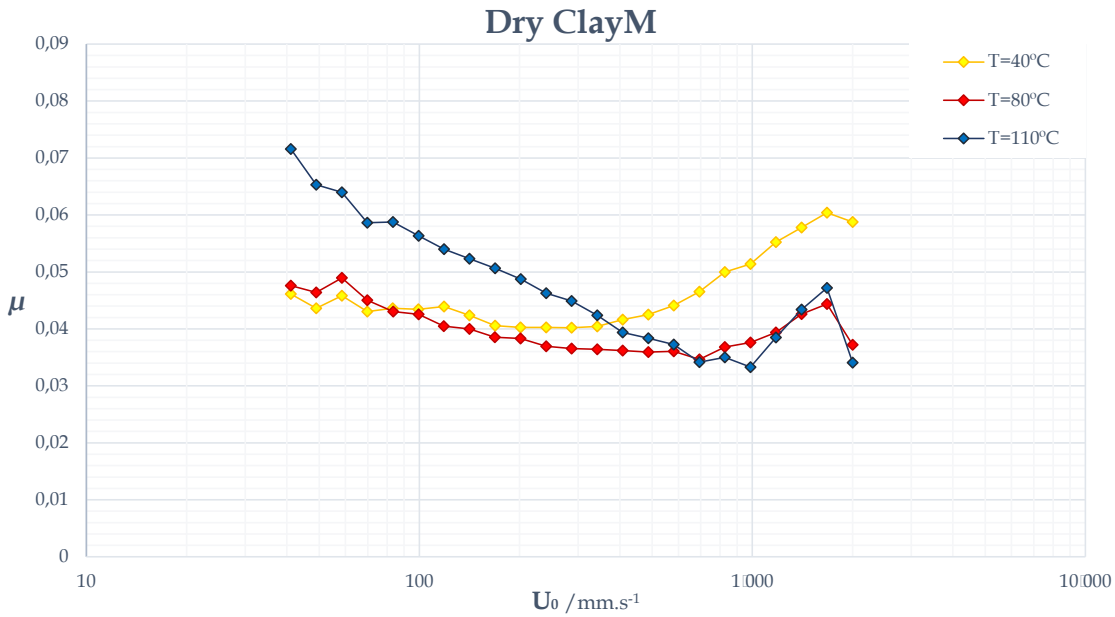


Figure A.37: ClayM Dry Grease Stribeck Curve Ra=100 nm

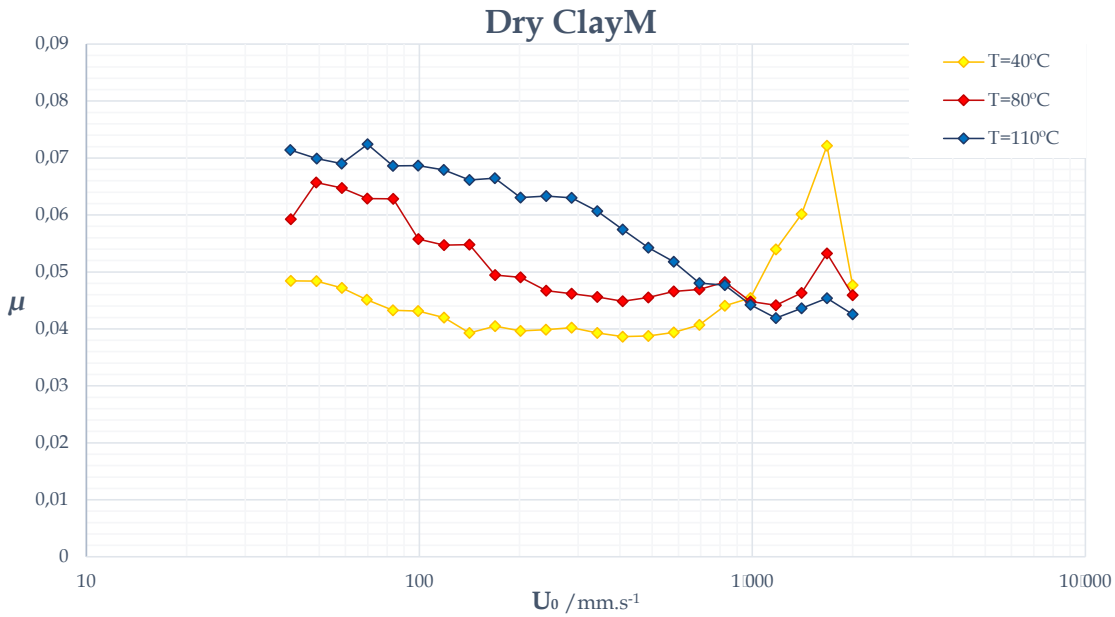


Figure A.38: ClayM Dry Grease Stribeck Curve Ra=500 nm

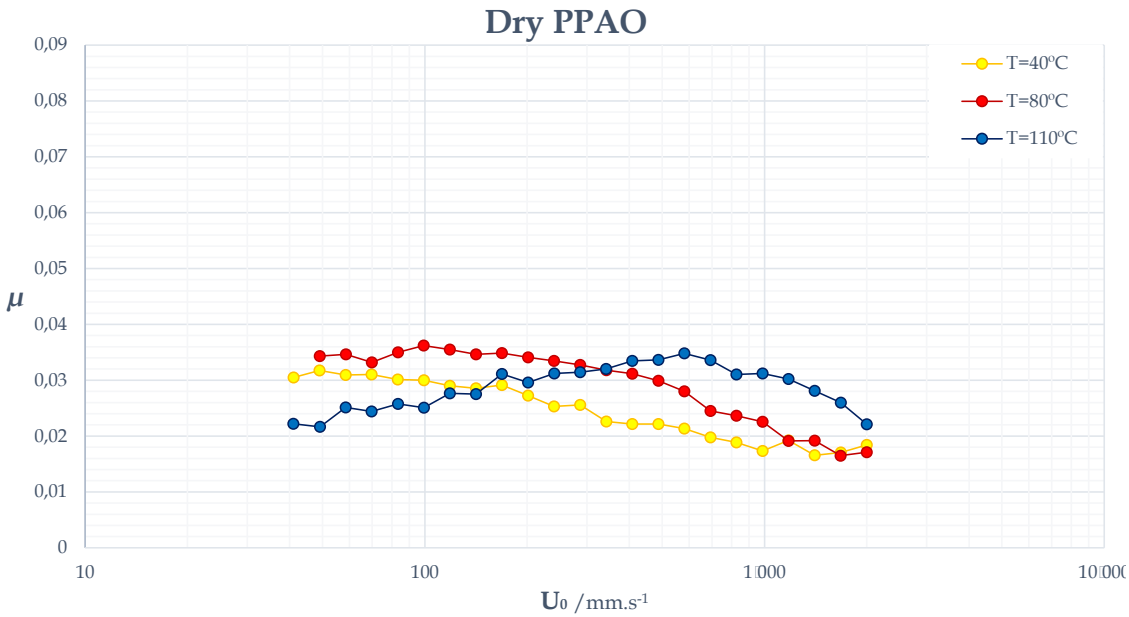


Figure A.39: PPAO Dry Grease Stribeck Curve Ra=100 nm

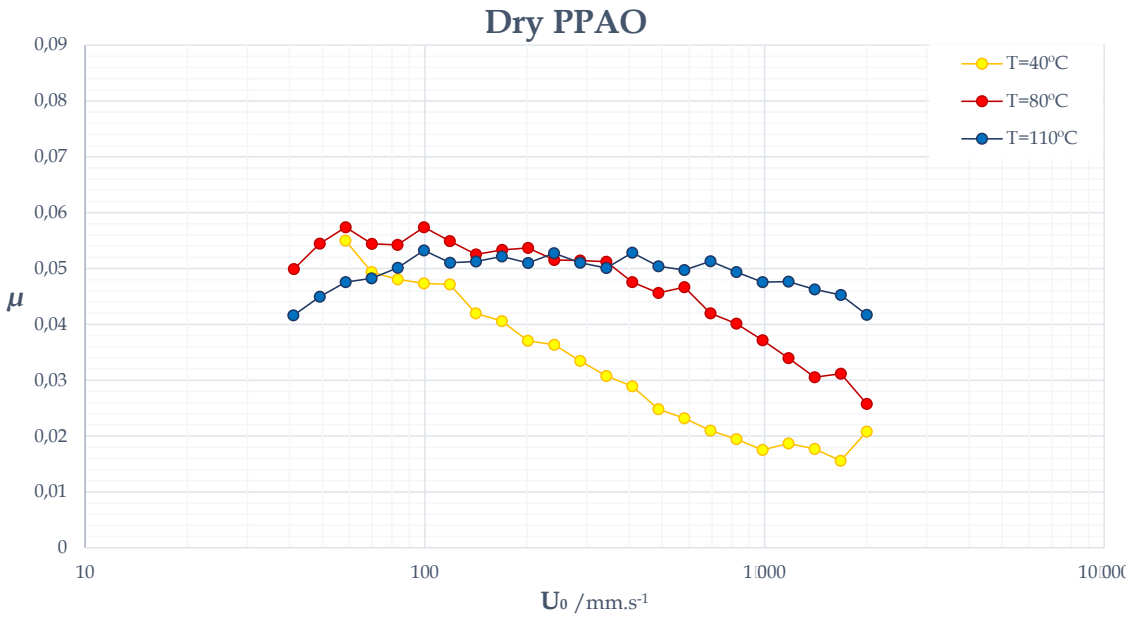


Figure A.40: PPAO Dry Grease Stribeck Curve Ra=500 nm